SEMIACTIVE VIBRATION ABSORBERS (SAVA) AT THE I-35 WALNUT CREEK BRIDGE

FINAL REPORT

Submitted to:

THE OKLAHOMA DEPARTMENT OF TRANSPORTATION

PROJECT: WALNUT CREEK BRIDGE

Submitted by:

William Neff Patten, Ph.D., P.E.

Director, Center for Structural Control
The University of Oklahoma
865 Asp Avenue, Room 212
Norman, Oklahoma 73019

September 1997

TECHNICAL REPORT DOCUMENTATION PAGE

1. REPORT NO. FHWA/OK 97(08)	2. GOVERNMENT ACCESSION NO.	3. RECIPIENT'S CATALOG NO.
4. TITLE AND SUBTITLE		5. REPORT DATE
		6. PERFORMING ORGANIZATION CODE
7. AUTHOR(S)		8. PERFORMING ORGANIZATION REPORT
9. PERFORMING ORGANIZATION NAME AND ADDRESS		10. WORK UNIT NO.
		11. CONTRACT OR GRANT NO. 2125
12. SPONSORING AGENCY NAME AND ADDRESS Oklahoma Department of Transportation Office of Research 200 N.E. 21st Street, Room 2A2 Oklahoma City, OK 73015		13. TYPE OF REPORT AND PERIOD COVERED 2125
		14. SPONSORING AGENCY CODE

15. SUPPLEMENTARY NOTES
U.S. Department of Transportation
Federal Highway Administration, 715 S. Metropolitan Avenue, Suite 700, OKC, OK 73018

16. ABSTRACT

The project was undertaken to develop and field test an automatically controlled bridge mounted vibration absorber. The system, referred to as a semiactive vibration absorber (SAVA) consists of a hydraulic cylinder coupled to structural steel elements that bolt on to an existing bridge. The hydraulic cylinder (HC) is equipped with a computer-controlled valve and sensors. The sensors are used to detect the motion of the bridge girders that results from the passage of heavy multi-axle trucks. The research resulted in the establishment of a smart software code that opens and closes the valve on the HC at appropriate times during the vibration. The modulation of the valve affords an optimized combination of both stiffness and damping, which results in a significant reduction of vibration amplitude and maximum stress in the girders. Field testing of the SAVA system was conducted on the Walnut Creek Bridge at the 92.7 mile marker on I-35 between Dallas, TX and Oklahoma City, OK. The bridge has a two-lane, 38' wide composite deck, supported by five 134 lb/ft girders mounted at 8' 6" centers. The continuous 400' long girders were supported at 100 foot intervals by three piers and abutments at either end of the bridge. The SAVA system was installed in the Summer 1996 on one span of the bridge, and field-tested for over 12 months. The results indicate a nominal reduction of truck-induced stress and deflection of over 55%. The tests were conducted using four multi-axle trucks with weights ranging from 27 klbs to 120 klbs, traveling at the posted speed limit. NCHRP 299 (1989) was used to determine the remaining safe life of the bridge. The most conservative estimate indicates that the span, in which the SAVA system is mounted, gained an additional 60 years of safe life and over 150 years of mean life. The estimated safe life of the bridge prior to the installation of the SAVA system was -7 years. The system operates on a 12-volt battery that is rated to last over two years. The instrumentation required include two sensors (per actuator). The entire SAVA system was mounted from below, without having to impede traffic. The estimated cost of the system is approximately 7% to 10% of the cost to replace the bridge. The performance of the system and the integrity of the electronics is routinely checked via a remote monitoring system. The work proved conclusively that the semiactive vibration absorber system is robust to climate conditions and is inherently safe. A patent has been awarded (# 5545372) for this technology.

17. KEY WORDS	18. DISTRIBUTION STATEMENT No restrictions. This publication is available from The Office of Research, Oklahoma DOT
19. SECURITY CLASSIF. (OF THIS REPORT) Unclassified	20. SECURITY CLASSIF. (OF THIS PAGE) Unclassified	21. NO. OF PAGES	22. PRICE

PROJECT FINDINGS

- **Maximum deflections routinely reduced by 60%+**

- **Maximum stress range routinely reduced by 55%+**

- **SAVA affords a minimum of 55 years additional safe life**
  150 years of mean life (per NCHRP-299)

- **SAVA system able to be installed from below without traffic delays**

- **Bolt up construction simple**

- **Minimum number of components**

- **Only 2 sensors required per actuator**

- **Remote monitoring**

- **Battery power (2 years refresh required)**

- **No painting necessary**

- **System useful for spans from 50 ft to 250 ft**
  (research now under way to extend to longer spans)

- **Cost at 8% of replacement cost for typical bridge**

- **Almost all truck suspensions resonate at or near**
  one of the fundamental modes of bridge

- **Impact factors over 1.8 were found to be routine for almost all trucks tested**

PROJECT OVERVIEW

TESTING OF AN INTELLIGENT HIGHWAY BRIDGE
AT THE I-35 WALNUT CREEK BRIDGE

Abstract

The decay of the U.S. bridge infrastructure has prompted a great deal of effort to discover remedies that are cost-effective. This report describes the concept of an intelligent bridge that is equipped with a controllable muscle that can be attached to the bridge superstructure (a smart bridge). The system works to increase the load-carrying capacity of a bridge as well as increase its service life by decades.

The paper describes a field test of the smart bridge concept. Preliminary results reported here indicate that the system can effect a 52% reduction of deflection and a commensurate reduction of stress range. The results also suggest that the system can increase the safe life of the span it is mounted in by over 50 years.

Introduction

There is growing interest in the development of smart, or intelligent transportation systems. While almost all of the effort appears to be aimed at providing automatic control of the trajectory of vehicles, there are other pressing problems that may also benefit from the synthesis of traditional transportation solutions with new and inexpensive systems that help to promote more intelligent use of the transportation infrastructure.

The U.S. bridge infrastructure is in need of remediation. A recent FHWA Report (1995) on the condition of bridges paints a dismal picture. The estimated cost to repair/replace deficient bridges is upwards of $6 billion per year for 25 years. Faced with that staggering outlay of funds, it makes sense to stop and consider the global picture, and make an assessment of how to proceed. Seriously deficient bridges are generally replaced. If each of the states were given enough monies to immediately upgrade their bridges, the impact on commerce would be nightmarish. Construction delays, especially on the interstate highway system, incur a significant cost to the interstate commerce, as well as a negative cost to communities along those routes that depend on vehicle volume to make local business viable.

What is desperately needed is an effort to determine alternative prescriptions for the remediation of bridges that avoid (at least in part) some of the serious negatives associated with the carte blanc replacement of deficient bridge structures. The Center for Structural Control (CSC) at the University of Oklahoma has been engaged in a program of research that has produced a working concept for an intelligent bridge.

The feasibility of the system will hinge on two important considerations. First, the cost of the system must be significantly less than the cost to replace a superstructure. Second, the installation of the system should be accomplished without impeding traffic significantly. This report recounts the results of a research project in which a technology was designed, developed and field-tested.

Background

The CSC has developed and field tested a prototype of a bridge vibration control system. The project was conducted with funds from the National Science Laboratory (NSF), the Oklahoma Department of Transportation

(ODOT) (with a NCHRP grant from the Federal Highway Administration) and the Oklahoma Center for the Advancement of Science and Technology (OCAST). The project was initiated in 1993. The system was installed on an in-service interstate bridge in the Fall of 1996. The ODOT investment in the project (including FHWA match) was appropriately 390K. NSF funds, to date, exceed 750K and OCAST has committed an additional 250K. The following paragraphs give a brief summary of the project and the progress achieved to date.

Semiactive Vibration Absorbers (SAVA) for a Bridge

The CSC has spearheaded the design and proof-testing of a new hydraulic control technology that uses simple hydraulic cylinders and a small valve to regulate the flow of fluid from one chamber to the other when the structure that the cylinder is attached to induces movement of the piston. By opening and closing the valve at the appropriate moments, the motion of the structure that is vibrating can be reduced dramatically. The physics of the device and the analysis that underlies the development of a control policy are discussed at length in the report.

Semiactive structural control represents a hybrid of active and passive control methodologies. The technique seeks to provide performance levels close to those achieved by an active system, without relying on external power or pumps to accomplish the design objectives. A semiactive design differs from a passive design in that the characteristics of the system are not fixed as they are in, for example, a tuned mass damper system. A most significant distinction between a fully active control system and the SAVA system is that a SAVA system is inherently stable; it cannot pump energy into the structure. When two points on a structure move relative to each other, then the SAVA can be used to resist the motion, and to dissipate the energy in the structure. The piston in the cylinder is outfitted with a system of rings which were designed to minimize flow leakage between the two chambers in the piston. This feature is in sharp contrast to passive dampers which include specially designed bypass orifices. The only way fluid can be exchanged between the chambers of the SAVA actuator is by opening the motor-controlled valve. When the valve is closed, the actuator "locks up", which produces a temporary stiffness element. Energy is dissipated via the flow of the viscous fluid in the actuator through an orifice (the valve) when the valve is open (much like an adjustable shock absorber). The CSC has developed a low cost valve/motor combination that can rotate a valve under pressure from the fully-opened to the fully-closed position in 10 milliseconds. The speed of the valve motion plays a significant part in the effectiveness of the design. It is also important to note that the compressibility of the fluid in the actuator plays an important and constructive role in the logical operation of a SAVA. When large forces are present, the fluid responds like a spring, which can store energy, and which can be used in turn to enhance the motion mitigation of a structure.

The Bridge

The 400' long bridge carries two lanes of north bound traffic on I-35, which is a national corridor connecting Mexico (at Laredo, TX) to Canada (at Duluth, MN). The superstructure consists of five continuous girders weighing 126 lbs./ft., with a 54" deep web and 14" flanges. The concrete deck is 7 ½ " thick with reinforcing. The bridge, which has a skew of 45° is supported by three intermediate concrete piers at 100' intervals. The superstructure includes diaphragms constructed of lightweight elements located at 20' intervals along the span. The scope of work of the project called for the accomplishment of three tasks; 1) the modeling and model verification of the bridge, 2) the

design and installation of the SAVA system, and 3) the subsequent monitoring of the smart bridge system performance.

A system of sensors was first constructed to establish the dynamic character of the entire bridge. Forty-eight sensors were installed, including 36 accelerometers, 2 string potentiometers, and 10 strain gauges. The long distances from sensors to the data acquisition system (as much as 600') made it impossible to achieve the goals of this project with conventional signal conditioning technology. Instead, the research team developed a low-cost frequency modulation system to convey sensor data to the central processor. The cost per channel for signal conditioning was approximately $300 (U.S.), which is modest when the long transmission distances are taken into account.

A finite element model (FEM) of the bridge was developed. The IDEAS® FEM software (by Structural Dynamics Research Corporation) was selected for the analysis, primarily because of the excellent modal analysis capabilities. In addition, IDEAS has a state-of-the-art graphics support module which makes it especially easy to illustrate the system. The model consisted of 410 thin shell element, 620 beam elements (including "I", "T", and angle), 316 rigid bars and 74 solid elements. The base model included 811 nodes, requiring 4,800 coupled equations of motion. Boundary conditions at the support piers were included in a routine manner.

In order to verify the analytical model, experiments were conducted to identify a modal model of the bridge. A drop hammer was constructed, with an instrumented 350 lb. head which, when released, would free fall 6'2", creating an impulsive force of 24 Kpsi. The hammer was dropped at six different locations and the output of the 36 accelerometers was recorded. The test data was then subjected to standard modal test techniques to establish modal frequencies and mode shapes.

The correspondence between the modal frequencies is exceptional. The test results made it clear that modes beyond 10 Hz contain only a small percentage of the system's response energy. Once a valid FEM of the bridge was established, then a test truck was used to compare the predicted *versus* actual response of the bridge. The suspension of the trucks was instrumented and the vibration of the truck chassis was recorded while the truck traversed the bridge in the right-hand lane. The motion of the bridge was also recorded. Using a standard chassis model for the truck, the wheel loads were determined using the recorded data. Those loads were then used as inputs to the model.

While the model of the bridge was being developed and validated, the CSC team was also engaged in the design of the basic bridge muscle structure. As the truck proceeds across the span, the output of bridge-mounted sensors (strain gauges, pressure sensors, and piston displacement sensors) are relayed to a small microcontroller. The data is then processed to determine how each valve should be adjusted. Much of the research conducted at the CSC has been aimed at developing appropriate numerical algorithms for the operation of SAVA. The simplest and most effective technique, developed to date, utilizes a bi-state logic; the valve is throttled between its fully-opened position and fully-closed position.

Once the general kinematic layout of the actuator was selected, then CSC conducted an in depth design trade-off study. The study examined the effectiveness and cost implications of the following design variables

- number of actuators (2, 3, 4 or 5)
- placement of actuators

- length between moment arms
- size of an actuator
- size of valving
- fatigue life of SAVA components
- stroke of the actuator
- stiffness and weight of assembly
- number and location of sensors
- bandwidth of control electronics
- maintenance and reliability
- fatigue life of the bridge

A series of increasingly more complex dynamic simulations were used to finalize the SAVA design.

Performance Simulation

The expected effectiveness of the design is best portrayed first by simulating the response of a simple 100' long girder when a truck with a compliant suspension travels over it. The parameters used in the single-span simulation were based on the actual structure of the test bridge. The parameters that describe the truck match the characteristics of a truck that is used to conduct proof tests. (A 5-axle, tractor-trailer, dump truck weighing 80,000 lbs. with a 34' wheel base.)   The truck was assumed to be traveling at 70 mph (posted speed limit at the test site).

A comparison was performed of the deflection that is expected when, on the one hand, the SAVA system is mounted and operational and, on the other hand, when no SAVA system is installed. The data indicates that the SAVA can reduce the maximum deflection by approximately 60%. The stresses (or moments) experienced along the bridge span during dynamic loading are also effected dramatically by the SAVA system. The data indicates that the SAVA system "flattens" out the moment curve, producing much lower local stresses.

The simple span simulations are an effective means of demonstrating the basic advantages of the SAVA design. Additional simulations, using a single continuous girder with four spans (each 100'), were also used to conduct performance studies. Assuming that a SAVA was mounted on the third span of the structure, and presuming the same vehicle loading conditions defined above, indicates the effectiveness of the SAVA system. Results depict a 65% reduction of maximum displacement. Many additional simulations of the full structure performance were conducted in order to tune the final design. The selected design required the installation of three SAVA actuators, with one located on the east girder, one on the center girder, and one on the west girder.

Installation and Testing

Subcontracts were awarded for the fabrication of the hydraulic actuators, the extension elements, and the moment arms. The actuators and extension elements were assembled at the CSC facilities. The installation on the bridge superstructure was accomplished using monorails and block & tackle systems. A temporary road was installed using fill from the creek bed. First, holes were drilled to install web stiffeners. Then, holes were carefully drilled in the flange of one girder at a time. The effectiveness of the design relied, in part, on the ability of the SAVA system to

transmit forces at a specified moment in time. To that end, the installation required considerable care in the location and size of the holes drilled in the flanges. The work also relied on the use of tapered bolts and reamed holes, to guarantee a no-slip condition. Next, the moment arms for the SAVA assembly were traveled into place, hoisted into position, and bolted.

Following the installation of the moment arms, the actuator/extension assembly was trucked to the site. The assembly was placed on rollers on a mat and dragged to a position under the span (recall that a temporary road was constructed that made this possible). The assembly was then hooked to the monorail system, traveled to its proper location, and hoisted into place with chain fall equipment. The process was repeated for each SAVA assembly. Traffic was never impeded during the construction effort. The installation of the SAVA structural hardware was completed in 21 continuous working days. Once the mechanical hardware was installed, the CSC team began the task of installing the computer systems and electronic components that were used to produce a smart actuation system. The installed SAVA system is shown in Photo 1.

Any time a laboratory experiment is scaled up to a full-size demonstration, then there are likely to be problems, and problems translate into project delays. Almost all of the delays incurred were associated with the installation and proof-testing of the microelectronics. For example, the west facing girder (the bridge runs from south to north) experienced surface temperatures in excess of 140°F in the summer months. Laboratory grade sensors and signal conditions are not usually designed for those high temperatures. The team spent a significant amount of time climatizing the electronics. Nature has a way of testing any design. An intermittent failure off one of the electronically-controlled valves was traced to a deposit of bird feces on the encoder that was mounted on the valve motor to sense the valve position. The valve motor assemblies have now been bird-proofed. The project had its share of software "bugs" as well. The reliance on a network of microcontrollers is now a standard…in the laboratory. It takes a concerted effort to make that architecture foolproof for field applications. The CSC was able to complete and debug the electronics, and the first calibrated tests of the system were run in November, 1996.

SAVA Test

The test program employed four different trucks. Two of those trucks were instrumented in order to verify the truck/bridge interaction when passing over the bridge. It is important to point out that the bridge SAVA intelligence system has no á priori information about the truck(s) that passed over the bridge. The SAVA system must function without any preview or forecast of the truck weight, its speed, its suspension characteristics, or the truck's vibration state. (Truck vibrations are almost always excited by the entrance ramp irregularities.) It is also important to note that there is no "one" bridge modal frequency that ensues once the bridge and truck couple. The response of the bridge to the truck usually consists of an ensemble of bridge modes, each representing a significant portion of the vibration energy imparted to the bridge as the truck passes.

A computation of the safe life remaining for the bridge before the SAVA system was installed suggested negative life. The re-computation of the safe life using data from the SAVA test indicates that, at a minimum, the safe life is extended by 50 years. The mean life extension is also indicated there. The results using the heavier (120K lb.) truck

also suggest a trade off may be possible between the increase of service life and the permissible load capacity of a bridge outfitted with a SAVA system.

The testing of the system is ongoing. The results strongly suggest that the life extension and increased capacity evidenced in the test reported here are typical. The CSC is now conducting multi-truck tests, and preliminary results indicate that the designed system affords an approximately 55% reduction of maximum stress range. The open challenge is to tune the algorithms used in the control to push the present performance closer to the analytical prediction of a 65% reduction of the stress range.

Discussion and Conclusions

The report provides a preliminary report on the test of an intelligent bridge motion mitigation system. To the author's knowledge, this project demonstrates for the first time the feasibility of a semiactive control system for bridges and for structures, in general. The results indicate that the concept is technically viable. The cost to install the system on a generic bridge should represent no more than 15% of the cost (of construction) to replace the superstructure of the bridge. If the economic costs incurred because of traffic delays are factored in the true cost of the SAVA retrofit is less than 5% of the economic impact that results when the bridge is replaced. The price is right.

A patent has been awarded for the new technology and a license has been issued to commercialize the concept. The CSC is now engaged in the redesign of the assembly to make it possible to tuck the equipment up between the girders in order to negate the effects that might threaten the system if a 500+ year flood were to strike the region. The free board depth below the girder flange is the driving design variable in this instance. The CSC hopes to demonstrate the "tucked up" design in the fall of 1998.

Project Highlights

1. Using the most conservative truckload data, the SAVA control system produced:
    a. a 55% reduction of maximum deflections
    b. a 50% reduction of maximum stress range and
    c. a minimum of a 50 year increase in the remaining service life of the span it is mounted on.

2. The research demonstrates that the fundamental chassis modes of all trucks tested were very close to the fundamental mode of the test bridge (2.5 Hz). An analysis of three additional type 402 plate girder bridges on I-35, with spans varying from 80 feet to 125 feet, found a similar result. The conclusion is that truck suspension resonate with these bridges to produce very large levels of impact.

3. The installation cost of a SAVA system makes it an ideal alternative to the replacement of a bridge superstructure.

Photo 1: The I-35 Walnut Creek Bridge with SAVA System Attached

SEMIACTIVE VIBRATION ABSORBERS (SAVA) AT THE I-35 WALNUT CREEK BRIDGE

A PROJECT FUNDED BY OKLAHOMA DEPARTMENT OF TRANSPORTATION

ODOT PROJECT ENGINEER: DAVID OOTEN, PE

SUB-REPORT # 1:

EXPERIMENTAL MODAL ANALYSIS, MODEL REDUCTION, AND MODEL MODIFICATION

CENTER FOR STRUCTURAL CONTROL

UNIVERSITY OF OKLAHOMA

http://www.coe.ou.edu/research/cstructc/

PROJECT MANAGER:

WILLIAM N. PATTEN, Ph. D, P.E., (PI)

RESEARCH ENGINEERS:

JINGHUI SUN, Ph. D.
GANG SONG, Ph. D.
JIAN PANG, Ph. D.
JEFFERY L. KUEHN
GUANGJUN LI

AUGUST, 1997

TABLE OF CONTENTS

NOMENCLATURE

A	Area	(ft^2 or in^2)
a	Acceleration	(m/sec^2)
A$_{lp}$	Residue	
C	Damping matrix	(kg/sec)
Cr	Reduced damping matrix	
E	Young's modules	(psi)
E$_K$	Stiffness Error	
F	Force	(lbf., N)
F	Average force	(lbf., N)
G	Fourier spectrum	
H	Transfer function	
I	Identity matrix	
J	Jacobi matrix	
J$_E$	Objective function	
K	Stiffness matrix	(lbf/in, N/m)
Kr	Reduced stiffness matrix	(lbf/in., N/m)
L	Modal participation factor	
m	Mass	(lb., kg)
M	Mass matrix	
Mr	Reduced mass matrix	(lb., kg)
N	Mode number	
N$_s$	Shape function	
P$_0$	Force peak	(lbf., N)
q	Modal coordinate	
T	Transformation matrix for the model reduction	
T$_i$	Initial kinetic energy of the system	
T$_f$	Final kinetic energy of the system	
U	Stain energy	
V	Velocity	(m/sec, mile/hr)
V$_f$	Final kinetic energy of the system	
V$_i$	Initial potential energy of the system	
X	Displacement	(in., m)
Xm	Remained displacement coordinate	
Xs	Omitted displacement coordinate	

Δt	Time duration	(Sec)
ϵ	Strain	
Λ	Eigenvalue matrix	
ω	Natural Frequency	(Hz, rad/sec)
ωr	Disturbance Frequency	(rad/sec)
Ω	Frequency matrix	(rad/sec)
Φ	Modal shape	
Φa	Remained modal shape	
Φo	Omitted modal shape	
Ψ	Complex modal matrix	
σ	Stress	(psi)
ξ	Damping ratio	

ABSTRACT

Dynamic testing and modal analysis can provide valuable information on the service behavior and working performance of the bridge structure. The experimental modal analysis and related theoretic works presented in this report are part of the principal investigations which were conducted in conjunction with a recently completed research project - Mitigating Vibration of a Steel Highway Bridge Using Semiactive Control, funded by the Oklahoma Department of Transportation.

The project was designed to test a new technology; Semiactive Vibration Absorbers (SAVA). These low cost adjustable shock absorbers, which require no external power were installed on the bridge to increase the service life and load capacity of the test bridge. The actual performance of the tested system is reviewed in a related report.

In order to accomplish the project, the Center for Structural Control (CSC) first embarked on an effort to develop a precise understanding of the test bridges behavior under load. Key to that understanding was the establishment of a rigorous Finite Element Model (FEM) that could be used to predict the vibratory motion and stresses that result from the passage of vehicles. The report recounts the various aspects of the research project that were undertaken in order to produce a high fidelity FEM of the bridge.

Included in the text is a description of a system of sensors that were installed to monitor the motion and strain through the entire bridge structure. The tests that were conducted to extract the modal signatures of the bridge are also reviewed. Next, the task of constructing a FEM that was able to mimic the field modal data is discussed. This report closes with a description of methods that were subsequently employed to reduce the order of the full FEM.

INTRODUCTION

1.1 Bridge and Project

The test bridge is located on I-35 at the 92.7 mile marker and crosses Walnut Creek near Purcell, Oklahoma (Figure 1.1). The bridge was built in 1971. It consists of five 400' long continuous steel girders with three intermediate piers and two abutments located at 100' intervals. The bridge deck is skewed at 45° to the center line of the roadway. The deck is 38' wide, including two 12' wide lanes of traffic, and has a 10' shoulder adjacent to the inside lane, and a 4' shoulder adjacent to the outside lane. The five steel girders are covered by the composite concrete deck. The superstructure is supported via a group of fixed shoes (on the middle pier) and four groups of expansion shoes (on the other two piers and the two abutments). The girders are equipped with diaphragms at 20' intervals. The diaphragms are orthogonal to the longitudinal centerline of the bridge. Recent traffic surveys indicate that approximately 18,000 vehicles cross the bridge on an average day.

The ultimate purpose of this project was to install and test an automatically controlled vibration suppression system on the bridge to mitigate vehicle induced vibration. Three semiactive vibration absorbers (SAVA) were mounted on the bridge.
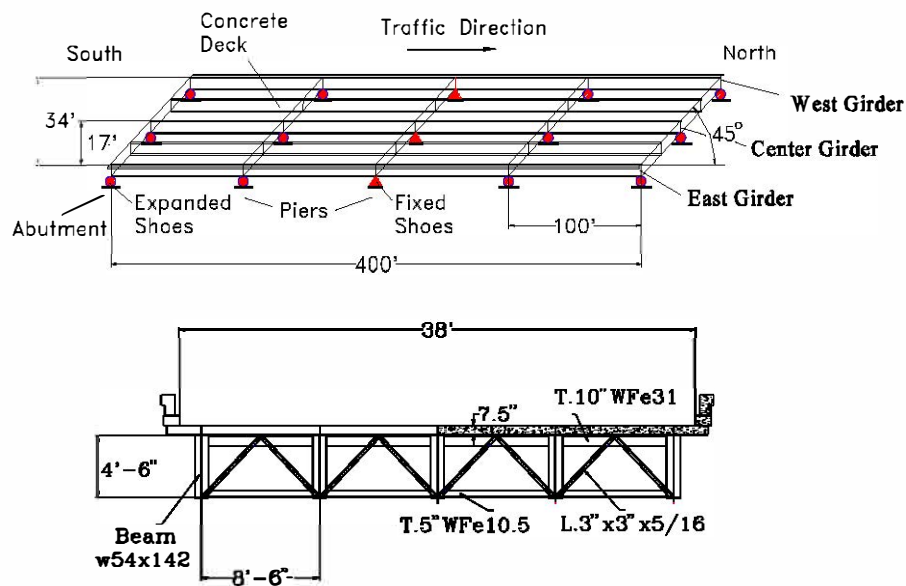
Figure 1.1 Superstructure of the Oklahoma I-35 Walnut Creek Bridge

This report focuses on the modal analysis of the Walnut Creek Bridge. An impact modal test technique was utilized. The measured impact response was used to identify the modal parameters of the system. The parameters were then compared to those obtained via a finite element (FE) based model of the structure. The work presented here is based in part on the experiments performed in November 1995 on the superstructure of the bridge before the SAVA system was installed. The results are also based on the data obtained from modal tests conducted after the SAVA system was mounted on the bridge.

A comprehensive dynamical model of the bridge was first established via the Finite Element Method (FEM). Next, a Reduced Order Model (ROM) was produced. The report discusses the fidelity of the ROM. The discussion provides a comparison of the accuracy obtained using various model reduction methods, including Guyan reduction, Dynamic reduction, Improved Reduction System (IRS), and the Modal Model Reduction Method (MMRM). The model produced by the reduction process was then used to generate frequency response functions (FRF), which were then used to predict the response of the bridge to the truck impact loads.

Experimental modal analysis begins with the measured forced response data (i.e., FRFs) and extracts the modes of vibration directly from the FRFs without having to make any assumptions about the mass and stiffness distribution. Experimental modal analysis produces a set of modes defined by frequency, damping, mode shape, and residues. Certain assumptions and post processing of the data are necessary to calculate modal mass or stiffness.

The process of developing a modal model included the following iterative procedures:

(1) Pretest analysis, using the theoretical FEM to determine optimal locations for sensors and test input actuators;

(2) Modal testing and subsequent modal analysis, to determine precise modal model parameters;

(3) Correlation analysis between the analytical FEM and the experimental modal model to assess the validity of the FEM; and

(4) Model updating to tune the analytical FEM. The objective is to improve the modal shape correlation and orthogonality coefficients, and to equalize the corresponding natural frequencies.

The process repeats itself until the level of correspondence sought is achieved.

1.2 Bridge Modeling and Testing

A finite element based physical model was established to make it possible to predict, with accuracy, the deflections and stresses of the structure when subjected to a vehicle load. Experimental modal analysis was employed in order to:

(1) validate the theoretical (finite element) model of the bridge. It must be noted that the FEM involved significant hypotheses. A comparison and correlation of the theoretical prediction with the actual measured response has lead to a better understanding of the structure;

(2) understand the dynamics of the bridge;

(3) increase the database for the dynamic behavior of similar structures. This is pertinent since there are many similar bridges built on the Interstate highway. Thus, the database can be used to predict the response of similarly constructed bridges. Since full-scale tests are extremely expensive, this database represents an invaluable tool for the evaluation of bridges;

(4) determine the integrity of a structure after the occurrence of an overload (for example, an unusually large permit load). The same approach can also be used to assess the effectiveness of remedial repairs to the bridge;

(5) provide a systematic means of monitoring the health of the structure. Changes, as a result of deterioration, can be detected by the variations in the system parameters --- mass, stiffness and damping --- which reflect the changes in the vibrational response (Results of tests have shown that the size of damage is proportional to the magnitudes of observed changes in identified system parameters.); and

(6) determine the remaining fatigue life for the bridge.

1.3 Literature Review of Bridge Modal Analysis

Dynamic tests have been conducted on bridges since the late 19th century [1]. Many of the earlier tests were conducted as a component of safety inspections and involved monitoring bridge vibration. Modern dynamic tests focus on improving analysis and design procedures so that when new bridges are built, they will exhibit improved vibration characteristics.

Experimental dynamic testing is now being conducted on many bridges. Dynamic testing includes an excitation source and response measurement. Response signals usually consist of acceleration, displacement, strain, etc. Types of excitation usually include ambient vibration and forced vibration testing. Ambient vibration includes wind, ocean wave, vehicle traffic, etc. Forced vibration testing includes hydraulic shakers, impact hammer, etc.

1.3.1 Ambient Vibration Testing.   Ambient vibration tests are usually conducted on medium to long span bridges (i.e., span is larger than 70 m) [2,3,4]. An extensive experimental investigation has been done on the Golden Gate Suspension Bridge [5] in order to determine dynamic factors such as: effective damping, three-dimensional mode shapes and resonant frequencies. The excitation was derived from wind, ocean waves and vehicular traffic. The testing results demonstrated similarities with the results of both the two- and three-dimensional finite element analysis.

Other modal tests using traffic inputs have also been reported [2,6]. To accomplish the investigation, a bump was normally constructed on the bridge deck. An input impulse was produced when a truck passed over the bump. Since the input force is not monitored, a reference accelerometer was chosen at a location where motion is most likely to occur for the first few modes, i.e., the reference accelerometer data was treated as the input signal and all other acceleration data as output signals. A finite element model was constructed using the results of the test. The lack of a precise knowledge of the actual input makes this approach to modal testing less reliable than other approaches.

1.3.2 Hydraulic Shaker Testing.   Excitation by hydraulic shaker has been found to produce excellent results for short to medium span bridges (span < 100 m) [3,7,8,9]. One recent example is the reported use of a servo hydraulic vibration generator to excite the West End Bridge in Berlin, Germany [7]. A 500 kg mass was connected to a hydraulic ram, which then excited the bridge. The maximum force produced was ±5 KN. Three load cells were mounted beneath the mass block to sense the dynamic force exerted on the structure. The experimental investigation provided the basis for adjusting a finite element model of the bridge structure to reflect actual behavior. The drawback to this testing approach is the expense of the equipment required.

1.3.3 Hammer Impact.   Hammer impact testing is often used for a shorter bridge with a span < 40 m [3,10]. It can, however, be effective for bridges with longer spans also (<150 m). There are two kinds of impact test devices:

a long-arm impact hammer [10] and vertical drop impact hammer [1,3]. Yantha, et al., described the building of a long-arm hammer which was used to excite a pony-truss bridge [10]. The hammer head had a mass of 20 kg fixed at the end of a 2 m long arm. A force transducer was mounted on the face of the hammer.

Green, et al., [3] have reported successful utilization of an instrumented hammer during the modal identification of two highway bridges. Impact hammers have been used to excite many small bridges, such as a three span railway bridge with a main span of 21 m [11], a six span (30 m for each) prestressed concrete bridge [12], and a truss bridge with a main span of 43 m [13].

1.4 Overview of Chapter.

In this report, a description of modal instrumentation fabricated and installed at the Walnut Creek Bridge is first presented in Chapter 2. The design and construction of the impact hammer used in the modal test are also discussed in Chapter 2. Chapter 3 recounts the steps involved in the construction of a finite element model of the bridge. The modal analysis and related results, as well as FEM correction of the project bridge are discussed in Chapter 4. The procedures used to produce a reduced order model of the bridge are recounted in Chapter 5. Conclusions and Recommendations are offered in Chapter 6.

CHAPTER 2

SAVA SYSTEMS AND EXPERIMENTAL SETUP

2.1 SAVA System

The kinematic assembly of the each SAVA system on the Walnut Creek Bridge consists of two moment arms, an automatically adjustable hydraulic actuator, an extension rod, web stiffeners, and connecting components. Three systems were installed; the east, west, and central bridge girder (W54x142) at the second span from the north (Figure 2.1). The longitudinal center of the SAVA assembly corresponds with the longitudinal center of the girder, to which it is attached. The designed stroke of each actuator is 6", and the diameter of the piston is 10". The dimensions of the SAVA components were selected based on a thorough design analysis that relied on supporting information from simulations using the bridge FEM. The actuators are designed to provide as much as 140 kips of force, at an operating pressure of 1,800 psi.

The semiactive control device installed on the test bridge was developed by the Center for Structural Control at the University of Oklahoma [14]. A U.S. patent (#5595372) for the system has been awarded. The SAVA actuator is shown schematically in Figure 2.2. The system is composed of a double action hydraulic cylinder and related plumbing. A high bandwidth flow (globe) valve (full open to full closed in 10 msec. under load), with a small battery-powered DC motor is used to regulate the valve orifice opening. The system operates with a pre-charge of 300 psi (nominal). Oil pressure sensors are provided to detect the pressure level in each cylinder and to indicate the direction of liquid flow. The system operates without an accumulator. The cylinder of the actuator is installed between the end of moment arm and the extension rod (Figures 2.1 & 2.2). An LVDT (Linear Voltage Displacement Transducer) is included to measure the movement of the piston. The stroke displacement of the piston in the cylinder for an 80,000 lb. truck load is typically of the order of ±3 mm, which corresponds to a maximum vertical deflection at the girder center of approximately 12 mm.

The design of the SAVA system components emphasizes lightweight construction, ease of installation, minimal cost and infinite fatigue life (of the SAVA components used). Also, critical to the success of the design was the need for high stiffness of the SAVA assembly relative to the girder to which it is attached. A stiff assembly was needed to assure the timely transmission of forces.

Table 2.1 lists the dynamic parameters (mass and effective stiffness) associated with each of the structural parts of the SAVA assembly. The total weight of the three devices is approximately 22,100 lb., which in effect adds about 5.8 lb./sf. to the span in which the SAVA are installed. The mass ratio of the three semiactive assemblies to the bridge superstructure is 5.5/134 = 4.1% (Table 2.2). An analysis of the combined system (bridge plus SAVA) indicates that the equivalent stiffness of the first mode of the bridge is increased to 231,000 lbf./in from the original first mode stiffness of 194,600 lbf./in.

Figure 2.1 Kinematic Assembly of the Semiactive Control System on the Walnut Creek Bridge

Figure 2.2 A Semiactive Control Device on the Walnut Creek Bridge

Table 2.1 Structural Parts for the SAVA Control Assemblies

Name of Elements	No.	Weight/Piece (lbs.)	Effective Stiffness (lbf./inch^2)
1. Moment Arm	6	987.2	6.0×10^6 on deflection
2. Mounting Block	12	30.8	
3. Pin	6	16.0	
4. Connect Block	6	41.8	
5. Actuator (East)	1	618.0	
(West)	1	628.8	
(Center)	1	874.3	
6. Extension (East)	1	(3672+165.8)	3.69×10^6 on axial deformation
(West)	1	(3672+165.8)	
(Center)	1	(3672+231.2)	
7. Stiffener	24	72.9	

Table 2.2 Evaluation of the Mass on the Four spans' Superstructure of the Walnut Creek Bridge

Material	Weight and Area
Structural Steel	392,500 lb.
Reinforcing Steel	120,280 lb.
Class #AA Concrete	426.2 yd^3 × 3934 lbs./yd^3 = 1,676,700 lb.
Weight of the Entire Superstructure	2,189,480 lb.
Total Square Foot of the Superstructure	15,980 ft^2
The Mass per Square Foot	137 lbs./ft^2

The operation of the actuator is fairly simple, with two general working conditions. When the control valve is open fully, the actuator acts like a standard shock absorber. The resistance to the flow of fluid through the valve orifice dissipates the vibration energy. When the valve is closed, then the fluid in the actuator acts like a stiff spring (Figure 2.3). The fluid (spring), compressed by the deflection of the bridge structure, provides an energy storage device. The operation of the SAVA under a dynamic load consists of the judicious addition of stiffness and or damping to the bridge superstructure during the passage of a heavy truck. The details of the control system operation are provided in an associated report.

Figure 2.3 Model Showing the Elasticity of the Fluid/Air Mix in the Cylinder

when the Control Valve is Closed

2.2 Sensor Layout and Testing Configuration

The work plan at the Walnut Creek Bridge required the multi-year monitoring of the bridge to determine the effectiveness of the SAVA system mounted on the bridge. The unique nature of the project, and the long term monitoring requirement, made it essential to develop a modal test system that could be relied on for highly precise measurements of the structure vibration over the life time of the project (approximately 4 years). The monitoring sensors consist of 36 piezoresistive accelerometers, 18 strain gauges, 6 absolute pressure sensors, and 5 displacement transducers (LVDTs and string pots). The acceleration data is used exclusively to obtain the dynamic properties of the bridge structure and to conduct the modal analysis. Strain gauge outputs were used to establish the stress in members, the deflection of the superstructure, and the location of the neutral axis of the girders. That information was typically stored and post-processed for evaluation. The output from at least five of the strain gauges are used in the feedback control system (discussed in a related report). The LVDTs, which are mounted on the SAVA actuators, sense the real time displacement of the hydraulic piston, which is subsequently used for control purposes. Specifications of each type of sensor are shown in Table 2.3. Accelerometers, strain gauges and string pots were placed on the bottom flange of the steel girders. Four additional channels of strain gauges were mounted on the head of the impact hammer. The geometric arrangement of 36 channels of accelerometers and the hammer drop locations are presented in Figure 2.4 and described in Table 2.4.

A key consideration in the development of the sensor system was the environmental conditions at the bridge site. The integrity of the components had to be assured in spite of the seasonal temperature changes. The temperature of the west facing girder had been recorded at over 140 $^\circ F$ in mid August, and the joints in the concrete deck allow torrents of rain run off to soak the surfaces of the girder during the storm conditions. In order to protect sensor circuits from high temperatures and moisture, PVC pipe was glued to the web of the girder with epoxy. Heat insulation material was included in the pipe in order to reduce heat to transfer to the sensor and circuit. Moisture absorbing material was also added to each sensor cell to keep the circuits dry.

Table 2.3 Specification of Sensors

Accelerometers (36 locations)

Maximum Response		Excitation Voltage	Frequency Response
±1.0g		+5.0V	1060KHz

Strain Gauges (18 locations)

Resistance	Gauge factor	Kt	Lot No.
350.0±0.015% ohms	2.105±0.5%	(+0.4±0.2)%	R-A56AD90

String pots (2 locations)

Measurement Range	Acceleration	Excitation Voltage	Temperature Range
0-2 inches	4 g	10Volts	-67 to 250 $^\circ F$

West

```
      24  23  22          21  20  19          18  17  16          15  14  13

    12  11  10          9   8   7          6   5   4          3   2   1

  36  35  34          33  32  31          30  29  28          27  26  25
```
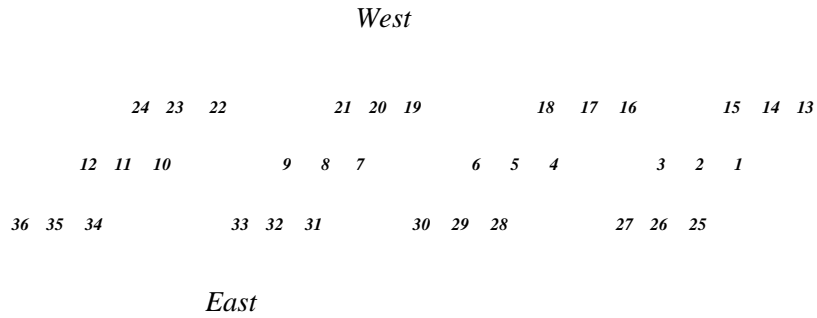
East

Figure 2.4 Sensor Channels' Layout and Hammer Impact Locations

Table 2.4 Accelerometer's Channel Number via Bridge Geometry, and Locations of Impact Hammer
(c=center girder, e=east girder, w=west girder; the number followed indicates
the distance (ft.) from the north end of bridge)

Channel Number	Location	Channel Number	Location	Channel Number	Location	Hammer Drop Locations
1	c, 33	13	w, 33	25	e, 33	e, 150
2	c, 50	14	w, 50	26	e, 50	e, 250
3	c, 67	15	w, 67	27	e, 67	c, 150
4	c, 133	16	w, 133	28	e, 133	c, 250
5	c, 150	17	w, 150	29	e, 150	w, 150
6	c, 167	18	w, 167	30	e, 167	w, 250
7	c, 233	19	w, 233	31	e, 233	
8	c, 250	20	w, 250	32	e, 250	
9	c, 267	21	w, 267	33	e, 267	
10	c, 333	22	w, 333	34	e, 333	
11	c, 350	23	w, 350	35	e, 350	
12	c, 367	24	w, 367	36	e, 367	

2.3 Impact Hammer

Modal testing of a structure consists of measuring the dynamic response to applied loading. The applied loading may be either deterministic (e.g., shaker, impact hammer) or random (e.g., ambient vibration). Ambient vibration methods have been found appropriate for medium to long span bridges (spans >70m) [1,2,4]; excitation via a shaker has been found to produce the best results for short to medium span bridges (spans <100m) [1,3,8,9]; and impact methods produced the best results for bridges with intermediate spans, 50m<span<150m [2,3,10]. There are two types of impact hammers used on the bridge modal test: the drop hammer [1,3] and the long-arm impact hammer [10]. A drop hammer was built and employed to excite the test bridge.

The easiest way of inducing an impact on a structure is by using an instrumented hammer or a suspended mass to deliver blows to the bridge. The impulse delivered to the bridge can be varied either by changing the mass of the impact device or by changing the drop height. The impact frequency range (bandwidth) can also be varied by changing the hammer type. The impulse function consists of a short duration broad-band spectrum. The width of the impulse function determines the frequency content, while the height and shape control the energy level of the spectrum. Impulse testing is susceptible to input noise, since the input force is applied over a short period of time compared to the record length of the measured response.

Figure 2.5 is the drawing of the drop hammer. Two vertical bars are fixed on the top and bottom frames. The hammer mass is attached to two sliding bearings, and the bearings move along the vertical bars. The drop mass is composed of six steel blocks, one weighs 100 lb. and the remaining five weigh 50 lb. The load cell, which weighs 40 lb., is bolted to the face of the drop mass. During impact, the force acting on the load cell is detected by strain gauges. Figure 2.6 depicts the impact force when the hammer is

Figure 2.5 Impact Hammer

11

dropped from a height of 6'2". The peak impact force is over 24,000 lbf. Figure 2.7 is the experimental auto-spectrum of the impact force. In the frequency range of interest (below than 20 Hz), the impact force spectrum is essentially flat with a maximum variation of less than 5 decibels (db). Impact hammer performance is typically restrained by the presence of a rebound impact. It is virtually impossible to avoid the second rebound, but it is possible to design an impact cushion that reduces the amplitude of the rebound and maximizes the time between the principal impulse and the second rebound. Examining Figure 2.6, it is clear that we successfully minimized the effect of rebound. The team spent some time trying various materials to cushion the impact, including viscoelastic material, and a polyurethane form. The best results were obtained using a sand filled rubber bladder (a hot water bottle that is commercially available in any typical drug store).
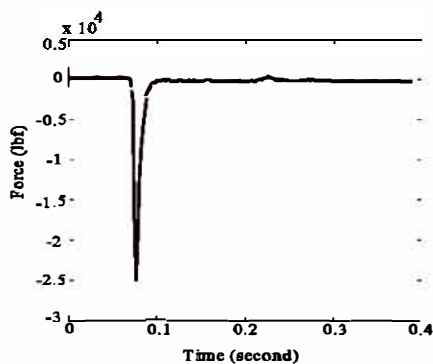
Figure 2.6 Hammer Impact Time History
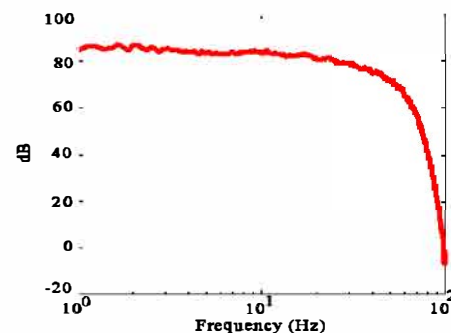
Figure 2.7 Auto-spectrum of Hammer Impact

2.4 Signal Conditioning

The acquisition of data from distant points on the bridge posed a severe problem. Conventional methods require the detection of a sensor voltage output which is usually proportional to the measurement (e.g., 1 Volt equals 200 psi). The long wires represent a large resistance which reduces the voltage signal. This is a problem because many of the sensors are located as much as 600 ft from the data acquisition system. One possible alternative is to transmit the data from each of the sensors using wireless technology. That approach is prohibitively expensive, given the large number of sensors involved. The CSC instead, developed an economical solution that relies on FM technology. The voltage output at a sensor was first converted to a proportional carrier frequency. While the voltage of the signal is subject to amplitude loss, the carrier frequency remains undistorted. The data acquisition system then demodulated the signal, to determine the actual voltage output of the sensor. The technique produces error free readings. The CSC produced printed circuit boards (PCB) to accomplish the design, which was based on analog devices AD650 F/M chip.

The following diagram (Figure 2.8) shows how the original signals are transferred and conditioned when the modal test is on going.
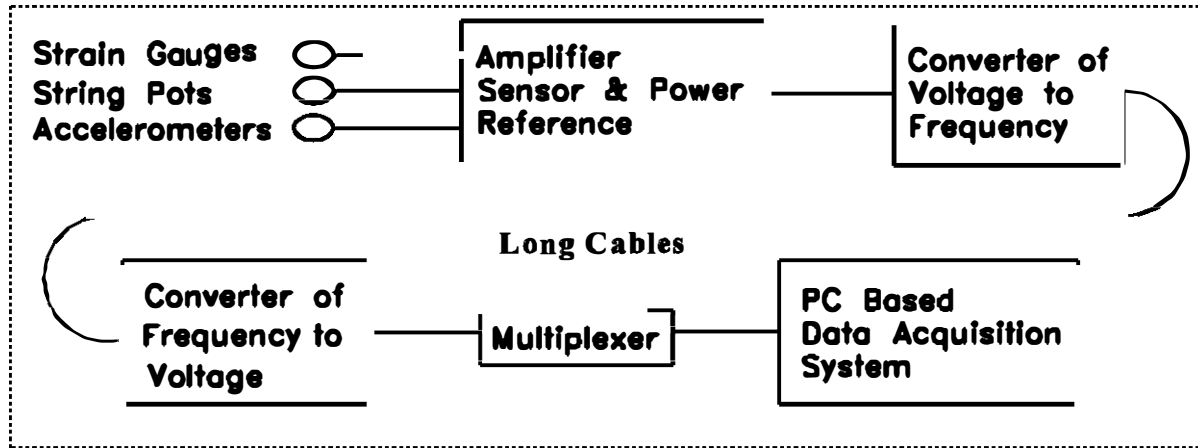
Figure 2.8 Signal Conditioning Network

A 64 channel PC-based data acquisition system was also installed on the test bridge. The system is capable of acquiring data from all 64 channels at a 500Hz sample rate. Data post-processing was conducted using PC Matlab™ on site, while a SUN Sparc station 20 was used for the off-line data analysis with SDRC I-DEAS™-TEST software.

2.5   SDRC I-DEAS™ Test Software

I-DEAS™ is an integrated package of mechanical and civil engineering software, mainly used for product design and structural analysis, as well as other applications. Many postprocessing tasks for this project were completed by using I-DEAS™-TEST software, including the processing of test data, mode shape analysis, the analytical correlation between a finite element and experimental modal model, and fatigue evaluation.

The time-domain signals, acquired from the modal tests, were transferred into the I-DEAS™-TEST system using universal files. Transfer functions between acceleration outputs and hammer input were calculated via Signal Processing software. Test-Modal Analysis provided several modal analysis methods such as SDOF (Single Degree of Freedom), Complex Modal Analysis, Parameter Direct, and Multi-Reference Analysis. In this project, a direct parameter technique was adopted to conduct the bridge modal analysis. This method identifies closely spaced modes with very high accuracy, and gives the bridge modal shapes, frequencies, modal damping, modal mass and stiffness.

2.6 Testing Procedure

The process of conducting a modal analysis is generally composed of three phases: (1) test preparation and system setup, (2) time and frequency response measurements, and (3) signal processing and modal parameter identification. Finite element simulations are also conducted for comparison as a reference and to help in the modal identification effort.

The modal tests on the Walnut Creek Bridge were performed several times. Two major tests events were conducted: (1) November 1995--on the superstructure of the bridge without the SAVA assemblies installed, and (2) July 1996--with the SAVA assemblies mounted on the bridge girders. During the field tests, The Oklahoma Department of Transportation (ODOT) provided traffic control. The impact hammer was moved to six test locations on the bridge deck and dropped three times at each position. Radio communication was utilized by the different teams involved in the work. Bridge impact response and hammer input signals were recorded. On-site modal analysis was then conducted by using PC MATLAB^{TM}.

CHAPTER 3

FINITE ELEMENT MODELING

3.1 Bridge FE Model (FEM)

A comprehensive FEM of the bridge was developed to establish a baseline for the work. The model was used to predict dynamic parameters, including the natural frequencies, mode shapes, modal mass and modal stiffness, modal damping, and to calculate stress range and deflections of the bridge structure in response to vehicular loads. Original drawings of the bridge, as well as field measurements were used to determine the physical parameters of the model. The I-DEAS™ analysis software, produced by Structural Dynamics Research Corporation (SDRC) was used to construct the model on a SUN Sparc 20 workstation.

The model was composed of 620 beam elements (shaped I,T, and Angle), 410 thin shell elements, 316 bar elements, and 74 solid elements (Figure 3.1). A total of 1,420 elements were employed. The assembled model consisted of 811 nodes, with over 4000 degrees-of-freedom (DOFs). Once the model was completed, it was used to conduct the dynamic simulations of the structure response to various truck loadings.

As an alternative, a PC-based FEM was built in "C" Language which had 85 nodes, 128 2-D beam elements, and 145 DOFs. This model is designed to correspond to the setup of the modal test system on the Walnut Creek Bridge (Figures 2.3 & 3.2). That reduced order model was developed in order to make it possible to process field data at the site. The field evaluation of data made it possible to pinpoint and repair problems with the data acquisition setup.

Figure 3.1 Full Finite Element Model of the Bridge Superstructure

Beam 4   Test Sensors

Beam 5

Figure 3.2 Low Order FE Model of the Bridge Superstructure

A second FEM of the bridge with the SAVA system attached was also developed (Figure 3.3). The bridge/SAVA model was used to simulate the response of the combined bridge/SAVA/truck system. The model with three semiactive assemblies was composed of 5,226 elements and 5,505 nodes. In this case, the element mesh for the bridge girder, in the vicinity of the control assembly, was made very fine for the purpose of examining the stress and strain pattern and the dynamic response of the connecting bolts, the girder bottom flange, the web stiffeners, and the moment arm top plates**.**

Figure 3.3 Finite Element Modeling of the Semiactive Control Assembly

The principles that underlie the modal analysis are reviewed next.

3.2 Bridge Dynamic Response Simulation

A generic model that represents the dynamic equations of the bridge/truck system was first derived using Newton's Laws. The dynamics take the following form

$$[M]\ddot{x} + [C]\dot{x} + [K]x = F \tag{3.1}$$

here $[M], [C], [K]$ are the global mass, damping and stiffness matrices, and $\ddot{x}, \dot{x}$ and x are the global nodal acceleration, velocity and displacement vectors, respectively. **F** is the external nodal force vector.

The nodal (physical) coordinate response is assumed to be representable using the following transformation

$$x = \sum_{r=1}^{N} \phi_{lr} q_r \tag{3.2}$$

where **x** is the vector of displacements (and rotations); ϕ is the modal transformation (determined by analysis from the modal response) and q_r is the modal amplitude.

The acceleration response can be written as

$$\ddot{x} = -\sum_{r=1}^{N} \phi_{lr} q_r \omega_r^2 \tag{3.3}$$

where, ω_r is the frequency of the r-th mode.

As an example, the impact signal input used on the bridge modal test at point p, can be presented by

$$F = [0, \dots 0, \dots, f_p(\omega), 0, \dots 0]^T \tag{3.4}$$

where $f_p(\omega)$ is the impact force acting at point p.

The modal force can be expressed as

$$F_r = \phi_{pr} f_p(\omega) \tag{3.5}$$

Substituting Equations 3.2, 3.3 and 3.5 into Equation 3.1, we can deduce

$$-\omega^2[M]\sum_{r=1}^{N}\phi_{lr}q_r + j\omega[C]\sum_{r=1}^{N}\phi_{lr}q_r + [K]\sum_{r=1}^{N}\phi_{lr}q_r = \phi_p f_p \tag{3.6}$$

If proportional damping is assumed, and considering the mode/mass and mode/stiffness orthogonality, then the decoupled modal response of acceleration at point l is

$$\ddot{x}_l = -\sum_{r=1}^{N}\frac{\phi_{lr}^T\phi_p f_p\,\omega^2}{k_r - \omega^2 m_r + j\omega c_r} \tag{3.7}$$

and, the transfer function between acceleration (output) at point l and the impact (input) at point p can be expressed as

$$H_{lp}(\omega) = -\sum_{r=1}^{N}\frac{\phi_{lr}^T\phi_p\,\omega^2}{k_r - \omega^2 m_r + j\omega c_r} \tag{3.8}$$

Usually only the first few lower modes are employed to calculate the system dynamic response. Higher modes contribute little to the structure. In order to compensate the truncated models, a residual flexibility will be introduced, and Equation 3.8 can be written as

$$H_{lp}(\omega) = \sum_{r=1}^{N_e}\frac{A_{lp}\,\omega^2}{\omega_r^2 - \omega^2 + j\,2\xi\omega_r\omega} + H_c \tag{3.9}$$

where, $A_{lp} = \phi_{lr}\phi_{pr}/m_r$; H_c is the truncated model transfer function. N_e is the number of the truncated modes. The acceleration residual of the bridge system can then be expressed as

The proceeding relationships are employed in the analysis described next.

3.3 Test Transfer Functions

An accurate estimation of a transfer function from experimental data is essential for successful modal analysis. Bridge modal frequency and mode shape are directly obtained from modal transfer functions. Figure 3.4 presents a system diagram that will help to explain the formation of the test transfer function, which is essential to the construction of mode shapes.

Noise Corruped
Command Input
Command   Plant Output
                                                                        Output
U(t)   F(t)   x(t)   y(t)

m(t)   n(t)
Noise   Output Noise
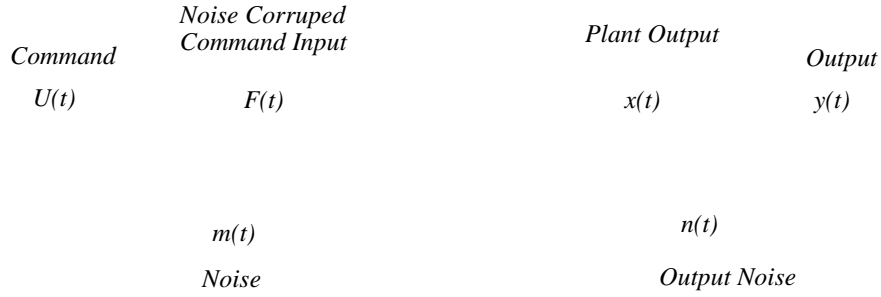
Figure 3.4 Bridge Signal Input and Output System

For the test-based modal analysis, the discrete Fourier transform is needed, in which the time-varying quantities can be described as a set of sinusoids, and transformed into a set of frequency components.

As mentioned in Chapter 2, the bridge modal test produced 36 channels of time responses and 1 channel of impact input. Using Fourier transform theory, the following equations relate the excitation and the response to these 36 channels;

$$
\begin{aligned}
S_{xx}(\omega) &= |H(\omega)|^2 S_{ff}(\omega) \\
S_{fx}(\omega) &= H(\omega) S_{ff}(\omega) \\
S_{xx}(\omega) &= H(\omega) S_{xf}(\omega)
\end{aligned}
\tag{3.11}
$$

where, $S_{xx}(\omega)$ are the auto spectrum of a channel response, $S_{ff}(\omega)$ are the auto spectrum of the impact input, and $S_{xf}(\omega)$ = $S_{xf}(\omega)$ are the cross spectrum between these two signals. $H(\omega)$ is the function estimate linking the quantities $x(t)$ (output) and $F(t)$ (input). Detailed definition can be obtained from References [15,16].

An experimental transfer function for a test can be calculated using

$$
H_1(\omega) = \frac{S_{fx}(\omega)}{S_{ff}(\omega)}
\tag{3.12}
$$

or

$$
H_2(\omega) = \frac{S_{xx}(\omega)}{S_{xf}(\omega)}
\tag{3.13}
$$

The quality of the measurement and its processing can be estimated by the coherence r^2, which is expressed by

$$r^2 = H_1(\omega) / H_2(\omega) \tag{3.14}$$

If all is well with the measurement, the coherence should be close to unity.

There are several situations in which an imperfect measurement might be made and a low coherence recorded. Noise in one or another of the inputs or outputs is an important consideration (Figure 3.4), because it can degrade the measured spectra. Considering the noise (Figure 3.4), then the transfer functions in Equations (3.12) and (3.13) will be rewritten as

$$H_1(\omega) = \frac{S_{fx}(\omega)}{S_{ff}(\omega) + S_{nn}(\omega)} = \frac{S_{fx}(\omega)}{S_{ff}(\omega)(1 + S_{nn}(\omega)/S_{ff}(\omega))} \tag{3.15}$$

$$H_2(\omega) = \frac{S_{xx}(\omega) + S_{mm}(\omega)}{S_{xf}(\omega)} = \frac{S_{xx}(\omega)(1 + S_{mm}(\omega)/S_{xx}(\omega))}{S_{xf}(\omega)} \tag{3.16}$$

Then, the $\mathbf{H_1(\omega)}$ will suffer most if there is noise included in the input signal, while the $\mathbf{H_2(\omega)}$ might be better. On the other hand, if the noise is involved with the output, $\mathbf{H_2(\omega)}$ will be worse, while $\mathbf{H_1(\omega)}$ might be better. If the nature of the noise is unknown, then the following algebraic average is recommended to minimize the errors

$$H_3 = \frac{H_1 + H_2}{2} \tag{3.17}$$

3.4   FE Simulation versus Testing

3.4.1 Impact Response. Once the bridge FEM is established, the modal solution of the bridge can be obtained via simulation. For this project, 40 fundamental modes were calculated and chosen to compute the response to the impact force. They were compared with the modal test results by using the measured impact force as the analytical input. Figures 3.5 and 3.6 indicate a very close match between the simulation and testing. The theoretical curves shown in Figures 3.7 and 3.8 are the transfer functions calculated from Equation 3.9, while the testing results are analyzed based on Equation 3.13.

20
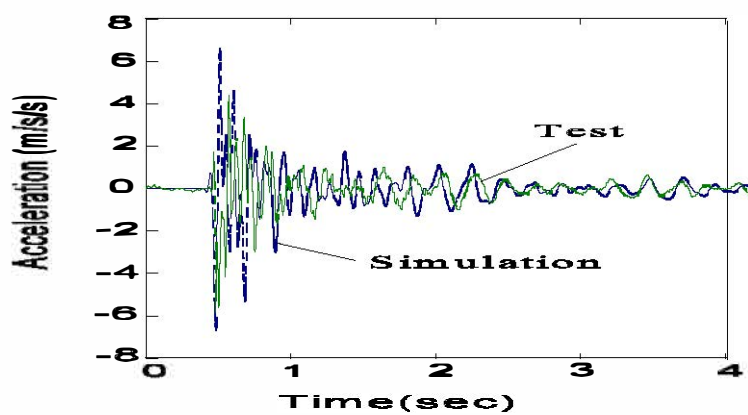
Figure 3.5 Time Response of Impact, Hammer dropped at location w250, Output from Channel 32
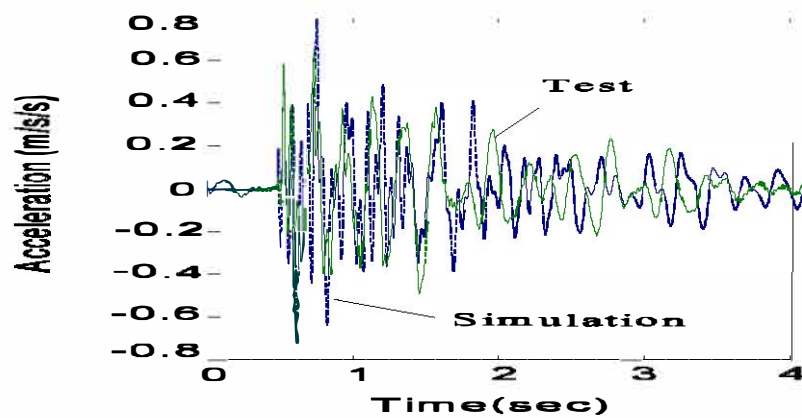
Figure 3.6 Time Response of Impact, Hammer Dropped at Location of e250, Output from Channel 29
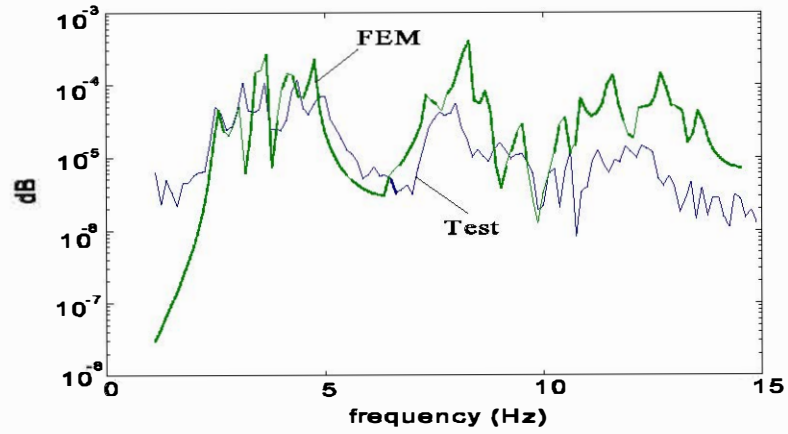
Figure 3.7 FEM Simulation vs. Test Transfer Function,

Output (Acceleration) at Channel 13 vs. Impact Input (Force) at e250
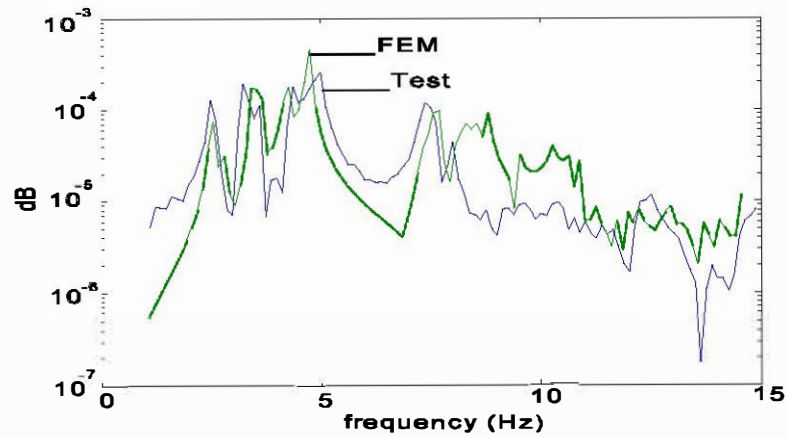
Figure 3.8 FEM Simulation and Test Transfer Function,

Output (Acceleration) at Channel 29 vs. Impact Input (Force) at e250

3.4.2 Traffic Response. The iterative correlation between the FEM and modal test data provides a reliable means of tunning the analytical model (FEM) of the bridge. Once the FEM matched the experimental data, simulations of the response of the bridge to various truck loads were made. The simulated response and the measured test response is shown in Figure (4.7).
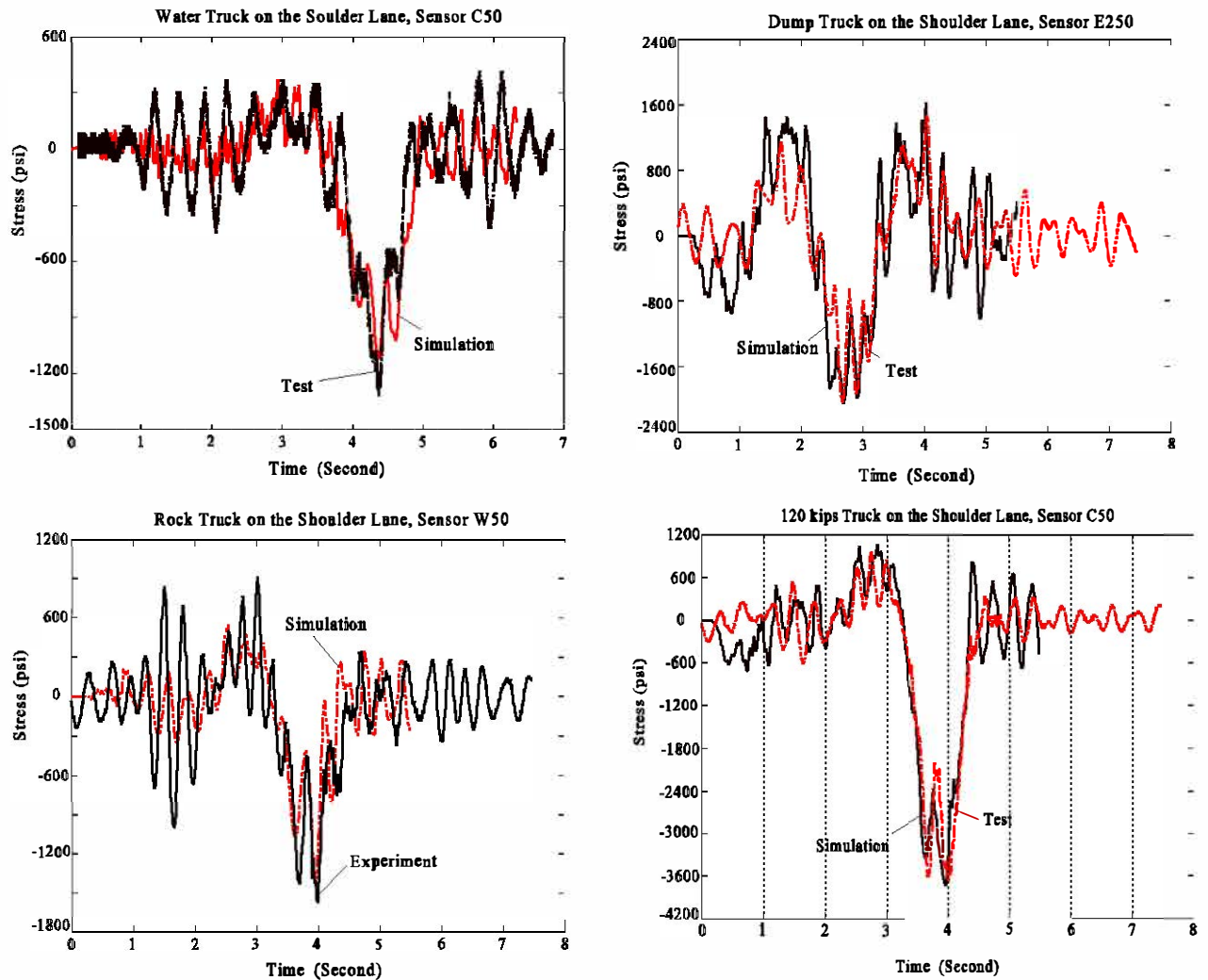
Figure 3.9 Simulations of Response to Various Truck Loading at 65 mph

The full FEM is far too large dimensionally to be of use in a design synthesis. The methods used to produce a more practical reduced order model of the bridge are reviewed next.

CHAPTER 4

MODAL ANALYSIS OF HIGHWAY BRIDGE

4.1   Introduction

Modal analysis has been used for several decades to determine the dynamics of structures [17]. Many modal analysis methods, such as SDOF (Single Degree-of-Freedom) curve fitting, circle fitting, complex exponential, direct parameter and ployreference techniques, have been developed [20, 47-49].

In this project, the direct parameter technique and multi-DOF (Degrees-of-Freedom) Real Modal Analysis Technique [50-52] were used to obtain the bridge modal parameters. The direct parameter technique relies on a frequency domain curve-fitting algorithm. This is a multi-DOF technique in which multiple output response functions, produced by a single input of the drop hammer, are post-processed to obtain a global least squares estimate of the modal properties of the bridge. Because it is a frequency domain method, it inherently accounts for the effects of residual modes during the estimation process. The algorithm is very useful for accurately defining closely spaced modes within a narrow frequency range. Since it works directly on the spectra in the frequency domain, it can account for modes outside the frequency range of interest as well. The direct parameter technique is implemented in SDRC I-DEAS™ post-processing software.

The Multi-DOF real modal analysis automatically identifies both the real and the imaginary part of test transfer functions. The method is simple and easy to use. A review of the method is described first. The test then provides a comparison of the analytical and experimental data.

4.2   Direct Parameter Modal Analysis

Recall that the equations of motion for the bridge have the following form

$$M\ddot{X} \; + \; C\dot{X} \; + \; KX \; = \; F \qquad\qquad (4.1)$$

Here **M** is the mass matrix, **C** is an equivalent damping matrix, **K** is the stiffness matrix, and **F** represents the dynamic input from the truck and gravity loads.

The impulse response **H(t)**, which occurs when the structure is excited by a direct impulse at one input point, can be expressed as [38]

$$\bar{H}(t) \; = \; \Psi \, e^{\,\Lambda t} \, L \qquad\qquad (4.2)$$

where, Ψ is the complex modal matrix; Λ is the eigenvalue matrix; and L is the modal participation factor. Modal participation factors are the weighing factors for different modes [18]. Physically, these factors indicate the extent to which a particular input excites each of the modes.

The representation of the displacement response in the Laplace domain can be derived by transforming Equation (4.2)

$$H(s) = \Psi (SI - \Lambda)^{-1} L = \Psi T(s) \tag{4.3}$$

where, $T(s) = (SI - \Lambda)^{-1} L$

The Laplace transform of the derivative of the impulse response is

$$\mathcal{L}|\dot{H}(\tau)| = SH(s) - H(\tau)|_{\tau = 0} = SH(s) - \Psi L \tag{4.4}$$

Combining Equations (4.3) and (4.4), the following matrix equation is produced

$$\begin{matrix} H(s) \\ SH(s) \end{matrix} - \begin{matrix} 0 \\ \Psi L \end{matrix} = \begin{matrix} \Psi \\ \Psi \Lambda \end{matrix} T(s) \tag{4.5}$$

For the eigenvalue matrix Λ and eigenvector matrix Ψ, a square non-trivial complex matrix A_1 exists such that

$$A_1 \Psi + \Psi \Lambda = 0 \tag{4.6}$$

The matrix A_1 is referred to system matrix (in physical coordinates) and contains information characterizing the complete set of modal parameters of the structural system. The desired modal frequency and damping ratio are determined from the eigenvalues of the system matrix A_1. The frequency is

$$\omega_r = Re(\lambda_r)^2 + Im(\lambda_r)^2 \quad (r = 1, 2, ..., n) \tag{4.7}$$

where ω_r are the eigenvalues (complex) associated with each of the r nodes.

The damping ratio is

$$\xi_r = Re(\lambda_r)/\omega_r \tag{4.8}$$

Equation (4.6) can be rewritten as

$$[A_1 \quad I] \begin{matrix} \Psi \\ \Psi \Lambda \end{matrix} = 0 \tag{4.9}$$

Multiplying Equation (4.9) by $T(s)$ then yields

$$[A_1 \quad I] \begin{matrix} \Psi \\ \Psi \Lambda \end{matrix} T(s) = 0 \tag{4.10}$$

Substitution of Equation (4.5) into Equation (4.10) yields

$$[A_1 \quad I \ ] \ \begin{matrix} H(s) \\ S\,H(s) \end{matrix} - \Psi\,L = 0 \qquad (4.11)$$

Defining $B_1 = \Psi\,L$, where B_1 is a n x 1 matrix. Then, Equation (4.11) can be rewritten as

$$A_1\,H(s) = -\,S\,H(s) + B_1 \qquad (4.12)$$

Letting $s = j\omega$, Equation (4.12) can be expressed as

$$A_1\,H(j\omega) = -j\omega\,H(j\,\omega) + B_1 \qquad (4.13)$$

Consider N modal frequencies at $\omega = \omega_1, \omega_2, ..., \omega_N$, then, Equation (4.13) can then be written as

$$\begin{aligned}
A_1\,H(j\omega_1) &= -j\omega_1\,H(j\,\omega_1) + B_1 \\
A_1\,H(j\omega_2) &= -j\omega_2\,H(j\,\omega_2) + B_1 \\
&\quad .... \\
A_1\,H(j\omega_N) &= -j\omega_N\,H(j\,\omega_N) + B_1
\end{aligned} \qquad (4.14)$$

or in vector matrix form

$$[A_1 \quad B_1] \ \begin{matrix} H(j\omega_1) & H(j\omega_2) & ... & H(j\omega_N) \\ I_1 & I_2 & ... & I_N \end{matrix} = [H(j\omega_1) \quad H(j\omega_2) \quad ... \quad H(j\omega_N)] \begin{matrix} -j\omega_1 \\ -j\omega_2 \\ ... \\ -j\omega_N \end{matrix} \qquad (4.15)$$

This expression indicates that the impulse response measurement data H and ω can be described by a model which is linear in the unknown A_1 and B_1. Equation (4.15) can be solved using a least-squares technique. After A_1 and B_1 are determined, then A_1 is substituted into Equation (4.6) and the eigenvectors are determined directly.

The dilemma with the formulation of the Direct Parameter Estimation technique is that the size of the matrix is equal to twice the number of physical DOF (or coordinates on the structure for a complex mode). However, for the bridge structure, only the first few modes are of interest. The Principal Response Analysis [19] is one of the techniques used to reduce a large number of physical coordinates to a smaller number of principal coordinates.

For N measurement points and one input point, the transfer function H is N x 1 matrix. H can be reduced into H'. That is, a transformation matrix Q exists which satisfies

$$H'(j\omega) = Q\,H(j\omega) \qquad (4.16)$$

Let R be a matrix of m response functions (in physical coordinates) defined for N frequencies. Each row of R is a frequency response function over the frequency range of $\omega_1 \le \omega \le \omega_N$. The Principal Response Analysis technique involves performing an eigen-decomposition as follows

$$R R^T = P D P^T \tag{4.17}$$

where D is a diagonal N x N matrix of real singular values or eigenvalues. Selecting the m largest singular values and corresponding singular vectors yields the rectangular m x N matrix Q in Equation (4.16). H' will be used to calculate A_1 and B_1 in Equation (4.15).

The Direct Parameter Estimation technique can be summarized as follows:

(1) Select the frequency response data points by band selection or other criteria, then construct the measured transfer function matrix;

(2) Determine the minimum realization system matrix by singular-value decomposition and Principal Response Analysis; and

(3) Solve the eigenvalue problem to obtain modal frequencies, damping ratios and modal shapes.

4.3 Multi-DOF Real Modal Analysis

For the steel bridge structure, the damping is relatively small (less than 3%), so real modal analysis theory can be directly used to analyze the bridge modal model and response. The transfer function between response point at l and input point at p can be written as

$$H_{lp}(\omega) = \sum_{r=1}^{N} \frac{1}{K_{er}[(1 - \bar{\omega}_r^2) + j2\xi_r \bar{\omega}_r]} \tag{4.18}$$

where K_{er} is the effective stiffness for the r-th mode; $\bar{\omega}_r$ is the r-th mode frequency ratio

$$\bar{\omega}_r = \frac{\omega}{\omega_r} \tag{4.19}$$

and, the damping ratio is expressed by

$$\xi_r = \frac{C_r}{2 M_r \omega_r} \tag{4.20}$$

The transfer function in Equation (4.18) can be rewritten as a composition of the real and the imaginary parts

$$H_{lp}(\omega) = \sum_{r=1}^{N} \frac{1}{K_{er}} \left[\frac{1 - \bar{\omega}_r^2}{(1 - \bar{\omega}_r^2)^2 + (2\xi_r \bar{\omega}_r)^2} + j \frac{-2\xi_r \bar{\omega}_r}{(1 - \bar{\omega}_r^2)^2 + (2\xi_r \bar{\omega}_r)^2} \right]$$

$$= H_{lp}^R(\omega) + j H_{lp}^I(\omega)$$

(4.21)

where, $H_{lp}^R(\omega)$ and $H_{lp}^I(\omega)$ are the real part and the imaginary part of the transfer function, respectively, and are written as

$$H_{lp}^R(\omega) = \sum_{r=1}^{N} \frac{1}{K_{er}} \left[\frac{1 - \bar{\omega}_r^2}{(1 - \bar{\omega}_r^2)^2 + (2\xi_r \bar{\omega}_r)^2} \right]$$

(4.22)

$$H_{lp}^I(\omega) = \sum_{r=1}^{N} \frac{1}{K_{er}} \left[\frac{-2\xi_r \bar{\omega}_r}{(1 - \bar{\omega}_r^2)^2 + (2\xi_r \bar{\omega}_r)^2} \right]$$

(4.23)

At the r-th mode, the real part of the transfer function $H_{lp}^R(\omega_r) = 0$ and the magnitude of the transfer function at ω_r is the imaginary part of the transfer function. The imaginary part of the transfer function at different points on the bridge defines the r-th mode shape.

4.4 Test Results and FE Simulation

As mentioned in Chapter 2, 36 channels of accelerometer output and one channel of load cell signal (input) were recorded during each modal test. The input and output signals were analyzed by using either PC Matlab™ or Workstation SDRC I-DEAS™. In the I-DEAS, transfer functions, mode shapes, and modal parameters were obtained using the Modal Testing-Signal Processing package. The results from the both methods are exactly the same.

The modal tests were conducted in three stages:

Stage 1: Original bridge construction without the SAVA control system attached;

Stage 2: Bridge with the SAVA control system attached with the control valves opened; and

Stage 3: Bridge with the SAVA control system attached with the control valves closed.

The data capture was started just prior to the impact of the hammer. A sample length for a single output consisted of 4,096 points. The frequency resolution was calculated by dividing the sample rate by the sample length, 512/4,096 = 0.125 Hz. This resolution is considered sufficient for the work conducted here. In fact, the differences observed in the higher modes of the modal results from Stage 1 to Stage 3 were so small (on the order of 0.1 Hz) that some steps were taken to artificially increase the resolution of the test data by padding out the time histories.

4.4.1 Time and Frequency Domain Results. All of the results (figures and tables) illustrated here include the three testing cases mentioned above. The experimental system and test environment were repeated for each of the three

modal tests. Figures 4.1 and 4.2 present some of the time domain responses of the acceleration at various points on the bridge. Figure 4.3 gives the corresponding frequency responses (transfer functions).

The time responses shown in Figures 4.1 and 4.2 indicate that the three different tests produced data that has similar frequency content but that the amplitude did change substantially from test to test. The transfer functions depicted in Figure 4.3 indicate that the addition of the control hardware does effect the amplitude of the response. It is clear that the SAVA control system produces significant reduction of certain modes. It is worth noting that the primary modal content is clearly a function of where the sensor is located.

Tables 4.1-4.3 are the mode shapes of the first eight vibrating modes post-processed from the modal test. Tables 4.4-4.6 present the same orders of mode shape obtained by finite element simulation. Although the difference on frequency from stage to stage is obvious, the mode shapes show no significant variation. Table 4.7 is a list of the modal frequencies for each of the three test stages. The longest change of frequency was less than 4%. The results suggest that it is not necessary to establish the natural properties of the bridge when doing semiactive control. Table 4.8 lists the expected variation in each mode frequency based on the analytical model. Table 4.9 lists the test modal damping of the bridge structure. It can be seen that the damping of this bridge structure is relatively small (less than 2.5%), and that the damping ratio increased with the installation of the semiactive control dampers.
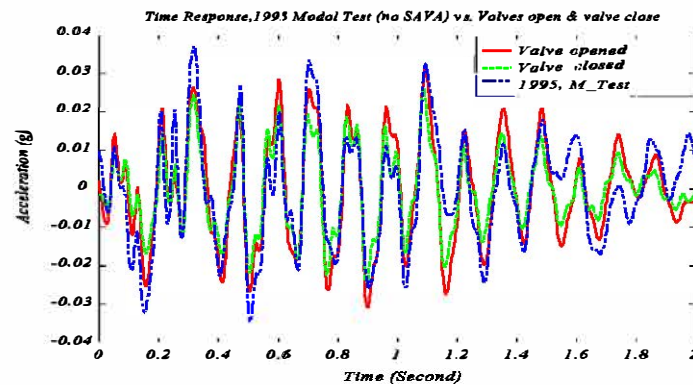
Figure 4.1 Time Domain Signals Measured in Three Modal Tests
Signal Channel 10, Input at Location e250
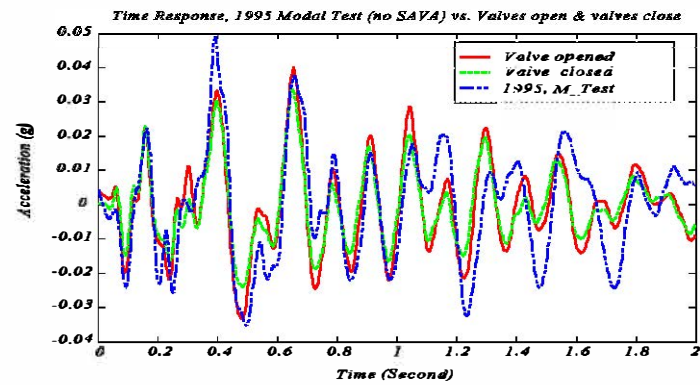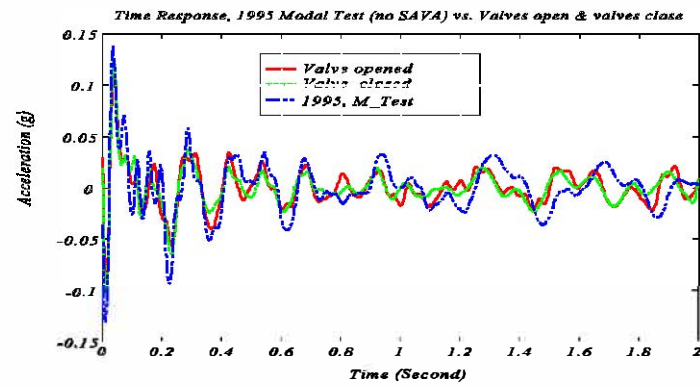
**Figure 4.2 Time Domain Signals Measured in Three Modal Tests
Signal Channels 23 (Top) and 43 (Bottom), Input at Location e250**
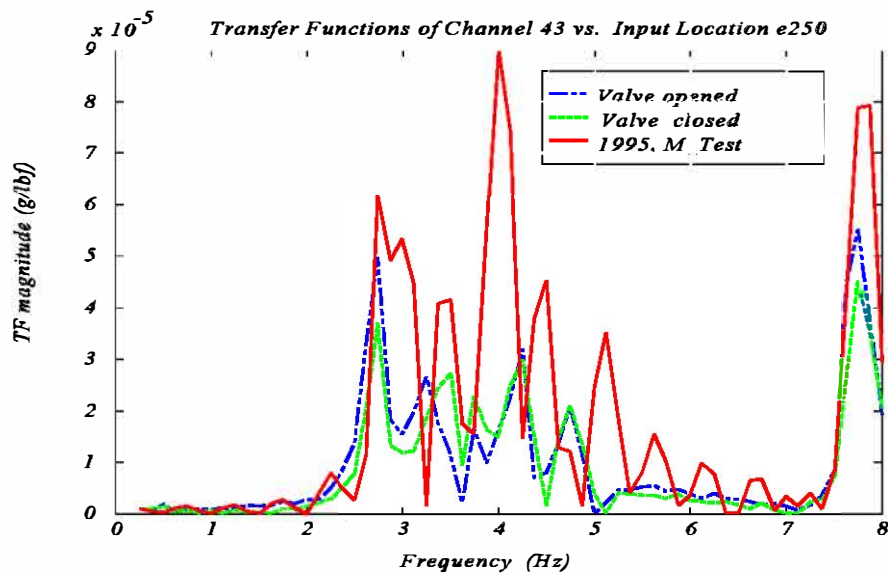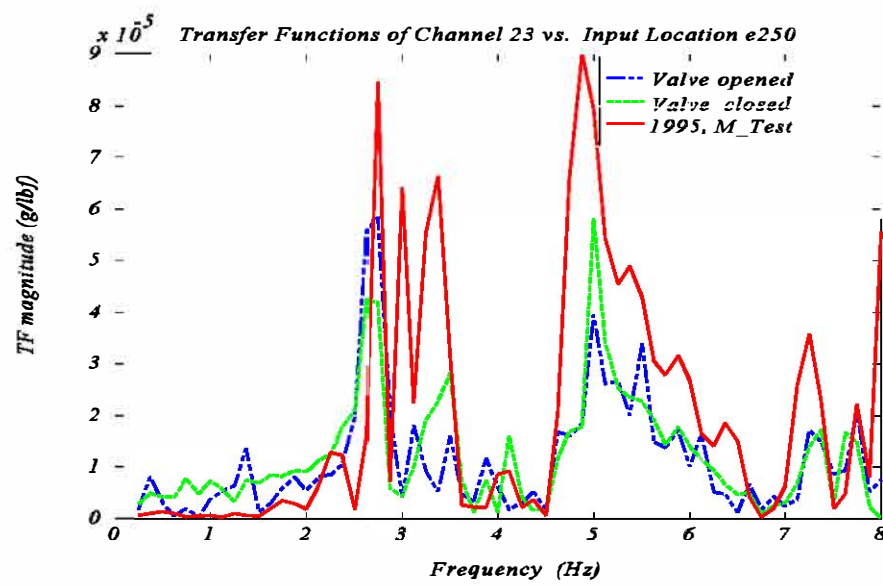
Figure 4.3 Transfer Functions of Bridge Acceleration Responses to the Hammer Impact Force

4.4.2 Test Mode Shape (Table 4.1, Table 4.2, and Table 4.3)

**Table 4.1 Test Mode Shapes of the Original Bridge Superstructure
with No Control Devices Installed (Tested in 1995)**

First Mode, Freq. = 2.502 Hz

Second Mode, Freq. = 3.021 Hz

Third Mode, Freq. = 3.204 Hz

Fourth Mode, Freq. = 3.571 Hz

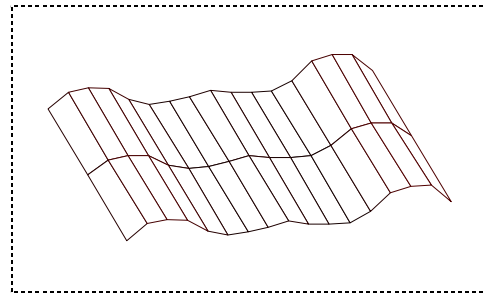Fifth Mode, Freq. = 3.845 Hz

Sixth Mode, Freq. = 4.211 Hz

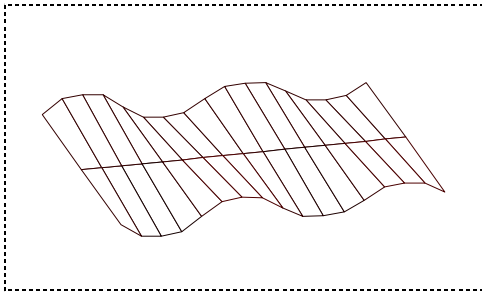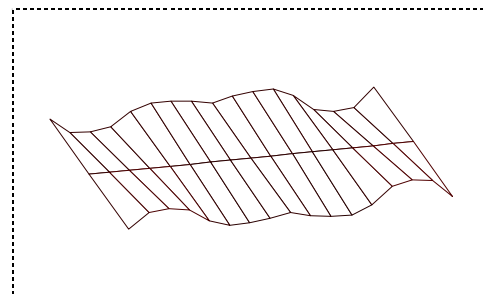Seventh Mode, Freq. = 4.517 Hz

Eighth Mode, Freq. = 4.761 Hz

Table 4.2 Test Mode Shapes of the Bridge Superstructure
with Control Devices Installed and Valves Opened
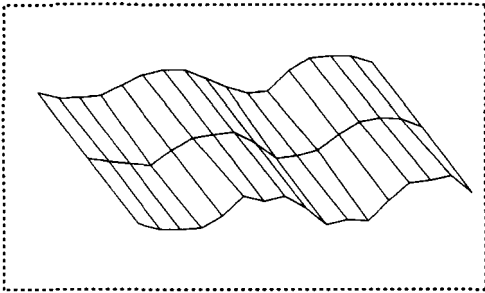
First Mode, Frequency = 2.563 Hz
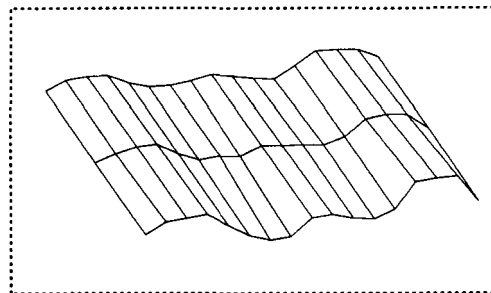
Second Mode, Freq. = 3.080 Hz
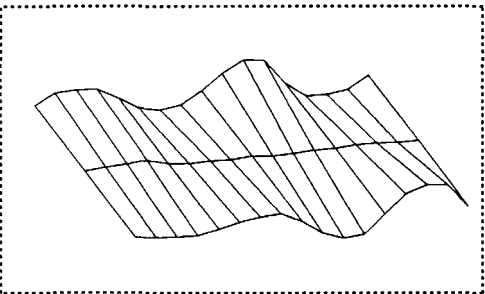
Third Mode, Freq. = 3.250 Hz
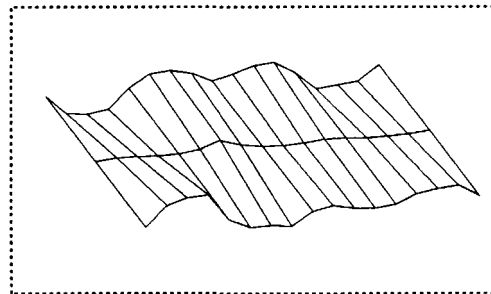
Fourth Mode, Freq. = 3.625 Hz
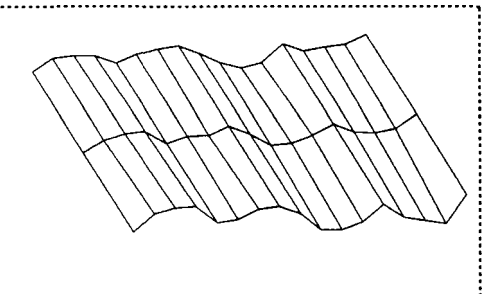
Fifth Mode, Freq. = 3.875 Hz
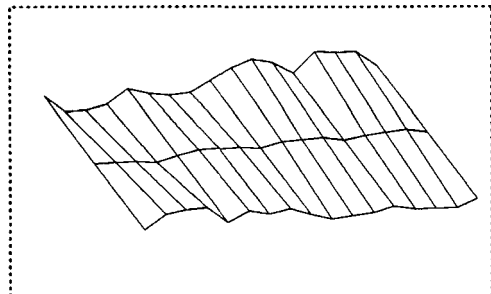
Sixth Mode, Freq. = 4.250 Hz
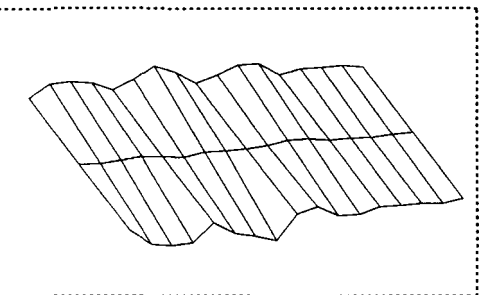
Seventh Mode, Freq. = 4.563 Hz
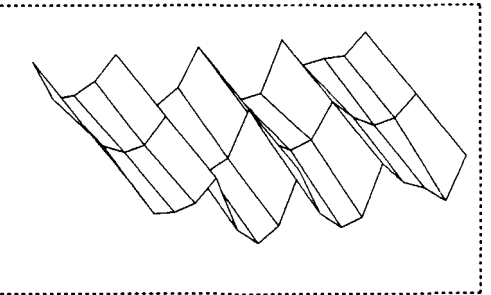
Eighth Mode, Freq. = 4.781 Hz

**Table 4.3 Test Mode Shapes of the Bridge Superstructure
with Control Devices Installed and Valves Closed**

First Mode, Frequency = 2.594 Hz

Second Mode, Frequency = 3.120 Hz

Third mode, Frequency = 3.310 Hz

Fourth Mode, Frequency = 3.660 Hz

Fifth Mode, Frequency = 3.938 Hz

Sixth Mode, Frequency = 4.281 Hz

Seventh Mode, Frequency =4.594 Hz

Eighth Mode, Frequency = 4.813 Hz

4.4.3 Simulated Mode Shapes (Table 4.4, Table 4.5, and Table 4.6).

**Table 4.4 FE Mode Shapes of the Original Bridge Superstructure
with No Control Devices Installed**

First Mode, Freq. = 2.522 Hz

Second Mode, Freq. = 2.938 Hz

Third Mode, Freq. = 3.288 Hz

Fourth Mode, Freq. = 3.626 Hz

Fifth Mode, Freq. = 3.915 Hz

Sixth Mode, Freq. = 4.346 Hz

Seventh Mode, Freq. = 4.483Hz

Eighth Mode, Freq. = 4.674 Hz

**Table 4.5 FE Mode Shapes of the Bridge Superstructure
with Control Devices Installed and Valves Opened**

First Mode, Freq. = 2.533 Hz

Second Mode, Freq. = 2.992 Hz

Third Mode, Freq. = 3.295 Hz

Fourth Mode, Freq. = 3.628 Hz

Fifth Mode, Freq. = 3.927 Hz

Sixth Mode, Freq. = 4.349 Hz

Seventh Mode, Freq. = 4.49 Hz

Eighth Mode, Freq. = 4.676 Hz

**Table 4.6 FE Mode Shapes of the Bridge Superstructure
with Control Devices Installed and Valves Closed**
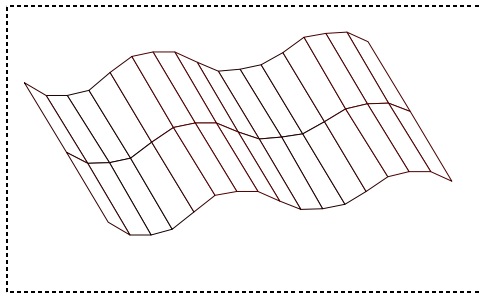
First Mode, Freq. = 2.592 Hz

Second Mode, Freq. = 3.056 Hz

Third Mode, Freq. = 3.334 Hz

Fourth Mode, Freq. = 3.645 Hz
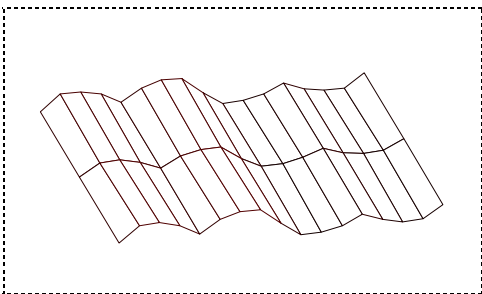
Fifth Mode, Freq. = 3.994 Hz
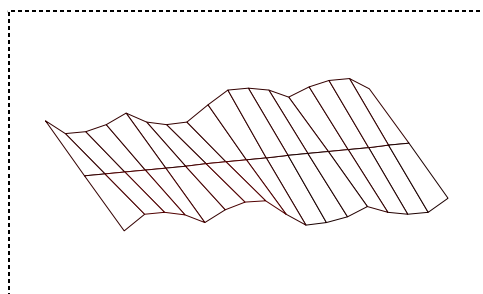
Sixth Mode, Freq. = 4.391 Hz
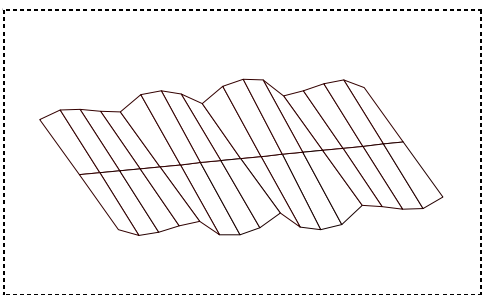
Seventh Mode, Freq. = 4.55 Hz
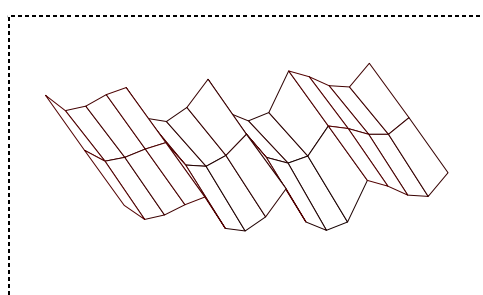
Eighth Mode, Freq. = 4.694 Hz

Table 4.7 Comparison of the Natural Frequencies from Experimental Modal Tests (Hz)

Test Cases, and No. of Frequency	Case 1, Original Bridge Structure	Case 2, Structure with SAVA, Valves Open	Case 3, Structure with SAVA Valves Closed	Case 2 vs. Case 1 (%)	Case 3 vs. Case 1 (%)	Case 3 vs. Case 2 (%)
1	2.502	2.563	2.594	2.44	3.68	1.21
2	3.021	3.080	3.120	1.95	3.28	1.30
3	3.204	3.250	3.310	1.43	3.31	1.85
4	3.571	3.625	3.660	1.51	2.49	0.96
5	3.845	3.875	3.938	0.78	2.42	1.63
6	4.211	4.250	4.281	0.93	1.66	0.73
7	4.517	4.563	4.594	1.02	1.70	0.68
8	4.761	4.781	4.813	0.42	1.09	0.67
9	5.001	5.025	5.050	0.48	0.98	0.51
10	5.525	5.625	5.660	1.81	2.44	0.62
11	7.625	7.750	7.760	1.64	1.77	0.13
12	8.101	8.150	8.200	0.60	1.22	0.61

Table 4.8 Natural Frequencies from Finite Element Simulation (Hz)

Simulation Case and No. of Mode	Case 1, Original Bridge Structure	Case 2, with SAVA, Valves Open	Case 3, with SAVA Valves Closed
1	2.522	2.535	2.592
2	2.938	2.992	3.056
3	3.288	3.295	3.334
4	3.626	3.628	3.645
5	3.915	3.927	3.994
6	4.346	4.349	4.391
7	4.483	4.490	4.550
8	4.674	4.676	4.694
9	4.934	5.012	5.120
10	5.517	5.630	5.700
11	7.548	7.625	7.760
12	8.132	8.250	8.310

Table 4.9 Modal Damping Ratios Obtained from Modal Test

No. of Modes	Original Structure (Test in 1995)	With Controller, Valves Open	With Controller, Valves Closed
1	0.024	0.026	0.030
2	0.014	0.021	0.024
3	0.016	0.035	0.035
4	0.018	0.023	0.028
5	0.014	0.017	0.019
6	0.014	0.025	0.025
7	0.022	0.025	0.027
8	0.025	0.028	0.031

The results shown above indicate that when the SAVA system is installed to the bridge, the mass and stiffness of the coupled system are increased when compared with the original system; therefore, the frequency and magnitude changed. The control system hardware, however, apparently weighs so little relative to the weight of the bridge superstructure, that it effects the signature of the bridge only minutely. The SAVA system has the potential function on mitigating the bridge vibration, but without significant variations on the bridge service behavior.

The proceeding results lead to the following conclusions:

(1)   The correspondence between the theoretical simulation and the measured mode shapes and modal frequencies indicates that the finite element modal model is an accurate representation of the bridge.

(2)   The addition of the SAVA hardware produces very little change in the modal frequencies of the base bridge. Reductions in base bridge modal amplitudes indicate that the uncontrolled (open valve) SAVA adds damping to the structure. The observation to be made here is that should the closed loop SAVA hardware cease to function, then the system can still be expected to provide some reduction of response because of the added damping.

4.5 Modal Assurance Criterion (MAC)

In engineering analysis and design, it is often desirable to compare and correlate results from a theoretical analysis with the measured data, in order to validate the theoretical model. The field of experimental and analytical modal analysis includes a number of methods that can be used for such correlation studies [20]. Most methods available for comparing theoretical and measured vibration data are applicable to any two sets of data. In addition, some of the methods are able to indicate which aspects of one model need to be modified to make it equivalent to the other (correct) model. If these methods are applied to test data for an original and modified structure, it is possible to infer which areas of the original structure were altered. The correlation of mode shapes can be achieved through the use of the modal assurance criterion (MAC). MAC is a scalar value between zero and one which represents the correspondence between two mode shapes. A MAC value near one indicates a high degree of correlation or consistency, and a value close to zero is indicative of an uncorrelated mode. The MAC therefor gives a numerical indication of the consistency of two sets of modal vectors and it can be used to indicate whether individual modes are related to each other. If an appropriate weighing matrix is available, MAC can also be used to access the orthogonality of the modal vectors.

The MAC between the q-th mode of the first data set A and r-th mode of second data set B is defined as follows

$$MAC\left(\{\phi_A\}_q, \{\phi_B\}_r\right) \ = \ \frac{\left|\{\phi_A\}_q^T \{\phi_B\}_r\right|^2}{\left(\{\phi_A\}_q^T\{\phi_A\}_q \{\phi_B\}_r^T\{\phi_B\}_r\right)} \tag{4.24}$$

where, $\{\phi_A\}_q$, $\{\phi_A\}_r$ are the mode shape vectors for q-th mode and r-th mode of data set A, respectively and $\{\phi_B\}_q$, $\{\phi_B\}_r$ are the mode shape vectors for q-th mode and r-th mode of data set B, respectively. Equation (4.24) is essentially the inner product of two vectors; if the vectors are co-linear, the value is 1 and if the vectors are orthogonal, the value is 0.

Table 4.10 presents the MAC values between the first eight FE modes, and Table 4.11 are the MAC values between the first eight test modes. They show that all the diagonal values are one, and off-diagonal values are almost zero, which mean that the modes are independent or orthogonal (as expected). Table 4.12 gives the MAC values between the test data and the FEM results. Almost all the diagonal values are close to one. In those cases, where they are not, the diagonal element is dominant relative to the off diagonal terms. This indicates that the FE modes and the test modes are closely correlated.

Table 4.10 MAC Values Between the First Eight FE Modes of the Model

1.0000	0.0000	0.0000	0.0000	0.0000	0.0680	0.0000	0.0000
0.0000	**1 0000**	0.0000	0.0000	0.0000	0.0000	0.0000	0.0689
0.0000	0.0000	**1.0000**	0.0000	0.0000	0.0000	0.0000	0.0000
0.0000	0.0000	0.0000	**1.0000**	0.0000	0.0000	0.0000	0.0000
0.0000	0.0000	0.0000	0.0000	**1.0000**	0.0000	0.0000	0.0000
0.0680	0.0000	0.0000	0.0000	0.0000	**1.0000**	0.0000	0.0000
0.0000	0.0000	0.0000	0.0000	0.0000	0.0000	**1.0000**	0.0000
0.0000	0.0689	0.0000	0.0000	0.0000	0.0000	0.0000	**1.0000**

Table 4.11 MAC Values Between the First Eight Testing Modes of the Model (With the Actuator Coupled System and Valve Open)

1.0000	0.0002	0.0003	0.0050	0.0003	0.0334	0.0054	0.2080
0.0002	**1.0000**	0.0286	0.0004	0.0069	0.0094	0.0000	0.0038
0.0003	0.0286	**1.0000**	0.1660	0.0006	0.0006	0.0017	0.0000
0.0050	0.0004	0.1660	**1.0000**	0.0009	0.0004	0.0225	0.0067
0.0003	0.0069	0.0006	0.0009	**1.0000**	0.0012	0.0085	0.0000
0.0334	0.0094	0.0006	0.0009	0.0012	**1.0000**	0.0192	0.2021
0.0054	0.0000	0.0017	0.0225	0.0085	0.0192	**1.0000**	0.0011
0.0208	0.0038	0.0000	0.0067	0.0000	0.2021	0.0011	**1.0000**

Table 4.12 MAC Values Between the First Eight FE Modes and Testing Modes

0.9211	0.0524	0.0061	0.0038	0.2147	0.0070	0.0173	0.0017
0.0356	**1.0030**	0.0074	0.0687	0.0154	0.0013	0.1264	0.0058
0.0056	0.0152	**0.8372**	0.1100	0.0138	0.0002	0.0120	0.0077
0.0479	0.0012	0.0363	**0.7016**	0.0878	0.0674	0.0001	0.0160
0.0022	0.0057	0.0100	0.0562	**0.6948**	0.0126	0.0046	0.0000
0.0415	0.0006	0.0001	0.0068	0.0372	**0.8539**	0.0372	0.0034
0.0000	0.0680	0.0007	0.0031	0.0496	0.0118	**0.8675**	0.0018
0.0000	0.0019	0.0002	0.0004	0.0013	0.0003	0.0035	**0.8952**

4.6 FE Model Correction

When the measured modal characteristics vary from those predicted by the analytical (base) FEM, then the investigator must employ one method or another to adjust or modify the base model, to obtain results (from simulation) that closely approximate the field measured response characteristics. This procedure is referred to as model modification.

The open literature includes descriptions of a wide variety of methods that have been employed to improve a FEM based on observed data. Those approaches can be classified as: (a) mass modification, (b) stiffness modification, and (c) combined mass stiffness modification techniques. Berman [38] presented a mass modification method which does not require the knowledge of the eigenvalues of the system. The method relies on the addition of a perturbation of the mass matrix to achieve orthogonality of the mode shapes (eigenvectors). Wei [39], on the other hand, provided a stiffness matrix correction method that relied on the test data. It was assumed, in his report, that the mode shapes and mass matrix are orthogonal. Baruch [40] proposed a combined mass and stiffness correction method using the measured data. The first step of that method is the selection of a matrix from the mass and stiffness matrices which was of higher confidence, and to correct that matrix in an optimal way to force the matrix to comply with the modal orthogonality conditions. The other matrix is then corrected by fulfilling the equilibrium equation of system dynamics. Luk [41] presented three different model modification methods: (1) modification in the physical coordinates, (2) modification in the modal coordinates, and (3) modification in both the physical and modal coordinate systems. Avitabile, et al., [43], used five examples to discuss the effects of model truncation on the model. Chou and Chen [44] and Zhang [45] have proposed a model modification method that uses sensitivity analysis. The sensitivity of each element is first analyzed, and the elements are then modified according to their sensitivity values. Chen [46] developed a matrix perturbation method to improve the analytical model via the testing frequencies and modal shapes. That approach was used by the CSC team to improve the FEM generated for the Walnut Creek Bridge.

We recall first that the unforced (homogeneous) model of the system can be written as

$$M_0 \ddot{X} \; + \; K_0 X_0 \; = \; 0 \tag{4.25}$$

where M_0 and K_0 are the uncorrected mass and stiffness matrices.

The solution of the FEM problem generates a system of eigenvectors, Φ_0 (the modal matrix), and a corresponding vector of eigenvalues (modes) associated one to one with each of the mode shapes.

The method begins by assuming that the corrected system characteristics can be determined by adding a small perturbation to each of the system parameter;

$$\begin{aligned} M_1 &= M_0 \; + \; \Delta M \\ K_1 &= K_0 \; + \; \Delta K \\ \Phi &= \Phi_0 \; + \; \Delta \Phi \\ \Lambda &= \Lambda_0 \; + \; \Delta \Lambda \end{aligned} \tag{4.26}$$

where M_0 and K_0 are the mass and stiffness matrices of the ROM; M_1 and K_1 are the corrected mass and stiffness (matrices) of the modified model; ϕ_0 and Λ_0 are the eigenvector and eigenvalue of the analytical model, and ϕ and Λ are the eigenvector and eigenvalue from the test data. The items prefixed with Λ are the differences between the test/modified model and the FEM, in which ΛM and ΛK are the unknown functions that will be determined by the known parameters, M_0, K_o, ϕ_0, ϕ and Λ.

A procedure is outlined here to identify the required perturbations. We first assume that the perturbation of the modal matrix is in fact a mapping of the original modal matrix

$$\Delta \phi = \phi_0 A \tag{4.27}$$

where A is a coefficient matrix with small values.

Substitution of Equation (4.26) yields

$$\phi = \phi_0 + \Delta \phi = \phi_0 (I + A) \tag{4.28}$$

The modified model is also required to satisfy the mode orthogonality [46]

$$\phi^T M_1 \phi = M^* $$
$$\phi^T K_1 \phi = K^* \tag{4.29}$$

where, M^* and K^* are the modal mass and stiffness of the modified model, and they are assumed as $M^* = M_0^*$ and $K^* = K_0^*$ at the initial iterative step. $M_0^* = \phi_0^T M_0 \phi_0$ and $K_0^* = \phi_0^T K_0 \phi_0$ are the modal parameters of the ROM.

Substitution of Equations (4.26) and (4.28) into Eq. (4.29) yields

$$(\phi_0 (I + A))^T (M_0 + \Delta M) \phi_0 (I + A) = M_0^*$$
$$(\phi_0 (I + A))^T (K_0 + \Delta K) \phi_0 (I + A) = K_0^* \tag{4.30}$$

Neglecting the higher-order terms of the expansion, then Equation (4.30) can be approximated with the following expressions

$$\phi_0^T \Delta M \phi_0 = M_0^* (-A^T - A)$$
$$\phi_0^T \Delta K \phi_0 = K_0^* (-A^T - A) = M_0^* (-\Lambda_0 A^T - \Lambda_0 A) \tag{4.31}$$

Assuming that the inverse of the modal matrix exists, then Equation (4.28) is used to determining the following forms

$$A = \varphi_0^{-1} \varphi - I$$
$$A^T = \varphi^T \varphi_0^{-T} - I \tag{4.32}$$

Pre and post multiplying Equation (4.310) by φ_0^{-T} and φ_0^{-1}, and inserting the above equations into Equation (4.31) yields

$$\Delta M = M_0 \varphi_0 (2I - \varphi_0^T M_0 \varphi - \varphi^T M_0 \varphi_0) \varphi_0^T M_0$$
$$\Delta K = M_0 \varphi_0 (2\Lambda_0 - \varphi_0^T K_0 \varphi - \varphi^T K_0 \varphi_0) \varphi_0^T M_0 \tag{4.33}$$

In Equation (4.33), M_0, K_o, φ_0 and Λ_0 are the dynamic values from the ROM; φ is obtained from the modal test or the combination of the test with the ROM. Then, ΔM and ΔK, as well as M_1 and $K_1 1$ of the first iterative step results, can be calculated. The next step is started by re-determining the modal mass and modal stiffness of the modified model from Equation (4.26), and applied to Equation (4.33) again, until a certain tolerance convergence is satisfied.

The actual correction procedure was realized by the multi-step modification using the following iterative assumptions

$$M_i = M_{i-1} + \alpha \Delta M$$
$$K_i = K_{i-1} + \beta \Delta K \tag{4.32}$$

α and β are the penalty factors, and their selection is arbitrarily. For this project, $\alpha = \beta = 1.1$ were chosen.

Figure 4.4 shows the comparison of the transfer functions between the corrected FEM and the test results without modification. The differences are obvious.

After two iterations, in which the full-scale model was taken as the reference, the system parameters realized a significant change.

Figure 4.5 indicates that the modified transfer functions match the test data closely. At this time, the modal test data was employed to form a reference system. It demonstrates that the modified model matches with the experimental results very well (Table 4.13).

45
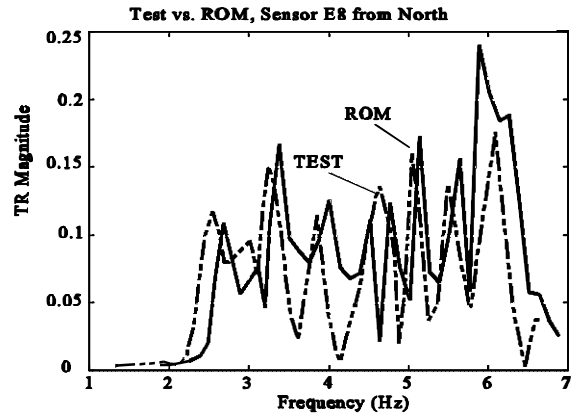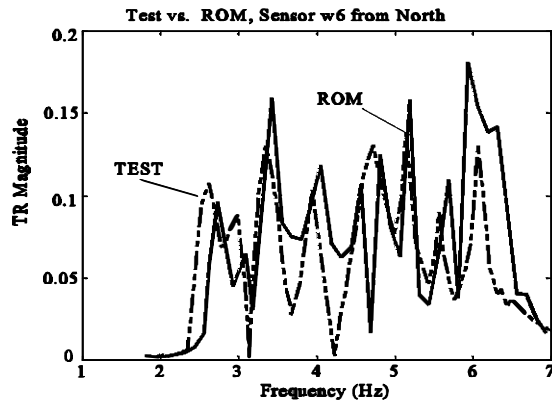
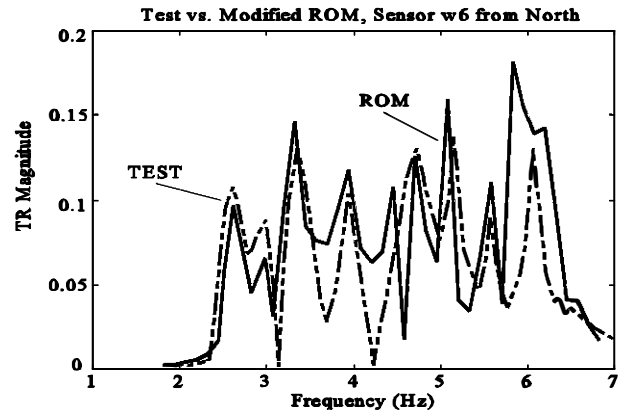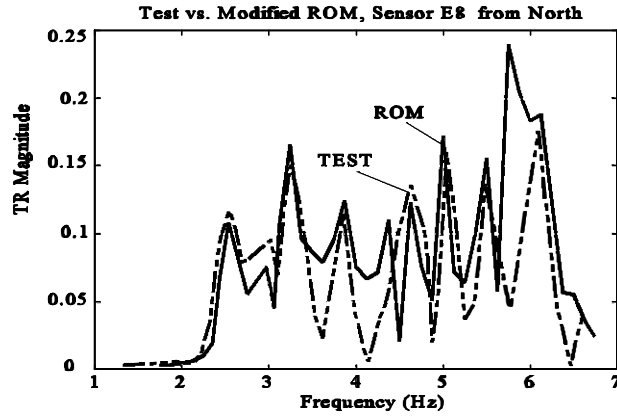**Figure 4.4 Transfer Functions of the FEM vs. Modal Test**

Figure 4.5 Transfer Functions of Modified ROM vs. Modal Test

Table 4.13 Frequency List, Modified FEM vs. Test (Hz)

Mode No.	Test	Modified FEM vs. Test	
1	2.56	2.566	0.12%
2	3.01	2.988	0.73%
3	3.25	3.217	1.02%
4	3.63	3.626	0.03%
5	3.88	3.857	0.59%
6	4.25	4.190	1.41%
7	4.56	4.506	1.25%
8	4.78	4.840	1.25%

Figure 4.6 depicts the variation of mode shape produced by the modification process. Next, the corrected modal matrix was used to compute the modal assurance values for the first eight modes. A comparison of those values before and after correction is given in Tables 4.14 and 4.15. The results indicate that the method produces major changes in those mode shapes that had the lowest MAC before correction.
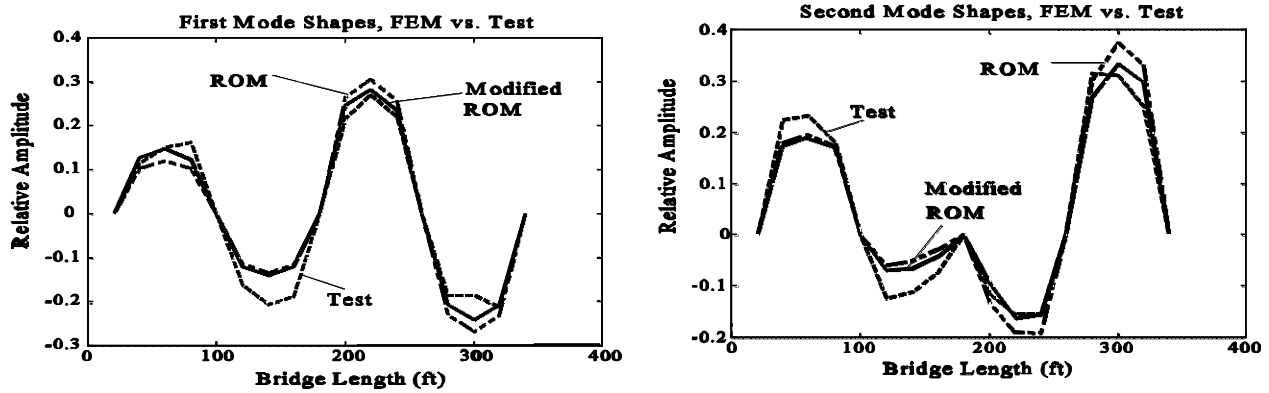
Figure 4.6 Bridge Mode Shapes Shown in One Lane

Table 4.14 MAC Values Unmodified FE Model vs. Test

0.9271	0.0524	0.0061	0.0038	0.2147	0.0070	0.0173	0.0017
0.0356	**1.0030**	0.0074	0.0687	0.0154	0.0013	0.1264	0.0058
0.0056	0.0152	**0.8372**	0.1100	0.0138878	0.0002	0.0120	0.0077
0.0479	0.0012	0.0363	**0.7016**	0.0000	0.0674	0.0001	0.0160
0.0022	0.0057	0.0100	0.0562	**0.6948**	0.0126	0.0046	0.0000
0.0415	0.0006	0.0001	0.0068	0.0372	**0.8539**	0.0372	0.0034
0.0000	0.0680	0.0007	0.0031	0.0496	0.0118	**0.8675**	0.0018
0.0000	0.0019	0.0002	0.0004	0.0013	0.0003	0.0035	**0.8952**

Table 4.15 MAC Values Modified FE Model vs. Test

0.9363	0.0046	0.0073	0.0028	0.0035	0.1311	0.0016	0.0009
0.0075	**1.0241**	0.0081	0.0772	0.0051	0.0001	0.1230	0.0001
0.0050	0.0397	**0.8602**	0.0286	0.0007	0.0011	0.0081	0.0013
0.0332	0.0009	0.0075	**0.8173**	0.0936	0.0040	0.0003	0.0000
0.0000	0.0019	0.0039	0.0821	**0.8775**	0.0066	0.0003	0.0147
0.0313	0.0000	0.0003	0.0265	0.0567	**0.9535**	0.0017	0.0002
0.0003	0.0791	0.0017	0.0005	0.0000	0.0037	**0.9287**	0.0145
0.0001	0.0031	0.0006	0.0007	0.0000	0.0005	0.0159	**0.9202**

CHAPTER 5

MODEL REDUCTION FOR DYNAMIC SIMULATION

5.1 Introduction

As shown in the previous chapters, the FEM given in Equation (4.4) (which has 4096 DOF) provides the frame work for the identification of a high fidelity modal model of the bridge. That model has intrinsic value because it can be used to determine the load carrying capacity of the structure and can serve also to gauge the expected service life of the bridge.

The focus of the ODOT project is the design and development of a structural control system that is to be affixed to the bridge. The synthesis of a control system requires a model that is able to simulate the response of the bridge to external loads. That requires the numerical integration of a system of equations. The time required to simulate the response of the bridge to truck and control inputs using a 4096 DOF model is extremely prohibitive. What is needed then is a procedure that will produce a model of the bridge that has a minimal number of generalized coordinates. The constraint is that the reduced order model must mimic the behavior that would have been predicted, had the large FEM been used. What is required then is a procedure that produces a model that has very few DOF, and which has eigenvalues and eigenvectors (modal frequencies and mode shapes), that are consistent with the lowest and dominate modes produced by the full FEM. This chapter recounts the approach used by the Center for Structural Control (CSC) to develop low order models of the bridge dynamics.

Various techniques are used routinely by practitioners in the structural control field to produce a reduced order model (ROM). Some of those techniques are reviewed below. One popular method is based on the premise that only a few of the lowest modes of a structure are needed to characterize the motion. The method assumes that external loads are band limited, and rarely excite higher modes. Researchers have developed several approaches that use this assumption. One method requires the direct truncation of the higher modal DOFs. The drawback to this approach is that the entire mass and stiffness matrices of the original model must be available. That is not possible in general.

A technique that produces a ROM using a subset of the original physical coordinates was first introduced by Guyan [21]. The crudest form of the method is called static condensation. It is accomplished by eliminating those DOFs which have no external forces applied to them. None of the structural complexity is lost since all elements of the original stiffness matrix contribute. A similar approach is used to reduce the order of dynamic model as well. Both static and dynamic Guyan reduction rely on a simple division of the coordinates into those that have mass associated with them and those that don't. The technique produces the classic master and slave node characteristics.

Kidde [22] and Miller [23] modified the static condensation procedure, in an effort to reduce the inherent error that occurred when it was applied to dynamic problems. The main advantages of using their approach is the relative efficiency and cost effectiveness, when compared with solving the same problem using the full system model. A disadvantage, however, is the approximate nature of the reduced system, which sometimes leads to serious error. A virtually complete elimination of errors can be attained by using the so-called dynamic condensation method proposed by Paz [24,25] and O'Callahan, et al., [26]. The algorithm for this method starts by assigning an approximate value

(e.g., zero) to the first eigenvalue ω_1^2, applying dynamic condensation to the dynamic matrix of the system $[D_1] = [K] - \omega_1^2[M]$, and then solving the reduced eigenproblem to determine the first and second eigenvalues ω_1^2 and ω_2^2. Next, dynamic condensation is applied to the dynamic matrix $[D_2] = [K] - \omega_2^2[M]$ to reduce the problem and calculate the second and third eigenvalues, ω_2^2 and ω_3^2. The process continues in this manner, with one virtually exact eigenvalue and an approximation of the next eigenvalue calculated at each step.

Other reduction techniques include: general dynamic reduction [27,28,29,30], extended Guyan reduction [31], improved reduced system [32], and system equivalent reduction [33]. O'Callahan [34] recently published a survey of the various reduction procedures, and gave numerical examples to illustrate the high accuracy of the more recently developed methods.

The general approach to dynamic reduction often relies on a transformation which neglects inertia effects in order to eliminate the DOFs. The transformation is then used to generate mass and stiffness matrices for the reduced system that results in the same kinetic and potential energies that are equal to the complete system.

5.2 Review of Methods

5.2.a Guyan and Iterative Improved Reduction System (IRS) Method. For the purpose of the discussion here, we assume first that the structural damping is very small. Neglecting damping, the structural model takes the form:

$$M\ddot{X} + KX = F \tag{5.1}$$

where M, K are the mass and stiffness matrices, and $M \in R^{(N,N)}$, $K \in R^{(N,N)}$. X is the physical coordinates (displacement vectors) and F is the force vector. Where, $X \in R^N$, $F \in R^N$.

M and K are first partitioned into subspace matrices related to the master DOFs, which are to be kept and the slave DOFs which are to be deleted. Then, Equation (5.2) can be rewritten as

$$\begin{bmatrix} M_{mm} & M_{ms} \\ M_{sm} & M_{ss} \end{bmatrix} \begin{Bmatrix} \ddot{X}_m \\ \ddot{X}_s \end{Bmatrix} + \begin{bmatrix} K_{mm} & K_{ms} \\ K_{sm} & K_{ss} \end{bmatrix} \begin{Bmatrix} X_m \\ X_s \end{Bmatrix} = \begin{Bmatrix} f_m \\ 0 \end{Bmatrix} \tag{5.2}$$

Here, the master coordinates are those that are subjected to external loads. The subscripts m and s relate to the master and slave coordinates, respectively.

The argument is next made that all of the structures can be lumped to the master coordinates, allowing us to eliminate the acceleration terms in the second row of Equation (5.2), which produces the following simple "static" relationship between slave and master coordinates

$$K_{sm}X_m + K_{ss}X_s = 0 \tag{5.3}$$

Solving, then

$$X_s = -K_{ss}^{-1} K_{sm} X_m \qquad (5.4)$$

This expression is used to determine the reduced coordinates

$$X = \begin{bmatrix} X_m \\ X_s \end{bmatrix} = \begin{bmatrix} X_m \\ -K_{ss}^{-1} K_{sm} X_m \end{bmatrix} = \begin{bmatrix} I \\ -K_{ss}^{-1} K_{sm} \end{bmatrix} X_m = T_s X_m \qquad (5.5)$$

where T_s denotes the static transformation between the full model and reduced model

$$T_s = \begin{bmatrix} I \\ -K_{ss}^{-1} K_{sm} \end{bmatrix} \qquad (5.6)$$

The reduced mass and stiffness are then given by

$$\begin{aligned} M_r &= T_s^T M T_s \\ K_r &= T_s^T K T_s \end{aligned} \qquad (5.7)$$

Substituting T_s and M, K in Equation (5.1) into Equation (5.7), M_r and K_r result in the Guyan static reduction.

O'Callahan improved the static reduction method by introducing the IRS method. The method perturbs the transformation from the static case by including the inertia term as pseudo-static forces. The derivation starts from the second equation of Equation (5.2) for the sinusoidal excitation with frequency Ω

$$[K_{ss} - \Omega^2 M_{ss}] X_s = -[K_{sm} - \Omega^2 M_{sm}] X_m \qquad (5.8)$$

The dynamic relationship between the master coordinates and slave coordinates is

$$X_s = -[K_{ss} - \Omega^2 M_{ss}]^{-1} [K_{sm} - \Omega^2 M_{sm}] X_m \qquad (5.9)$$

or

$$-X_s = [I - \Omega^2 K_{ss}^{-1} M_{ss}]^{-1} [K_{ss}^{-1} K_{sm} - \Omega^2 K_{ss}^{-1} M_{sm}] X_m \qquad (5.10)$$

Equation (5.10) can be expanded by using Taylor series

$$-X_s = [I + \Omega^2 K_{ss}^{-1} M_{ss} + \Omega^4 (......)] [K_{ss}^{-1} K_{sm} - \Omega^2 K_{ss}^{-1} M_{sm}] X_m \qquad (5.11)$$

Truncating this expression for orders of Ω beyond 2, then

$$X_s = [-K_{ss}^{-1} K_{sm} + \Omega^2 (K_{ss}^{-1} M_{sm} - K_{ss}^{-1} M_{ss} K_{ss}^{-1} K_{sm})] X_m \tag{5.12}$$

For the static reduction model, the lower Ω of the full model is satisfied with the reduced model, which implies that

$$\Omega^2 M_r X_m = K_r X_m \tag{5.13}$$

Substituting Equation (5.13) into Equation (5.12), then

$$X_s = [-K_{ss}^{-1} K_{sm} + K_{ss}^{-1} (M_{sm} - M_{ss} K_{ss}^{-1} K_{sm}) M_r^{-1} K_r] X_m \tag{5.14}$$

The slave coordinate can be eliminated using following expression

$$X = \begin{bmatrix} X_m \\ X_s \end{bmatrix} = \begin{bmatrix} I \\ -K_{ss}^{-1} K_{sm} + K_{ss}^{-1} (M_{sm} - M_{ss} K_{ss}^{-1} K_{sm}) M_r^{-1} K_r \end{bmatrix} X_m = T_{irs} X_m \tag{5.15}$$

where T_{irs} is referred to as the general transformation of the IRS method, expressed as follows

$$T_{irs} = \begin{bmatrix} I \\ -K_{ss}^{-1} M_{sm} \end{bmatrix} + \begin{bmatrix} 0 \\ -K_{ss}^{-1} K_{sm} + K_{ss}^{-1} (M_{sm} - M_{ss} K_{ss}^{-1} K_{sm}) M_r^{-1} K_r \end{bmatrix} \tag{5.16}$$

$$T_{irs} = T_s + S M T_s M_r^{-1} K_r \tag{5.17}$$

where

$$S = \begin{bmatrix} 0 & 0 \\ 0 & K_{ss}^{-1} \end{bmatrix} \tag{5.18}$$

The reduced mass and stiffness matrices obtained by the IRS method are then

$$\begin{aligned} M_{irs} &= T_{irs}^T M T_{irs} \\ K_{irs} &= T_{irs}^T K T_{irs} \end{aligned} \tag{5.19}$$

51

The transformation in Equation (5.17) relies on the static reduced mass and stiffness matrices. Once the transformation has been computed, an improved estimate of these reduction matrices is available using Equation (5.20), which provides the basis for an iterative improvement of the estimate [50]

$$T_{irs,i+1} = T_s + S M T_{irs,i} M_{irs,i}^{-1} K_{irs,i} \tag{5.20}$$

$$\begin{aligned} M_{irs,i+1} &= T_{irs,i+1}^{T} M_{irs,i} T_{irs,i+1} \\ K_{irs,i+1} &= T_{irs,i+1}^{T} K_{irs,i} T_{irs,i+1} \end{aligned} \tag{5.21}$$

The iterative process has excellent convergence characteristics and can be used to produce a reliable reduced order model.

5.2.b Modal Model Reduction Method (MMRM). This method begins by expressing the physical coordinate as a linear combination of modal vectors

$$X = \Phi q \tag{5.23}$$

where, Φ is the modal matrix of the structure (N x N), $\Phi \in R^{(N,N)}$; q is the modal coordinate (N x 1), $q \in R^{N}$.

The full system model is then partitioned to separate the modal coordinates that will be kept from those modal coordinates omitted in the reduced system model. Equation (5.23) is then rewritten as

$$X = \begin{bmatrix} X_m \\ X_s \end{bmatrix} = \begin{bmatrix} \Phi_{ma} & \Phi_{mo} \\ \Phi_{sa} & \Phi_{so} \end{bmatrix} \begin{bmatrix} q_a \\ q_o \end{bmatrix} \tag{5.24}$$

The subscripts a and o relate to the kept and omitted coordinates, respectively.

Expanding Equation (5.24) then gets

$$X_m = \Phi_{ma} q_a + \Phi_{mo} q_o \tag{5.25}$$

$$X_s = \Phi_{sa} q_a + \Phi_{so} q_o \tag{5.26}$$

Assuming that the omitted modes are neglectable, then

$$X_s \cong \Phi_{sa} q_a \tag{5.28}$$

52

$$X_m \cong \Phi_{ma} \, q_a \tag{5.27}$$

In order to obtain the desired relationship between X_m and X_s, Equation (5.26) must be solved for the vector q_a. The matrix Φ_{ma} will in general be rectangular and of dimension m x a. Therefore, a direct inversion of Φ_{ma} matrix cannot be used to solve q_a. Instead, Equation (5.27) is pre-multiplied by Φ_{ma}^T, resulting in the expression

$$\Phi_{ma}^T \, X_{ma} = \Phi_{ma}^T \, \Phi_{ma} \, q_a \tag{5.29}$$

If the FEM-based mode shapes can be obtained using the selected set of retained DOFs, the matrix Φ_{ma} will be of full column rank. Thus, the a-th order square matrix, $\Phi_{ma}^T \, \Phi_{ma}$, is non-singular and invertible. Equation (5.28) can be solved for q_a, yielding

$$q_a = [\Phi_{ma}^T \, \Phi_{ma}]^{-1} \, \Phi_{ma}^T \, X_m \tag{5.30}$$

where, $[\Phi_{ma}^T \, \Phi_{ma}]^{-1} \, \Phi_{ma}^T$ represents the generalized inverse of Φ_{ma}.

Equation (5.29) is substituted into Equation (5.27), resulting in an expression for the omitted partition of the physical-displacement vector X_s, in terms of the kept partition X_m. It is given by

$$X_s = \Phi_{sa} \, [\Phi_{ma}^T \, \Phi_{ma}]^{-1} \, \Phi_{ma}^T \, X_m \tag{5.31}$$

Combining X_m and X_s, the relationship between the master coordinates and slave coordinates is then given as follows

$$X = \begin{bmatrix} I \\ \Phi_{sa} \, [\Phi_{ma}^T \Phi_{ma}]^{-1} \, \Phi_{ma}^T \end{bmatrix} X_m = T \, X_m \tag{5.32}$$

where

$$T = \begin{bmatrix} I \\ \Phi_{sa} \, [\Phi_{ma}^T \Phi_{ma}]^{-1} \, \Phi_{ma}^T \end{bmatrix} \tag{5.33}$$

The transfer matrix T can be used to reduce the original FEM, and the reduced mass and stiffness matrix can be written as

$$M_r = T^T M T$$
$$K_r = T^T K T$$
(5.34)

5.3 Accuracy Checking of ROM.

In order to evaluate the fidelity of the reduced order model (ROM), the actual frequency, mode shapes and dynamic responses must be compared to the predicted values given by the full order model. The dynamic responses analysis of the ROM is described here.

The reduced model can be written as

$$M_r \ddot{X}_m + K_r X_m = F_r$$
(5.35)

where, M_r, K_r are the reduced mass and stiffness matrices, respectively, $M_r \in R^{(m,m)}$, $K_r \in R^{(m,m)}$. X_m, F_r are the physical coordinates (displacement vectors) and force vector, respectively, $X_r \in R^m$, $F_r \in R^m$.

As a typical case, a one point impact input is considered here, which is the modal testing. F_r can be written as

$$F_r = [0, 0, ,......, f_i, 0, 0]$$
(5.36)

where f_i is the impact force at i point.

In order to compare the dynamic response of a reduced model and that of its full model, the impact force F_r and F should be the same

$$F = [F_r, 0, ..., 0, 0] = [0, 0, ,......, f_i, 0, ... 0]$$
(5.37)

Introducing the state space vector

$$X_1 = X_r$$
$$X_2 = \dot{X}_r$$
(5.38)

Equation (5.35) can be written as

$$\begin{bmatrix} \dot{X}_1 \\ \dot{X}_2 \end{bmatrix} = \begin{bmatrix} 0 & I \\ M_r^{-1} K_r & 0 \end{bmatrix} \begin{bmatrix} X_1 \\ X_2 \end{bmatrix} + \begin{bmatrix} 0 \\ F_r \end{bmatrix}$$
(5.39)

The transfer function provides the basis for a comparison of different models. The transfer function of Equation (5.35) can be written as

$$H(\omega) = \frac{X_r(\omega)}{F_r(\omega)} = \frac{1}{K_r - M_r \omega^2} \tag{5.40}$$

5.4 Application of ROM at Walnut Creek Bridge

The simulation of the dynamics of the bridge using the large FEM developed in SDRC I-DEAS™ was far too time consuming. To make matters worse, the I-DEAS™ software has no provision for the generation of reduced order models. The CSC had planned to use the modal truncation method and apply it directly to the I-DEAS model (4096 DOFs). That proved to be impossible, because there is no means provided to extract the mass and stiffness matrices (4096 x 4096) that were automatically generated in I-DEAS™ for the large FEM bridge mode.

We chose instead to produce a reasonably exact model of the bridge structure that utilized a much coarser mesh of the elements. A stick diagram of the mesh is shown in Figure 5.1. The bearing points (0) are restrained to rotation in about the X direction (perpendicular to centerline of bridge) only. Intermediate nodes between bearings are allowed to rotate in the X direction and translate in the Z direction. The model consists of 145 DOFs. Masses were lumped at nodes. The modal frequencies and mode shapes of this base (simple) model and the I-DEAS™ model are listed in Tables 5.1 and 5.2. For the lowest eight eigenmodes, the base model and the IDEAS™ model provide a nearly exact match of characteristics. The base model, while considerably simpler than the full I-DEAS™ model, was still far too cumbersome to conduct the design and simulation studies needed. We next applied different methods to construct reduced order models that were extracted not from the I-DEAS™ full model but from the base model (written in "C" language).
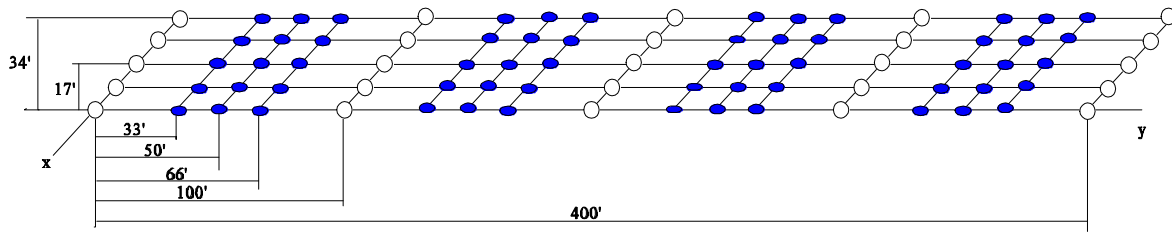
Figure 5.1 Simple FE Model of the Walnut Creek Bridge
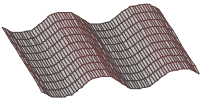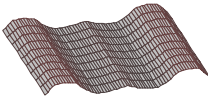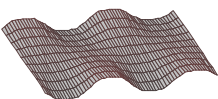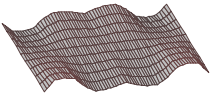
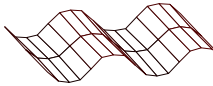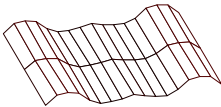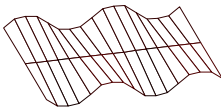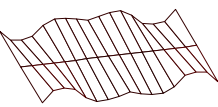In order to demonstrate the technique, we constructed a local FEM to establish a low order system that could be used to quickly establish the deflections of a span subjected to a moving vehicle load. The wire diagram of the system is shown in Figure 5.2. The nine interior nodes shown there are restrained to vertical translation. A first impression is that the model is at best a very poor representation of the motion of the bridge. We then applied the Guyan method, the standard IRS and the iterative IRS methods to compare the effectiveness of each approach. Table 5.3 contrasts the modal frequencies obtained using each method versus the frequencies of the full FEM mode. The first two methods fail miserably. The iterative IRS method, on the other hand, provides an excellent reconstruction of the mode

frequencies. A comparison of the transfer functions obtained at one point (Figure 5.3) for the large model and the ROM is also an indication of the accuracy that can be obtained using the iterative IRS method. While not presented here, it is also helpful to compare the degree of eigenvector orthogonality (the MAC) between the full model and ROM. The results of that test were acceptable.

Table 5.1 Comparison of Frequencies of the Simple (145 DOFs) Model
vs. Full (4098 DOFs) Model

Mode Number	Frequencies & Mode Shapes of Full Finite Element Model		Frequencies & Mode Shapes of Reduced Order Model		
1	2.522,	Bending	2.549,	Bending,	1.1%
2	2.938,	Bending	2.970,	Bending,	1.1%
3	3.288,	Torsion	3.317,	Torsion,	0.8%
4	3.626,	Torsion	3.658,	Torsion,	0.9%
5	3.915,	Bending	3.958,	Bending,	1.1%
6	4.346,	Torsion	4.377,	Bending,	0.7%
7	4.483,	Torsion	4.523,	Bending,	0.9%
8	4.674,	Bending	4.709,	Bending,	0.8%

Table 5.2 Comparison of the Lowest Mode Shapes of the Simple (145 DOFs) Model
vs. Full (4098 DOFs) Model

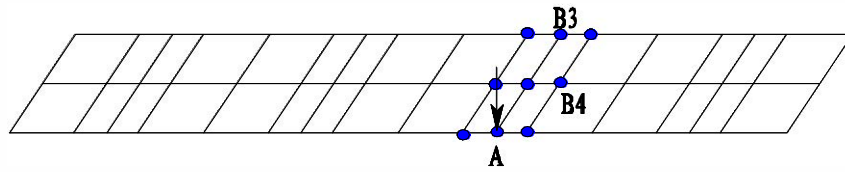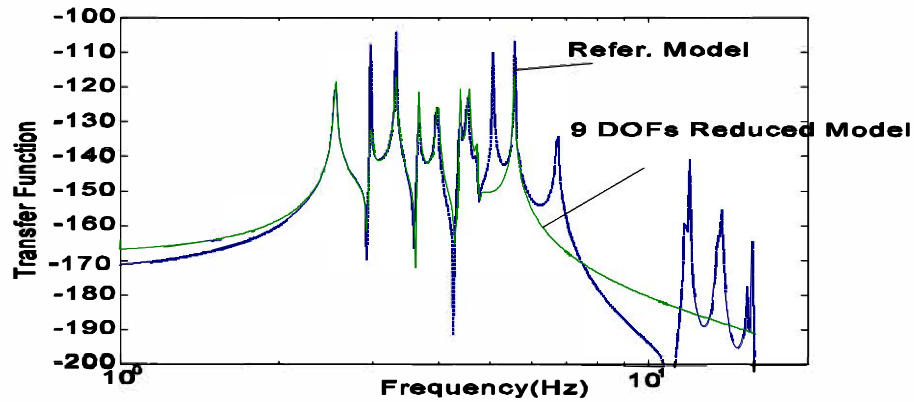|	1st Mode	2nd Mode	3rd Mode	4th Mode
Full FEM				
Simple FEM				

Figure 5.2   9 DOFs Pattern of Model Reduction

Figure 5.3 Transfer Functions Between Response at B3 and Input at A for 9 DOFs Reduced Model By Iterative IRS and Reference Model

Table 5.3 Natural Frequencies of three 9 DOFs Reduced Models

Mode Number	Mode Frequency and Errors (%)			
	Reference Model	Guyan (%)	Standard IRS (%)	Iterative. IRS (%)
1	2.5490	3.5815(40.51)	3.0425(19.36)	2.5512(0.086)
2	2.9695	4.3414(46.20)	3.9257(32.20)	2.9780(0.286)
3	3.3168	5.4931(65.61)	5.1107(54.08)	3.3236(0.205)
4	3.6579	12.560(243.38)	7.850(114.60)	3.6743(0.448)
5	3.9580	14.975(278.35)	9.372(136.77)	3.9863(0.715)
6	4.3773	35.097(700.18)	11.53(163.43)	4.3915(0.324)
7	4.5233	35.119(676.41)	19.39(328.18)	4.5591(0.791)
8	4.7091	36.097(666.54)	22.22(371.77)	4.7383(0.620)
9	5.0664	41.051(710.26)	26.91(431.17)	5.5563(9.660)

Example utilization of ROM

In order to demonstrate the utility of the method, the ROM was employed to predict the motion of the center of the east most girder in the third span of the bridge when a truck with known chassis characteristics passed over the bridge in the right lane. The truck was a "Low Boy" tractor trailer combination. The tractor was equipped with a steering axle, a tandem rear axle, and the trailer was outfitted with three solid axles. The truck weighed 120,000 lb. A comparison of the response predicted using the full model and the reduced order model is shown in Fig. 5.4.

Figure 5.4 Comparison of Dynamic Response, 12 DOFs ROM vs. Full FEM

5.5 Conclusion

Techniques were presented that can produce extremely accurate reduced order models of the bridge that provide an excellent basis for the study of the dynamic (motion) response of the structure. The ROM also provided a working format for the design of a suitable control.

The user is cautioned on one point; while the ROM produced here is an acceptable method for motion simulation, it provides a very poor estimate of the stresses that result from the motion. Stress studies are best accomplished with higher order models

CHAPTER 6

CONCLUSION

This report describes the results of an effort to develop an accurate mathematical model of the two lane, Walnut Creek Bridge (north bound) on I-35. The procedures used to conduct modal tests at the site were reviewed in detail. The post processing of that modal test data defined the modal frequencies, modal damping and mode shapes of the actual structure. Next, the construction of a FEM of the bridge was described. There followed a discussion of the model modification methods that were invoked to resolve the differences between the predicted modal characteristics and those measured in the field. The text also described the methods that were employed to generate reduced order model that was more amendable to dynamic simulation and control analysis than was the very large dimension FEM.

The work presented in this report provides the basis for the design of a vibration suppression system for the bridge. The work also provides a blue print of the process that can be relied on to study any other bridge. The procedures are all implemented in software, and are essentially independent of the type or description of the bridge. Modal modeling and modal testing can provide the bridge engineers with a crisp, and precise measure of a bridge's behavior and response characteristics. It also provides the engineer with a means of ascertaining highly accurate estimates of stress, load distribution and the general health of the structure. The existence of an accurate modal also makes it possible to examine other questions including, for example, what effect the diaphragms have on the characteristics of the bridge?

REFERENCE

[1] O.S. Salawu, C. William, 1995, *Review of Full-scale Dynamic Testing of Bridge Structure*, Journal of Engineering Structure, Vol.17, No.2, pp. 113-121.

[2] C.E. Ventura, et al, 1995, *Experimental Investigation of Dynamics of Queensborough Bridge*, Journal of Performance of Constructed Facilities, Bathel, Connecticut, pp. 146-155.

[3] M.F. Green, 1995, *Modal Test Methods for Bridges: A Review*, 13th International Modal Analysis Conference, Nashville, Tennessee.

[4] A. Ghaffan, et al, 1985, *Ambient Vibration Studies of the Golden Gate Bridge: 1. Suspended Structure*, ASCE, EMD, Vol.III, No.4 April 1985, pp. 463.

[5] G.S. Vincent, 1985, *Golden Gate Bridge Vibration Studies*, Journal of Structure Division, ASCE, 84(ST6).

[6] P. Paultre, J. Proulx, M. Tabot, 1995, *Dynamic Testing Procedures For Highway Bridge Using Traffic Loads*, ASCE, Journal of Structural Engineering, Vol.121, No.2, Feb. 1995.

[7] Y. Deger, et al, 1995, *Modal Analysis of a Highway Bridge: Experiment, Finite Element Analysis and Link*, 13th International Modal Analysis Conference, Nashville, Tennessee, pp. 1141-1149.

[8] N. Haritos, 1995, *Modal Testing of A Skew Reinforced Concrete Bridge*, 13th International Modal Analysis Conference, Nashville, Tennessee.

[9] O.S. Salawu, C.William, 1995, *Bridge Assessment Using Forced-Vibration Testing*, ASCE Journal of Structural Engineering, Feb. 1995, Vol.121, No.2, pp. 161-173.

[10] P.J. Yantha, et al, 1995, *Dynamic Testing of an FRP Vehicle Bridge*, 13th International Modal Analysis Conference, Nashville, Tennessee.

[11] R.T. Kohoutek, G. Marusiak, 1994, *Modal Analysis of Railway Bridge in Mlada Boleslav*, 12th International Modal Analysis Conference, Honolulu, Hawaii, pp. 1316-1320.

[12] R. Kohoutek, P. Marshall, 1994, *Use of Modal Analysis of Nattai Bridge Mittagong Bypass*, 12th International Modal Analysis Conference, Honolulu, Hawaii, pp. 706-712.

[13] R. Kohoutek, 1993, *Tests on Bridge Over Talbrager River at Dubbo*, 11th International Modal Analysis Conference, Bathel, Connecticut, pp. 1168-1174.

[14] W. N. Patten, R.L Sack, Q. He, 1996, *Controlled Semiactive Hydraulic Vibration Absorber for Bridges*, ASCE, J. of Struct. Engng., Vol. 122, No. 2, Feb. 1996, pp. 179-192.

[15] Y.F. Chou, J.S. Chen, 1985, *Structural Dynamic Modification Via Sensitivity Analysis,* 3rd International Modal Analysis Conference, pp. 483-489.

[16] L. Zhang, B. He, M. Yau, 1993, *Sensitivity Analysis Based on Lanczos Approach In Structural Dynamic Math Model Updating*, 11th International Modal Analysis Conference, Bathel, Connecticut.

[17] O. Dossing, 1995, *Going Beyond Modal Analysis on IMAC in A New Way*, 13th International Modal Analysis Conference, Nashville, Tennessee.

[18] F. Lembregts, J. Leuridan, 1987, *Multiple Input Modal Analysis of Frequency Response Functions Based on Direct Parameter Identification*, 5th International Modal Analysis Conference, London, England, pp. 589-598.

[19] SDRC, 1994, I-DEAS System Dynamic Analysis User's Guide Book, Structural Dynamic Research Corporation.

[20] D.J. Ewins, 1984, Modal Testing: Theory and Practice, Research Studies Press Ltd., Letchworth, Hertfordshire, England.

[21] Guyan, R. J., 1965, *Reduction of Stiffness and Mass Matrices*, AIAA Journal, Vol.3, (2).

[22] Kidder, R. L., 1975, *Reduction of Structural Frequency Equations*, AIAA Journal, Vol.13, (5), pp. 892-895.

[23] Miller, C. A., 1980, *Dynamic Reduction of Structural Models*, Journal of Structural Division, ASCE, pp. 2097-2108.

[24] Paz, Mario, 1984, *Dynamic Reduction Method*, contributed chapter for Structural Mechanics Software Series, Vol. V, The University Press of Virginia.

[25] Paz, Mario, 1985, *Dynamic Condensation*, AIAA Journal, Vol.22, (5), pp. 724-727.

[26] O'Callahan, J. C., Chou, C. M. and Koung R. T. F., 1986, *Improved Starting Vectors for Subspace Iteration Eigensolution Using Dynamic Condensation*, 4th Intel. Modal Analysis Conf., Los Angeles, CA, Feb. 1986.

[27] Kaufman, S., and Hall, D. B., 1968, *Reduction of Mass and Loading Matrices*, AIAA Journal, Vol.6, (3).

[28] Irons, B. M., 1965, *Structural Eigenvalue Problems: Elimination of Unwanted Variables*, AIAA Journal, Vol.3, (5).

[29] Fuh, J. S, Gustavson, B. and Berman, A., 1986, *Error Estimation and Compensation in Reduced Dynamic Models of Large Space Structures*, AIAA-Structural Dynamics and Material Conference, May 1986.

[30] Craig, R. R., Jr., and Bampton, M. C. C., 1968, *Coupling of Substructures for Dynamic Analysis*, AIAA Journal, Vol.6, July, 1968.

[31] Conti, P., 1989, *A Higher Order Generalization of the Guyan Reduction Method*, 7th Intel. Modal Analysis Conf., Las Vegas, Nevada, Feb., 1989.

[32] Avitabile, P., O'Callahan, J. and Pechinsky, F., 1990, *Understanding Structural Dynamic Modification Truncation*, 8th Intel. Modal Analysis Conf., Kissimmee, Florida.

[33] O'Callahan, J., 1989, *A Procedure for an Improved REDUCED System (IRS) Model*, 7th Intel. Modal Analysis Conf., Las Vegas, Nevada, Feb., 1989.

[34] O'Callahan, J., 1990, *Comparison of Reduced Model Concepts*, 8th Intel. Modal Analysis Conf., Kissimmee, Florida.

[35] K.P. Chiao, M.K. Abdelhamid, 1990, *Application of Least Squares Model Reduction to Optimal Active Vibration Control Problem*, 8th Intel. Modal Analysis Conf., Kissimmee, Florida, pp. 759-767.

[36] T.Chalko, V. Gershkovich, and N. Haritos, 1995, *Optimal Design of Modal Experimental For Bridge Structure*, 13th International Modal Analysis Conference, Nashville, Tennessee, pp. 571-577.

[37] J. Ocallahan, P. Avitabile, R. Piemer, 1989, *System Equivalent Reduction Expansion Process (SERED)*, 7th International Modal Analysis Conference, Las Vegas, Nevada, pp. 29-36.

[38] Berman, A., 1979, *Mass Matrix Correction Using an Incomplete Set of Measured Modes*, AIAA Journal, Vol.17, No.10, pp.1147-1148.

[39] Wei, F., 1980, *Stiffness Matrix Correction From Incomplete Test Data*, AIAA Journal, Vol.18, No.10, pp. 1274-1275.

[40] Baruch, M., 1982, *Optimal Correction of Mass and Stiffness Matrices Using Measured Modes*, AIAA Journal, Vol. 20, No.11, pp.1623-1626.

[41] Luk, Y. W., 1982, *System Modeling and Modification via Modal Analysis*, First International Modal Analysis Conference, Kissimmee, Florida, pp.423-429.

[42] Avitable, P., Ocallahan, J., and Pechinsky, F., 1990, *Understanding Structural Dynamic Modification Truncation*, Eighth International Modal Analysis Conference, Kissimmee, Florida, pp.43-53.

[43] Chou, Y. F., and Chen, J. S., 1985, *Structural Dynamic Modification Via Sensitivity Analysis*, Third International Modal Analysis Conference, pp.483-489.

[44] Zhang, L., He, B., and Yau, M., 1993, *Sensitivity Analysis Based on Lanczos Approach In Structural Dynamic Math Model Updating*, Eleventh International Modal Analysis Conference, Bathel, Connecticut, pp.350-355 .

[45] Chen, J. C., 1983, *Direct Structural Parameter Identification by Modal Test Results*, AIAA Paper 83-0812.

[46] Clough, R. W., and Pehzien, J. (1975). "Dynamics of structures." *McGraw-Hill Inc.*

[47] DeSilva, C. W. (1983), "Dynamic testing & seismic qualification practice", LexingtonBooks, D. C. Health and Company.

[48] Smith, J. D. (1989), "Vibration measurement & analysis", Butterworths & Co. (Publisher) Ltd.

[49] Liu, G. L. and Garibald, L. (1991), "Global MOF curve fitting with separated global parameter using frequency response function", Proc. Of 9th Intel. Modal Analysis Conf.,Firenze, Italy, pp. 254-260.

[50] Vold, H., and Leuridan, J. (1982), "A generalized frequency domain matrix estimation method for structural parameter identification", 7th Seminar on Modal Analysis Journal of AIAA.

[51] Leuridan, J., Brown, D., Alemang, R., "Direct system parameter identification of mechanical structures with application to modal analysis", 23rd Structural Dynamics and Materials Conference.

[52] Leuridan, J. and Brown, D. (1983), "Advanced matrix methods for experimental modal analysis --- a multi-matrix method for direct parameter extraction", 1st Intel. Modal Analysis Conf..

SEMIACTIVE VIBRATION ABSORBERS (SAVA) AT THE I-35 WALNUT CREEK BRIDGE

A PROJECT FUNDED BY OKLAHOMA DEPARTMENT OF TRANSPORTATION

ODOT PROJECT ENGINEER: DAVID OOTEN, PE

SUB-REPORT # 2:

FATIGUE ANALYSIS WITH THE DEVELOPMENT OF SEMIACTIVE STRUCTURAL CONTROL

CENTER FOR STRUCTURAL CONTROL
UNIVERSITY OF OKLAHOMA
http://www.coe.ou.edu/research/cstructc/

PROJECT MANAGER:

WILLIAM N. PATTEN, Ph. D, P.E., (PI)

RESEARCH ENGINEERS:

JINGHUI SUN, Ph. D.
GANG SONG, Ph. D.
XITIAN FANG
JEFFERY L. KUEHN
GUANGJUN LI

AUGUST, 1997

TABLE OF CONTENTS

NOMENCLATURE

AASHTO	American Association of State Highway and Transportation Officials
ADT	Average Daily Traffic
ADTT	Average Daily Truck Traffic
DLA	Dynamic Load Allowance
ECCS	European Convention for Constructional Steelwork
NCHRP	National Cooperative Highway Research Program
NSF	National Science Foundation
ODOT	Oklahoma Department of Transportation
a	age of bridge (years)
C	stress cycles per truck passage of bridge (cycles)
C_s	suspension damping coefficient (kips.sec/in)
D	fraction of life used up by an event or a series of events
f	factor to account for the difference between mean and allowable SN curve
f_d	damping natural frequency (Hz)
f_n	natural frequency (Hz)
K	detail constant
k_{rr}	ride rate
k_s	suspension stiffness (kips/in)
k_t	tire stiffness (kips/in)
k_m	lane moment ratio
k_r	effective relationship factor accounting for different lane truck loading
k_v	lane truck volume ratio
m	unsprung mass (kips)
M	sprung mass (kips)
N_e	equivalent number of cycles for a complex cycle (cycles)
R_s	reliability factor
R_p	peak ratio ($= S_{rp} / S_{re}$)
S_c	compressive dead load stress (ksi)
S_r	nominal stress range (ksi)
S_{re}	effective stress range (ksi)
S_{rlc}	constant-amplitude fatigue limit (ksi)
S_{rlv}	variable-amplitude fatigue limit (ksi)
S_{FL}	fatigue limit (ksi)
S_{rp}	peak stress range (ksi)

S_t	tension portion of the stress cycle
T_a	lifetime average daily truck volume
W_{er}	effective section modules (in^3)
W_r	section modules (in^3)
ζ_s	damping ratio

ABSTRACT

A recent report on the health of the bridges in the U.S. indicates that almost 28% of all U.S. bridges are considered deficient, and 10% of all bridges are in the structurally deficient category. Estimates to repair/replace and upgrade deficient bridges exceed 6 billion dollars per year for the next two decades. Almost as formidable is the pressure from the transportation industry to increase the non-permit weight limit on highways in order to satisfy an ever increasing pressure to make truck traffic more economic. That pressure is exacerbated by the recent call for more international truck traffic via recent international trade agreements. Our neighbors in Mexico and Canada allow non-permitted truck weight in excess of 110,000 lb, while the U.S. has an 80,000 lb limit.

The research project reported on here demonstrates a new technology that can on the one hand increase the useful service life of a highway bridge by several decades, while making it possible to increase the non-permit load limit without compromising remaining service life. The report utilizes the result of field tests of the new technology to compute the remaining safe and mean life of a test bridge on I-35 in Oklahoma using the NCHRP Report 299 (1989) as a guideline. Several calibrated trucks were used in the study to develop a spectrum of results. The study supports the contention that a bridge, outfitted with a load/vibration control system, is likely to last many more decades then originally designed for.

CHAPTER 1

IMPORTANCE OF THIS RESEARCH

There is no "best" approach to the fatigue analysis of bridges. At least three methods of fatigue analysis (the Stress Life method, the Strain Life method and the Fracture Mechanics method) are routinely used. Each method has unique advantages and limitations. Depending on the predictive capability and accuracy required in the fatigue analysis, any of these fatigue life estimation techniques can be used to determine the expected fatigue lives of new or existing bridges.

The Stress Life method is the easiest-to-apply method of fatigue analysis. It can be used in almost any situation to obtain an accurate estimate of fatigue life, and the method works very well in situations involving constant (or nearly constant) amplitude loading and long fatigue life. This method is routinely used during the design of new bridges and for the evaluations of remaining fatigue lives of existing bridges.

The work presented in this report relies on the application of the Stress Life method for the assessment of remaining fatigue life of the test bridge -- Walnut Creek Bridge on Interstate 35. The field test and simulation results of the dynamic response of the test bridge made it apparent, however, that the prescription of static stress ranges and impact factors, described in the basic procedure of the NCHRP Report 299 [1], provide at best a poor estimate of actual dynamic stresses. When the study was conducted, the investigators established moment ranges for bridge girders by loading the bridge with the static weight of the "Fatigue Truck" at various locations along the span to determine the maximum and minimum moments. That approach shows a complete disregard for the dynamic effects imposed by heavy truck vehicles, that are invariably outfitted with suspension that tend to shed (by design) vibratory loads to the bridge, rather than excite and possibly damage the conveyed load. An impact factor, or static load multiplier, is generally applied to the extreme static moments to provide an indication of the predicted effect that dynamic loads can produce. The procedures tend to underestimate the effect that vibration oscillations might have on useful life. The cumulative effect of cyclic loads can only be measured if each reversal is accounted for. The work here utilizes the rather conservative but more realistic rainflow counting method.

In order to render a more accurate representation of the actual impact loads that are imparted to the bridge, many field tests were conducted. Those test results provided a reliable understanding on the actual loading and bridge working performance. Once the field tests were completed, then the Center for Structural Control (CSC) developed a computer code of that was designed to simulate the dynamic response as a truck(s) passes over the Walnut Creek Bridge. That code consists of a dynamic finite element based model of the bridge, coupled with a truck. In order to replicate the actual field data, the CSC found it necessary to model the trucks chassis suspension system with complient elements. The parameters that define those springs, dampers, tire stiffness, the weight of the axle assemblies and the sprung weight of the truck were established via testing.

The research team used the field test results of the controlled and uncontrolled response of the bridge to determine the effect on service life that the SAVA system produced. Comparisons of the results are offered. The results indicate that the SAVA system extends the service life of the controlled span by at least 50 years.

It is noted, finally, that the results obtained here were based on standard practices, a fair and impartial estimate, the distribution of the loads, and a thoughtful determination of the prior history of the bridge/truck interaction loads imposed on the test bridge over the period from initial use to the present. The work provides an educated guess at the condition of the bridge as it exists, and an indication of how the bridge might fare once outfitted with the SAVA system.

CHAPTER 2

FATIGUE LIFE ANALYSIS STRATEGY FOR STEEL BRIDGES AND STRUCTURES

The purpose of this section is to provide the reader with a comprehensive review of the guidelines that are presently relied on by the bridge engineers to assess bridge fatigue life.

2.1 Review of Fatigue Evaluation Procedures

2.1.1 AASHTO Manual. The AASHTO Manual is perhaps the most widely followed prescription for the assessment of bridge health. The evaluation of the fatigue condition is based on a balanced assessment that selects both field observation and calculated effects. The Manual, which requires $\sigma - \epsilon$ inspection of the structure at least once every two years, provides a detailed recipe for the evaluation of the fatigue condition of a bridge based on the field observations made during inspections. The Manual suggests the use of more elaborate procedures, defined in the Specifications section of the AASHTO Regulations, be used when a more precise evaluation of bridge fatigue life is required.

2.1.2 AASHTO Specifications.   The drawback to utilizing the AASHTO Fatigue Specifications is that they were adopted prior to the development of an experimental basis for the prescription of fatigue assessment. Many of the particulars described in the Specifications fail to reflect the actual sources of fatigue-producing complications in bridge structures. Instead, they combine an artificially high stress range with an artificially low number of stress cycles to produce a reasonable design. Furthermore, the fatigue provisions in the Specifications are presented in terms of allowable stresses and do not indicate how to calculate the remaining life of an existing bridge, which is needed to make cost-effective decisions regarding inspection, repair, rehabilitation, replacement, and research. Neither the Manual nor the Specifications consider secondary bending effects or cracked or repaired members.

2.1.3 European Convention for Constructional Steelwork (ECCS). For several years the ECCS has been preparing recommendations [5] for the fatigue design of steel structures, which are intended for application to highway and railway bridges, crane and machinery supports, and other structures. The ECCS recommendations follow the AASHTO approach of classifying structural details according to their fatigue strength. However, ECCS uses 14 different detail categories instead of the seven presently used by AASHTO
 and includes details not covered by AASHTO. Furthermore, ECCS gives a complete design SN curve (stress range vs. life) for each fatigue category, instead of allowable stresses corresponding to specific life categories. Those curves are similar to the ones used to develop the AASHTO allowable stress range values. The ECCS uses an effective stress range concept, similar to that developed in NCHRP Project 12-12 [7], to define variable-amplitude spectra. This effective stress range is based on Miner's Law [9]. When conducting a fatigue evaluation, the effective stress range corresponding to the design loading is used with the appropriate SN curve. For highway steel bridges, ECCS also uses the fatigue-truck concept developed in the NCHRP Project [7,8]. In that approach, the variation of truck position in typical traffic, is represented by standard fatigue vehicles. The fatigue evaluation can be made in terms of either stress or life and absolute allowable stresses are not imposed.

2.1.4 British Fatigue Code. The recent British Fatigue Code [6], which applies to both highway and railway bridges, gives three different analysis procedures for highway bridges. All three procedures use the same design SN curves to define the fatigue strengths of various detail categories. The classification of details into categories is similar to that used in the ECCS recommendations [5]. Also, the finite-life portions of the SN curves, for the various categories, are essentially the same as those used by ECCS [5]. The British code, however, uses a constant-amplitude fatigue limit for each category of ten million cycles, and the SN curve is projected below this stress range at a slope of five. There is no cutoff level below which stress cycles have no effect. In the simplest of the three procedures, an effective applied stress range for each detail is calculated by loading the bridge with standard fatigue trucks that represent typical truck traffic. This calculation must be below an allowable stress range corresponding to a life of 120 years, and to a truck volume that is defined for various types of highways. Each truck passage is assumed to cause one stress cycle. The highest of the specified truck volumes is 2 million per year in one lane; this corresponds to 240 million stress cycles over the expected 120-year life of the bridge. The effective stress range and fatigue truck concepts, used in this procedure, are based on concepts developed in a previous NCHRP study [7] and are consistent with Miner's Law [9].

2.1.5 NCHRP Report 299. In recent years, information has been developed on variable-amplitude fatigue behavior, high-cycle, long life fatigue behavior, actual traffic loadings, load conditions, and other important parameters related to fatigue. This information, together with the extensive information previously accumulated on the fatigue behavior of various steel bridge details, is sufficient to permit the development of realistic procedures, the "**Fatigue Evaluation Procedures for Steel Bridges**", National Cooperative Highway Research Program Report 299 (hereinafter, referred to as **NCHRP Report 299**). The evaluation procedure used in this report was based on the application of the NCHRP Report 299.

The objective of the NCHRP Report 299 was to develop practical fatigue evaluation procedures that:

(1) realistically reflect the actual fatigue conditions of a bridge,

(2) give an accurate estimate of the remaining fatigue life of a bridge and permit this estimate to be updated in the future to reflect changes in traffic conditions,

(3) provide consistency and reasonable levels of reliability,

(4) permit different levels of effort to reduce uncertainties and improve predictions of remaining life,

(5) consistently apply to both the evaluation of existing bridges and the design of new bridges,

(6) can conveniently be modified to reflect future research, and

(7) are suitable for inclusion in the AASHTO maintenance manual and design specifications.

2.2 Similarities of Procedures

2.2.1 Evaluation Steps. Most fatigue evaluation procedures proposed for structural applications, are intended to reflect the actual fatigue conditions that occur in the structure under consideration. Consequently, they generally involve three steps: (1) calculate the variable-amplitude stress spectrum caused by the actual loading, (2) relate this variable-amplitude stress spectrum to an equivalent or effective constant-amplitude stress by some cumulative damage

approach, and (3) compare the resulting applied stress parameter with a fatigue strength (SN) curve to obtain the fatigue life. Stress range is the main stress parameter in most of the proposed procedures; some also consider the effects of mean stress. Factors of safety may also be used to modify the applied stress value.

2.2.2 Truck Loading. The uncertainty in the calculated variable-amplitude stress spectrum depends on how accurately the loading can be defined and how stresses can be calculated from the loading. For highway bridges, truck traffic produces the main fatigue loading, and a gross weight histogram for such traffic is the most important parameter defining this loading. Therefore, most of the proposed procedures define a typical histogram and/or permit the use of an actual histogram for the site. The wheel spacings and distributions of the gross weights to various axles are also important and are defined in most of the proposed procedures. Calculation of the stresses from the loading involves factors that account for lateral distribution, impact, and multi-truck loading. These parameters are usually included in a different formation in each proposed procedure.

2.2.3 Damage Accumulation. Miner's Law [9] is used in almost all of the proposed procedures to relate variable-amplitude fatigue behavior to constant-amplitude behavior. Although Miner's Law is often criticized by researchers, especially those dealing with special types of loadings, an extensive NCHRP study [7] of simulated bridge members reports that it is unbiased for such members and that the scatter in predicting the life is not large. For convenience, many of the proposed procedures use the effective stress range (see below) concept that was developed in the NCHRP study [7], which was based on Miner's Law. In that approach, a variable-amplitude spectrum is represented by an equivalent constant-amplitude stress cycle. Several of the proposed methods carry this concept one step further and use an effective fatigue truck to represent typical truck traffic [7].

2.2.4 Effective Stress Range. In most of the proposed procedures pertaining to highway bridges, the effective stress range for that bridge is compared with fatigue strength curves that are consistent with the present AASHTO allowable fatigue stresses [10] for various detail categories. The finite-life portion of these curves represents approximately 95 percent of the confidence limit for the worst detail in each category. Mathematical expressions are often given to define the curves, and parallel lines, representing different confidence levels, are sometimes provided. Also some of the proposed procedures give allowable stresses for various details that are based on the fatigue strength curves. These allowable stresses are based on heavy traffic volumes that are considered appropriate for specified types of highways (e.g., interstates) and on a desired level of useful service life for the bridge. Some procedures, however, give allowable stresses for any estimated lifetime average truck volume and desired design life. Thus, appropriate truck volumes for the actual site can be used. **Very few procedures [1] recognize that a truck passage may cause more than one stress cycle and give procedures to define the appropriate number of stress cycles per truck passage.**

2.2.5 Fatigue Limit. A limited number of the proposed procedures [1] use a variable-amplitude fatigue limit that is some fraction of the constant-amplitude fatigue limit. If the effective stress range for the spectrum is below this variable-amplitude fatigue limit, the fatigue life is assumed to be infinite. A limited number of those procedures project the finite-life portion of the fatigue strength curve downward without limit and; thus, assume that the constant-amplitude fatigue limit is still to be determined. Generally, a uniform slope of -3 on a log-log plot is used to represent

5

the decrease in fatigue life versus stress. Some of the proposed procedures assume that the fatigue life is infinite if all of the stress cycles in the variable-amplitude spectrum remains in compression. This is consistent with the present AASHTO [10] approach.

2.2.6 Probability and Safety. Many of the procedures use probabilistic concepts for assessing safety, and NCHRP 299 [1] is intended to indicate the probability that the actual fatigue life will exceed a particular value. Some procedures use reliability calculations to assess or adjust the level of safety associated with a particular design procedure or to obtain a consistent level of safety over a range of design cases. The values of key parameters in a design procedure can be adjusted to improve this consistency. Some factors that affect the fatigue stresses in actual bridges, such as unintended end fixity at abutments, may also be included in the reliability analysis to assure uniformity in safety level [1].

2.3 Fatigue Life Evaluation Strategies of the Walnut Creek Bridge

Walnut Creek bridge is located on I-35 at the 92.7 mile marker and crosses Walnut Creek near Purcell, Oklahoma (Figure 2.1). The bridge was built in 1971. It consists of five 400' long continuous steel girders with three intermediate piers and two abutments located at 100' intervals. The bridge deck is skewed at $45°$ to the centerline of the roadway. The deck is 38' wide, including two 12' wide lanes of traffic, a 10' shoulder adjacent to the inside lane, and a 4' shoulder adjacent to the outside lane. The five steel girders are covered by the composite concrete deck. The superstructure is supported via a group of fixed shoes (on the middle pier) and four groups of expansion shoes (on the other two piers and the two abutments). The girders are equipped with diaphragms at 20' intervals. The diaphragms are orthogonal to the longitudinal centerline of the bridge. Recent traffic surveys indicate that approximately 18,000 vehicles cross the bridge on an average day.

Data about the bridge that was used in the fatigue life evaluation included:

(1) measured truck weight,

(2) actual stress cycles per truck passage for each truck used in the study;

(3) actual and codified truck superpositions factors;

(4) codified lateral distribution factors for the girders;

(5) measured impact effects caused by bridge/truck vibration and rough road surface on the bridge,

(6) effective section modules for different sections of the composite bridge,

(7) indirectly measured moment ratios or moment ranges for different truck loads;

(8) constant-amplitude fatigue strength for the steel girders (the AASHTO category of the Walnut Creek Bridge is defined as category C), and

(9) cumulative damage relationship.

The analysis includes the significant effects caused by the resonant coupling that occurs between the bridge and the truck's suspension. The truck wheel load input to the bridge and the dynamic response of the bridge were all carefully simulated and then validated with the field test results. Other observations, such as fatigue limit, compression cycling, long-span loadings, and vibration cycles for the bridge, are also discussed.
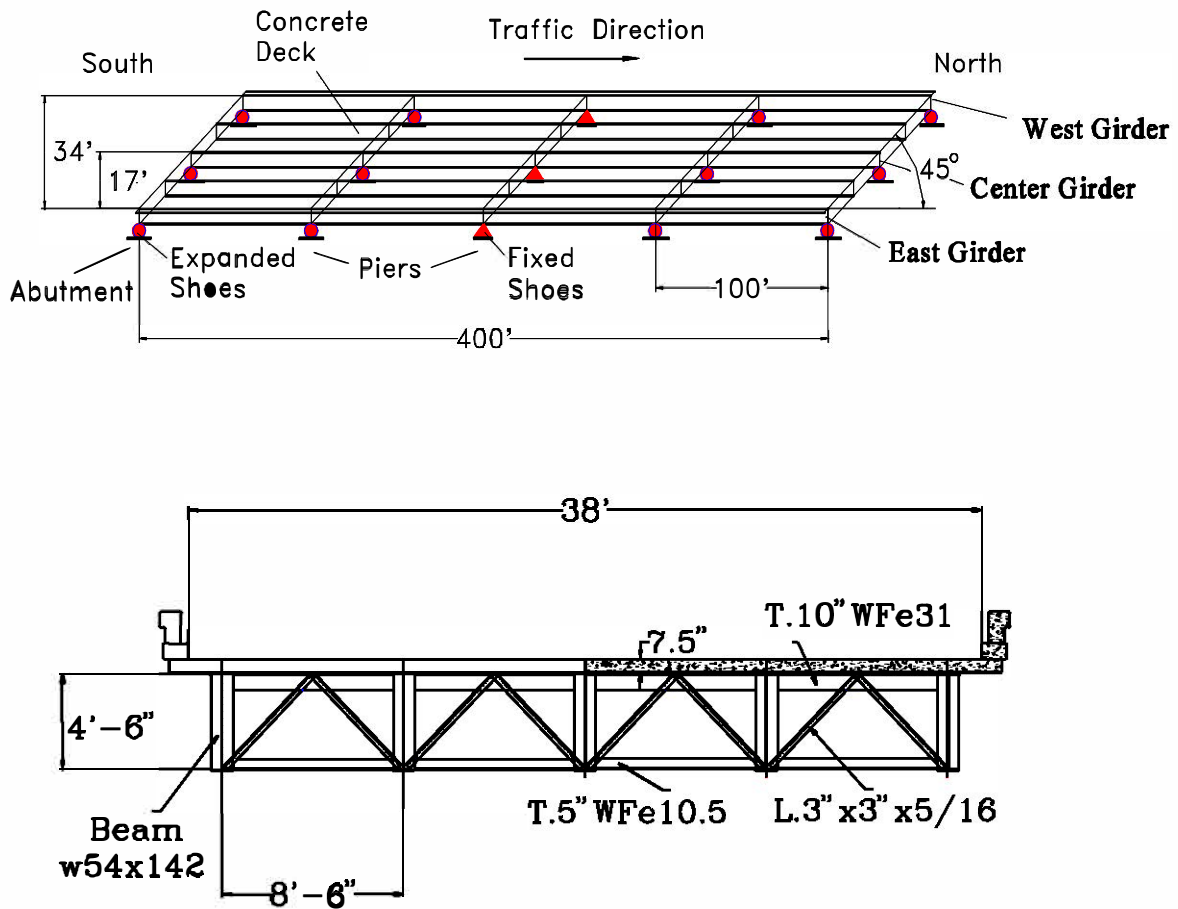
Figure 2.1 Layout and Cross Section of the Superstructure, Walnut Creek Bridge on I-35, Oklahoma

The analysis includes the significant effects caused by the resonant coupling that occurs between the bridge and the truck's suspension. The truck wheel load input to the bridge and the dynamic response of the bridge were all carefully simulated and then validated with the field test results. Other observations, such as fatigue limit, compression cycling, long-span loadings, and vibration cycles for the bridge, are also discussed.

2.3.1 SN Curve. It is generally accepted that the fatigue life of a bridge will be infinite if all of the stress cycles in a variable-amplitude spectrum, obtained from simulation and field tests, are below the constant-amplitude fatigue limit, S_{ric}. Figure 2.2 clearly shows that this occurs when the effective stress range, S_r, for the spectrum is less than S_{ric}/R_p, and this level of S_r can be considered the variable-amplitude fatigue limit, S_{riv}, for the spectrum. R_p is the peak ratio for the spectrum and is defined as the peak stress range, S_{rp}, in the spectrum divided by the effective stress range.
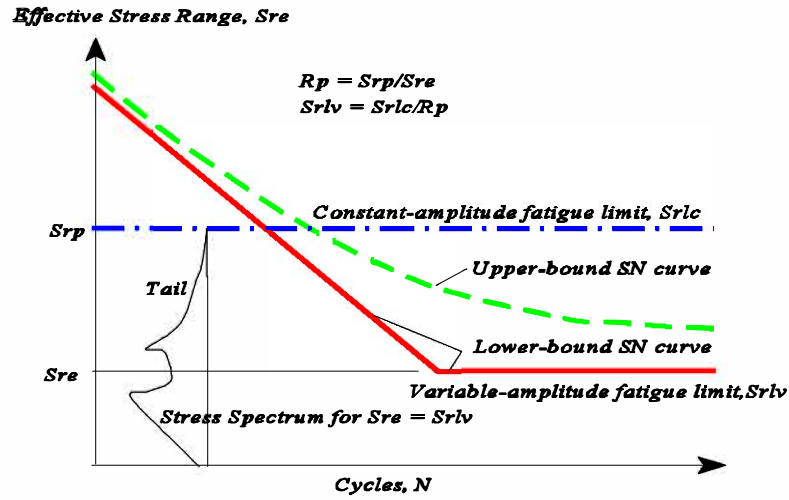
Figure 2.2 Effect of Fatigue Limit on Variable-Amplitude Fatigue Behavior [1]

If $S_{re} > S_{riv}$, some of the cycles, S_{riv} S_{ra}, are above the constant-amplitude fatigue limit and others, S_{rb}, are below. In the past, it was thought that the cycles, S_{riv}, below the constant-amplitude fatigue limit cause no fatigue damage and can could therefore be ignored. The dashed SN curve in is based on this assumption and represents an upper bound on the fatigue life. It becomes asymptotic to the variable-amplitude fatigue limit at a very long life.

More recently, it was concluded that the S_{rb} cycles cause damage by propagating cracks initiated by the S_{ra} cycles. At worst, the S_{rb} cycles cause the same fatigue damage as if the constant-amplitude fatigue limit did not exist. Therefore, the solid SN curve in Figure 2.2 defines the lower bound for fatigue life. The actual SN curve must lie between these two limiting curves, but sufficient data is not yet available to define its position precisely [1].

The difference between the upper- and lower-bound SN curves depends primarily on the peak ratio and the shape of the probability-density curve defining the stress spectrum. If this curve has a long low tail, R_p will be large and S_{riv} will be well below upper-bound curve. Consequently, the difference between the two curves will be large if the tail is long.

The SN curve for a "C" category bridge, which is recommended in NCHRP Report 299 [1], was used here to calculate the fatigue life. The effect of the fatigue limit on this evaluation procedure depends on the level of the actual SN curve at a practical design life. If the actual SN curve is well above the SN curve assumed in this procedure, the effect will be large. Therefore, tests will be needed to define the actual SN curve for the girders.

2.3.2 Compression Cycling. In this procedure, it is assumed that the fatigue life of the bridge is infinite, if all of the stress cycles in the spectrum from simulation and test are compressive. This is consistent with present AASHTO

fatigue design procedures. In practice, bridges in the category are considered fatigue risks. Although the fatigue life of an I-beam is shown to be infinite if the stress ranges at the critical locations are below or close to the compressive dead load, the slight difference or calculation error in dead load stress probably does not actually have a large effect on the fatigue life. Therefore, even if the stress ranges are a little above the compression dead load, the infinite life of the bridge can be assumed. This is the situation that is likely to occur on the controlled bridge.

2.3.3 Long-span Bridge Loadings. In a long-span bridge, the traffic loading causes long periods of continuous stresses of varying magnitude rather than a large number of individual cycles assumed in the procedures. The large magnitudes of these continuous traffic stresses suggest that special fatigue loadings need to be considered for such bridges. Further study of fatigue loadings in long-span bridges would be desirable to provide more definitive data on the nature and effects of such loadings.

A continuous stress time history can be generated from available data based on (1) the percentage of vehicles of various weights and types in typical traffic, and (2) the variation of traffic volume with time over a 24-hour period. Certain methods can be applied to the data to determine the positions of the vehicles on the bridge at any time, and appropriate influence lines can be used to calculate the resulting stresses. The effects of the continuous stress-time curves on fatigue behavior can be assessed by methods using the cycle counting technique.

2.3.4 Vibration Cycles. For some bridge types, the effects of vibration stresses on fatigue behavior are generally small enough to be neglected. **The vibration levels that occurred at the test bridge have been shown to be significant**. The specific site conditions including grade, bump, and deck surface roughness, may cause large vibrations of the bridge**. In addition, the research conducted here strongly suggests that the close correspondence between the fundamental frequencies of the bridge and the truck's suspension can cause near resonance vibration amplitudes.**

2.4   Bridge Data

The **critical locations** of the bridge for the fatigue analysis are determined by comparing the maximum stress ranges calculated from simulations and field tests. For the uncontrolled service condition, the critical locations are usually at the bottom flange of the girder near the middle points of the each span. For controlled load conditions, the critical locations correspond (approximately) to the third points of the span.

2.5   Additional Notes

The remaining safe life is a more conservative life estimate, which provides a level of reliability comparable to present AASHTO fatigue provisions of the bridge.

The **Stress Range** is determined directly from field measurements and/or simulation.

Standard **Fatigue Trucks** are used to represent the variety of trucks of different types and weights in the actual traffic. The gross weight of a standard fatigue truck is 54 kips, with main axle spacings of 14' and 30'. The effects of more than one truck on the bridge at a time was not examined here.

NCHRP 299 suggests that the **Impact Factor**[1] usually varies between 1 and 1.3 [1]. Also, the impact factor used for fatigue evaluation is for the stress range rather than for peak stress. Because actual stress time histories were employed in the study here, the impact factor was assumed to be 1.

The fatigue evaluation is generally based on the **Moment Load Range** caused by the passage of the fatigue truck across the bridge. The dynamic moment range [1] is used in this fatigue evaluation procedure, rather than the static moment range typically used in the NCHRP Report 299 [1], or the maximum moment method used in general procedures. (Note: The research here suggests that if the investigator prefers to rely on simulations using a fatigue truck, then the simulation should include a typical suspension compliance on that fatigue truck to discover the extent to which the bridge modes might couple with the truck suspension modes to produce near resonance vibrations.)

Reliability Factors are provided to assure adequate safety and consistent levels of reliability in calculating the remaining safe life for different cases. Basic factors (1.35) are recommended for bridges with **redundant** girder construction, which is the type of design employed on the test bridge studied here. The corresponding probability that the actual remaining fatigue life will exceed the calculated remaining safe life are about 97.7%. The reliability factors used in this procedure were 1.35 and 1.0, which were used when calculating the remaining safe life and mean life, respectively.

If the **Compressive Dead Load Stress** is high enough so that essentially all of the stress cycles caused by normal traffic are completely in compression, the fatigue life is assumed to be **infinite** (the calculated fatigue life exceeds the design fatigue life of bridge, 75-100 years). This situation will occur only when the compressive dead load stress is equal to the tension portion of the (factored) stress range caused by heavy trucks (e.g., 120 kips in weight) traffic. **For this estimate, it is assumed that the heaviest truck weighs twice as much as the fatigue truck**; less than 0.2% of trucks weighs more than this value, and their passage over a bridge is strictly regulated.

If the maximum factored stress range in tension falls below the **Fatigue Limit** (3.58 ksi) for the steel girders of this bridge, crack growth of the girder will not occur theoretically and infinite fatigue life of the bridge may be assumed [1]. **However, even if only one high stress cycle occurs and its stress range is larger than the fatigue limit, then the finite fatigue life of the bridge will be determined.**

It will be shown in a later section that the bridge being examined here fails to satisfy the infinite life check; therefore, the **Finite Remaining Life** (in years), corresponding to the factored stress range, is calculated for a lifetime average truck volume.

Detail Constants are obtained for this bridge from the present AASHTO specifications [11].

The passage of the fatigue truck across a short-span bridge usually produces a complex **Stress Cycle Per Truck Passage** that has two major peaks (corresponding to the main axles) and the shape of the complex cycle is obtained from simulation and field tests. The stress cycles per truck passage are determined using the rainflow counting

---

[1] Footnote: The project test data suggests that the correct standards (NCHRP 299) are in serious error with regard to the upper limit of 1.3 for the impact factor. That finding is discussed in a later section.

technique applied to field measurements [3]. The net effect of the complex stress or moment cycles is represented by an equivalent number of individual cycles.

The **Lifetime Average Daily Truck Traffic (ADTT)** for this bridge has been estimated using the Oklahoma Department of Transportation (ODOT)-suggested present traffic volume at the site, the present age of the bridge, and a projected ADTT annual growth rate of 4%. The heavy truck volume at a site is presumed to represent 30% of the ADT.

FIELD TEST ON THE WALNUT CREEK BRIDGE

3.1   Experimental Set-up

The work plan at the Walnut Creek Bridge includes the multi-year monitoring of the bridge motion to determine the effectiveness of a system of automatically controllable shock absorbers (SAVA) that have been mounted on the bridge. A multi-channel sensor system has been installed on the superstructure of the Walnut Creek Bridge in order to provide long-term monitoring of dynamic response of the bridge, and to validate the fidelity of the finite element model (FEM) of the structure.

Three types of transducers were employed, including 42 channels of ICS piezoelectronic accelerometers, 12 channels of EA-series strain gauges, and 2 channels of potential displacement sensors (string pot). Most of the sensors are situated on the bottom flange of W-shape beam (girder) to detect the vertical acceleration, the strain (stress), and the vertical deflection of the superstructure. Figure 3.1 shows the layout of sensors on the bridge.
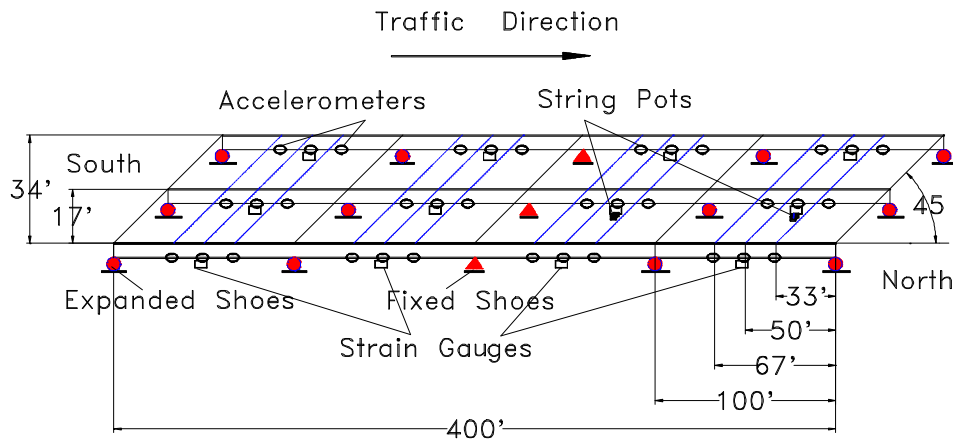
Figure 3.1   Sensors Layout on the Walnut Creek Bridge

A key consideration in the development of the sensor system was the environmental conditions at the bridge site. The integrity of the components had to be assured in spite of the seasonal temperature changes. The temperature of the west facing girder had been recorded at over 140 °*F* in mid August, and the joints in the concrete deck allow torrents of rain runoff to soak the surfaces of the girder during the storm conditions. In order to protect sensor circuits from high temperatures and moisture, PVC pipe was glued to the web of the girder with epoxy. Heat insulation material was included in the pipe in order to reduce heat transfer to the sensor and circuit. Moisture absorbing material was also added to each sensor cell to keep the circuits dry.

The acquisition of data from distant points on the bridge posed a severe problem. Conventional methods require the detection of a sensor voltage output which is usually proportional to the measurement (e.g., 1 Volt equals 200 psi).

The long wires represent a large resistance which reduces the voltage signal. This is a problem because many of the sensors are located as much as 600' from the data acquisition system. One possible alternative is to transmit the data from each of the sensors using wireless technology. That approach is prohibitively expensive, given the large number of sensors involved. The CSC instead, developed an economical solution that relies on FM technology. The voltage output at a sensor was first converted to a proportional carrier frequency. While the voltage of the signal is subject to amplitude loss, the carrier frequency remains undistorted. The data acquisition system then demodulated the signal to determine the actual voltage output of the sensor. The technique produces error-free readings. The CSC produced printed circuit boards (PCB) to accomplish the design, which was based on analog devices AD650 F/M chip. Figure 3.2 shows how the original signals are transferred and conditioned.
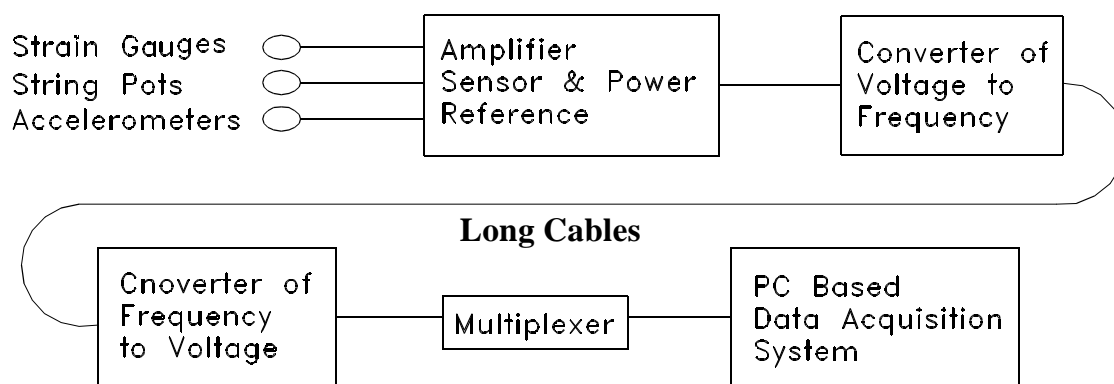
Figure 3.2 Signal Conditioning Network

3.2 Static and Dynamic Field Test

A large number of field tests have been conducted to establish the nature of the bridge/truck dynamic response. Four different types of heavy trucks were involved in the field tests. They were a Water truck (weight 26.6 kips), a Dump truck (weight 54.7 kips), a Rock truck (weight 79.5 kips) and a 120K Heavy truck (weight 120 kips). The water truck and rock truck were instrumented with accelerometers and displacement sensors for the purpose of identification of truck dynamics and analysis on the bridge/truck coupling. Figure 3.3 depicts the truck's wheel load and axle spacing pattern. A typical example of the type and number of truck tests conducted on a particular day is given in Table 3.1.
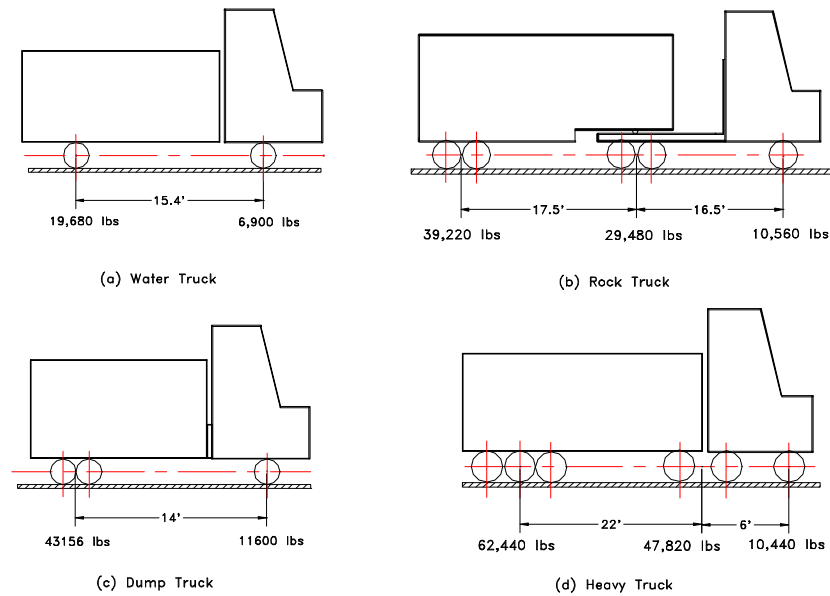
Figure 3.3 Test Trucks' Wheel Loads and Axle Spacing

Table 3.1 The Items of Field Test Fulfilled on January 5, 1997

Test Plan & Truck Moved Lane		Water Truck	Dump Truck	Rock Truck	Heavy Truck
Slow Motion	Right	+	+	+	+
	Left	+	+	+	
SAVA Open Valves	Right	+	+	+	+
	Left	+	+	+	+
SAVA Close Valves	Right	+	+	+	+
	Left	+	+	+	
SAVA Control Valves	Right	+	+	+	+
	Left	+	+	+	

3.3 Field Test Results

Figure 3.4 shows the locations of the stress sensors (strain gauges), which were installed at the bottom flange of the girder at locations noted. All the analytical and test results shown in the following texts will be described by referring to this diagram.

14
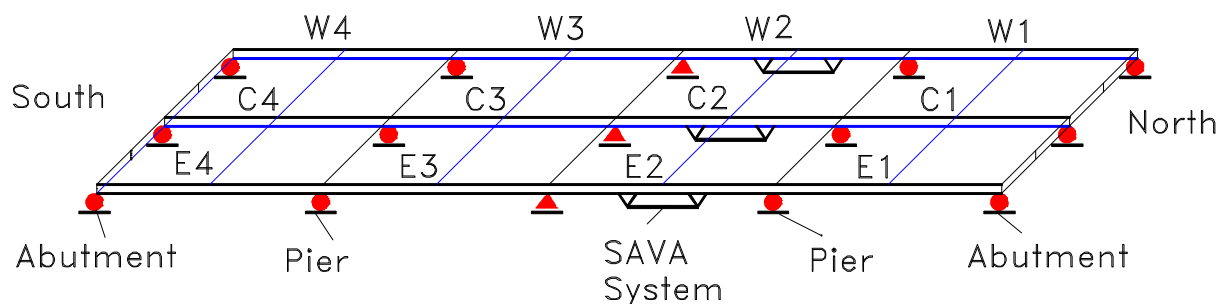
Figure 3.4 Strain Gauges Locations

3.3.1 Slow Motion (Crawl) Tests. In order to understand the dynamic interaction of the bridge and truck, it is essential to first establish a clear concept of the quasi-static effect that a vehicle has on the bridge. Once the quasi-static response is established, then that component of the total response at higher speeds can be subtracted out to yield the dynamic component only. This approach assumes that for all practical purposes, the bridge can be considered a linear system.

The results of a select number of quasi-static (crawl) tests of the project vehicles are reproduced here. Figure 3.5 shows the strain gauge outputs of the bridge at different locations for each of the four test vehicles. In each case, the truck traveled at approximately 1 mph in the right lane. One apparent anomaly worth pointing out is the nearly equivalent stress levels imposed by the rock truck and dump truck at the span centers of the center girder; this, in spite of the fact that the rock truck GVW was 80,000 lb while the dump truck GNW was 55,000 lb. The difference in wheelbase (rock truck @ 34 ft. and the dump truck @ 14 ft.) is the feature that most strongly affects this result, exclusive of weight.

The result of crawl tests in the left (passing) lane using the rock truck is shown in Figure 3.6. The data there, when compared with the result when the rock truck traveled in the right lane, suggests that the loading in the two girders that are closest to the wheel loads experience similar loads in spite of the different locations.

A second sequence of tests were conducted to establish the extent to which the SAVA system affects the quasi-static behavior of the bridge. During the first stage of testing, the valves of the SAVA system were fixed open, and the crawl tests were repeated. A close comparison of the strains measured in this test, with those measured during a crawl test before the SAVA system was mounted, confirms the expected result; the SAVA system does not produce any resistive moment at low speed. This is to be expected, since when the valve is open, the resistive force available from the SAVA is functionally related to the relative velocity between the SAVA moment arms. At slow speed, the relative velocity is essentially zero.

15
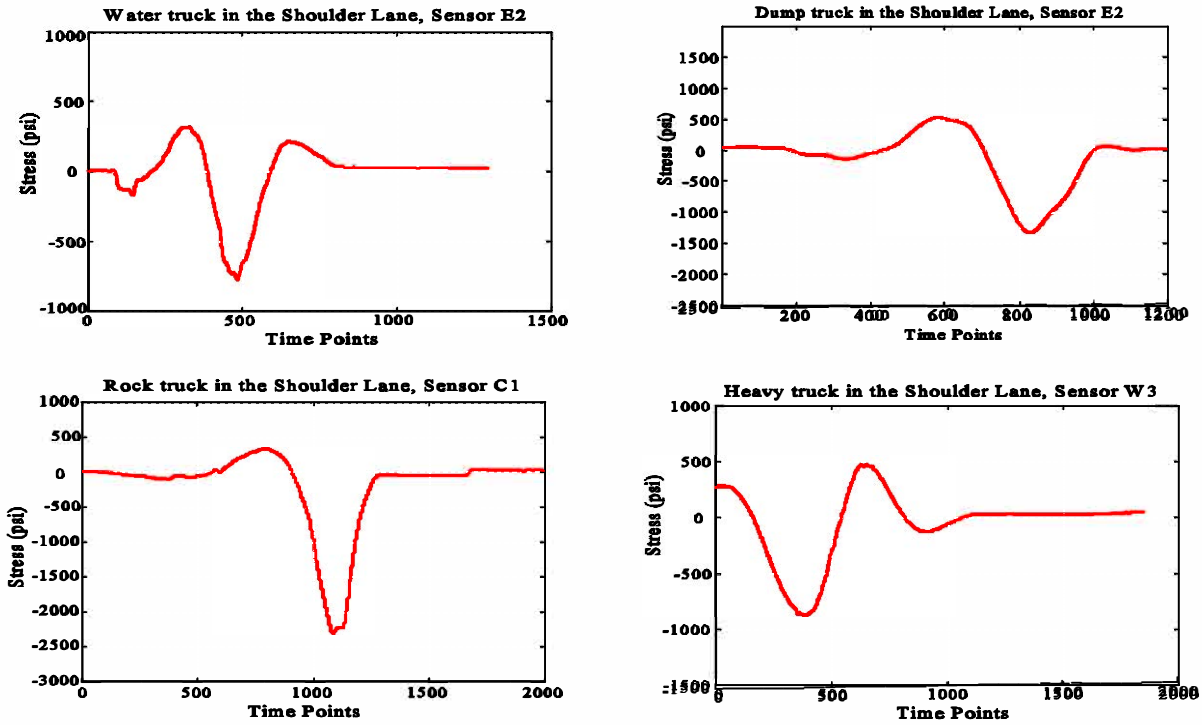
Figure 3.5 Stress Response of a Crawl Test, Right Lane, No SAVA System
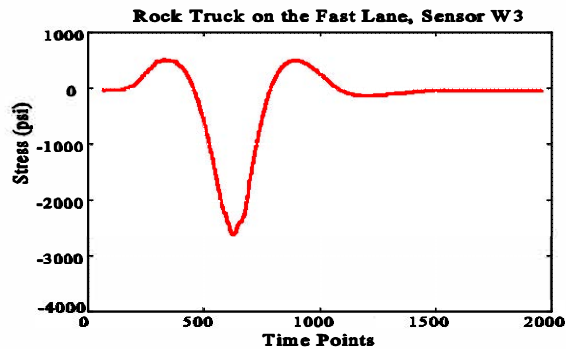

Figure 3.6 Stress Response of a Crawl Test, Left Lane, No SAVA System

The next sequence of crawl speed tests was conducted with the valves on the SAVA actuators closed. When the valve is closed, the SAVA assembly becomes in essence a stiffener. Figure 3.7a depicts time histories of the stress measured at the center of the girders in the span, in which the SAVA are mounted. It is compared for the valve open and valve closed. The results were obtained using the 5 axle rock truck (80,000 lb, 34' wheel base) at a 1 mph crawl, traveling in the right lane. Figure 3.7b shows the position of the wheels relative to the girders. A

16

catalog of peak stress range for each truck at the center of the west, central and east girders is given in Table 3.2, when the test vehicles were traveled at crawl speed in the right lane. Table 3.3 gives similar test data, when the test vehicles were traveled in the left lane.
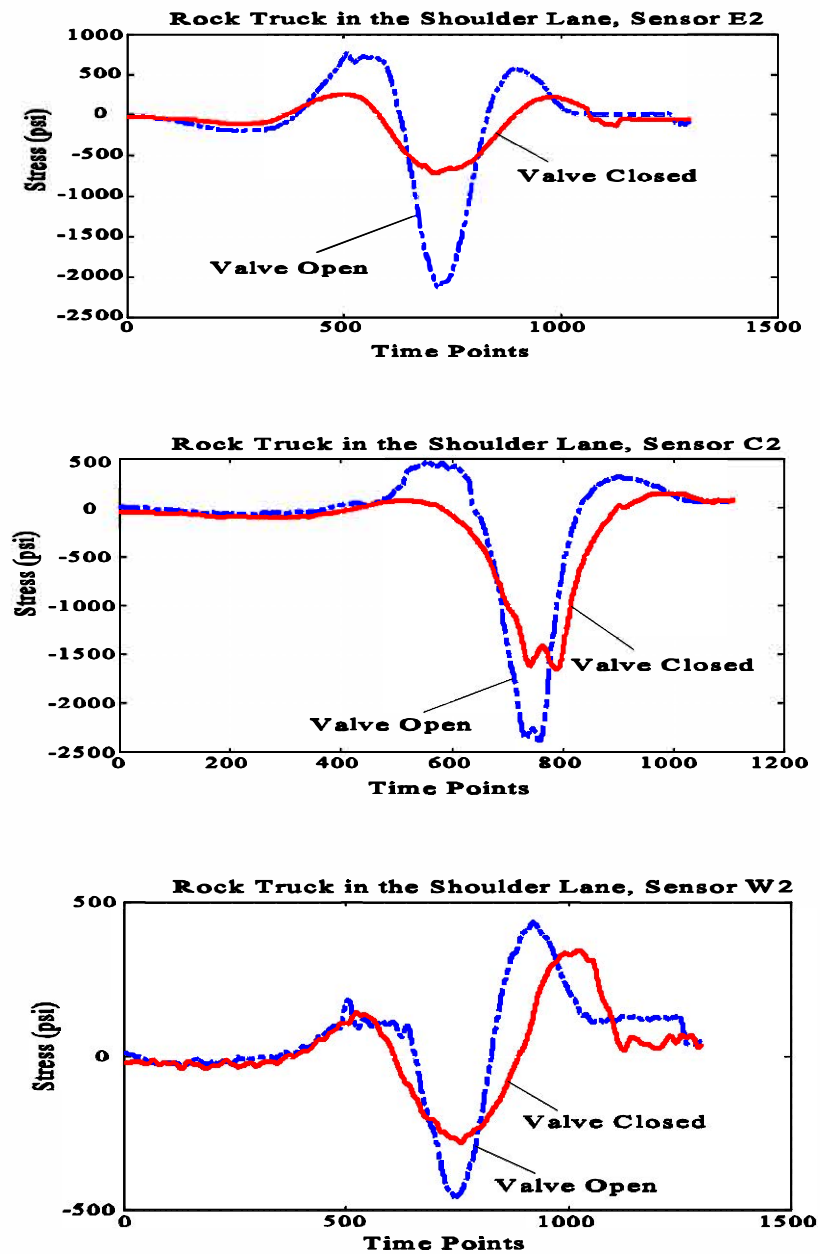
Figure 3.7a Stress Response of a Crawl Test, Right Lane, SAVA Control vs. SAVA Passive
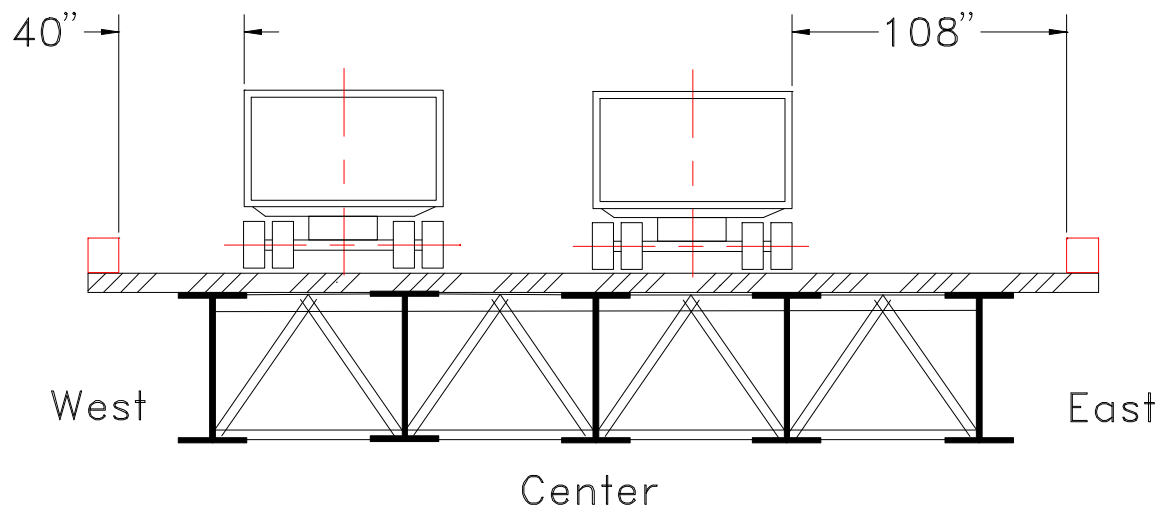
Figure 3.7b Truck Locations on the Bridge Deck when Doing the Crawl Test

Table 3.2 Static Stress Range under the Different Truck Test (Trucks Moving in the Right Lane)

(psi)

Test Trucks	Sensors (Strain Gauges) Location											
	E1	E2	E3	E4	C1	C2	C3	C4	W1	W2	W3	W4
Water Truck (25k)	879	1084	1188	1016	1222	1358	1415	1291	433	476	430	/
Dump Truck (54.7k)	1875	2127	2614	1741	2560	3107	2855	3078	886	813	737	/
Rock Truck (79.5k)	2668	2880	2985	2157	2392	2851	2785	3077	885	891	846	/
Rock Truck (79.5k) (with Valve Closed)	2217	(975)	3118	2317	2419	(1837)	2822	3060	843	(623)	897	/
Heavy Truck (120k)	3297	3497	4043	3599	3441	4026	4045	4323	1468	1393	1349	/

E --- East Girder, C --- Center Girder, W --- West Girder; Data inside ( ) are from the span with SAVA

Table 3.3 Static Stress Range under the Different Truck Test (Trucks Moving in the Left Lane)

(psi)

Test Trucks	Sensors (Strain Gauges) Location											
	E1	E2	E3	E4	C1	C2	C3	C4	W1	W2	W3	W4
WaterTruck (26k)	233	358	366	236	752	728	775	824	1161	1284	1327	/
Dump Truck (54.7k)	533	696	725	427	1713	1651	1718	1664	3200	2583	2726	/
Rock Truck (79.5k)	614	753	830	517	1975	1888	1975	1930	3827	3024	3139	/
Heavy Truck (120k)	/	/	/	/	/	/	/	/	/	/	/	/

E --- East Girder, C --- Center Girder, W --- West Girder

3.3.2 Dynamic Tests. A large number of dynamic field tests have been conducted using each of the test vehicles. Figure 3.8 depicts typical time histories for vehicle speeds at approximately 65 mph. In each case, the vehicle traveled in the right lane. The tests were conducted with two vehicles trailing the test truck. At a point two miles south of the test bridge, the two trailing vehicles pulled along side of each other and deliberately slowed the following traffic to approximately 55 mph. This allowed the test truck to cross the bridge (a 4 second event) with a long interval of time before or after any other vehicle crosses the bridge. The closest vehicle was typically more than 30 seconds (2600') behind or ahead of the test truck. This made it possible to assure that the bridge was not in motion prior to the truck's entrance. It is noted in the model testing report that the modal damping for the system is approximately 1.0% to 2.5% of critical. The data confirmed that observation; the bridge continues to oscillate long after the wheel loads have passed. An examination of the qualitative nature of the plots is instructive. Note, first that the heavy (120,000 lb) truck excites very little vibration, relative to the peak load values. Also apparent in the heavy truck load response is the double peak. This corresponds to the time delay that occurs between the passage over the center of the girder of first the tractor tandem axles and then the rear axle set of the truck.
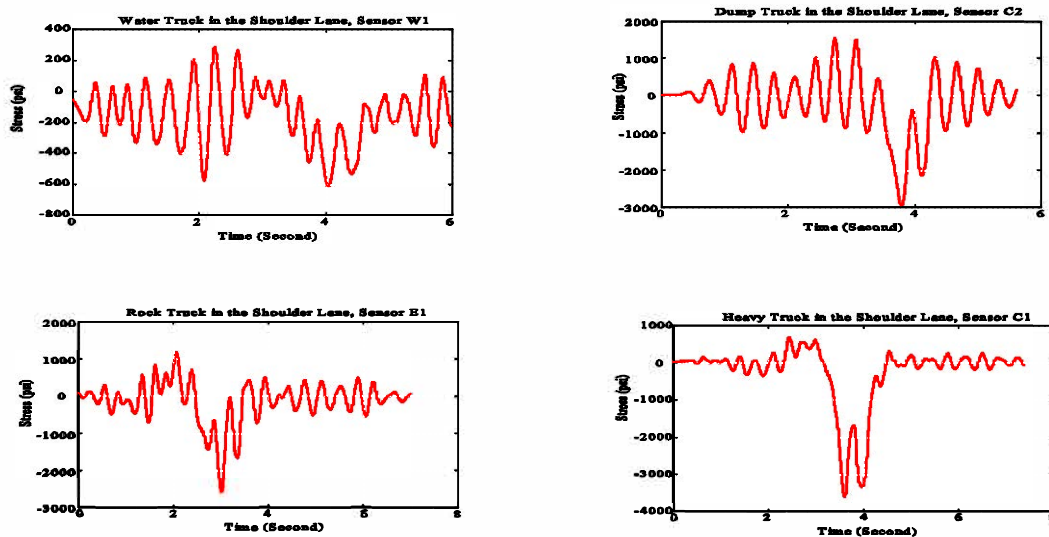
Figure 3.8 Time Domain Samples of a Dynamic Test

Another observation that gives some insight, is that the ratio of the weights of the rock truck and heavy truck (2:3) is approximately the ratio of the maximum stress for both trucks. This suggests that, given similar axle spacing, the bridge acts linearly. The maximum stress induced by the passage of the dump truck (3,000 psi) relative to the heavy truck (3,400 psi) is disconcerting. Recall that the dump truck weighs 55,000 lb, with a wheelbase of 14'. If one groups the heavy truck axles into three groups (steering axle, tractor tandems and trailer axles) and notes the distribution of weight at each axle set (15,000, 50,000, and 55,000 lbs), then it becomes evident that the load imposed by the dump

20

truck (peak) is approximately equal to the load imposed by the heavy truck. One could note that the longer truck produces two cycles of the maximum load.

Once the SAVA system was operational, a number of field tests were conducted to determine the effectiveness of the control system. Figure 3.9 provides several examples of how the untuned control architecture performed, relative to the uncontrolled response. **<u>The stress range reduction for the heavier vehicles (Rock, Dump and Heavy) is nominally 50% at those girders that carry the greatest portion of the moving load.</u>**

A tabulation of the maximum stress range values recorded for each of the tests is given in Table 3.4 (right lane test) and Table 3.5 (left lane test). A careful study of the data in Table 3.4 raises a question. When the truck is in the right lane, the center beam would normally be expected to see near maximum loads, which is generally the case. Surprisingly, the east beam is seeing similar peak stress values. The anomaly is that when the control is invoked, the largest (percentage) reduction is accomplished at the east girder. The reason for this was not clear at first. A thorough check of the hardware revealed that there was no malfunction of the controller. Because the bridge torsion and bending modes are close together in the frequency domain, then it is conjectured that the east girder realizes larger global deflections when a truck travels in the right hand lane. Had the truck been traveling at a crawl rate of speed, the center beam would have realized the largest load. **The difference between the static and dynamic loading, is that the dynamic bending and torsion modes combine to produce increased deflection at the outermost girders**. Figure 3.7 is an overlay of the east and west girder response when the rock truck travels in the right lane. A careful inspection of the dynamic response indicates that the east and west girders are moving down under the static weight of the truck, but are also vibrating out of phase; a clear indicator of the torsion effect.
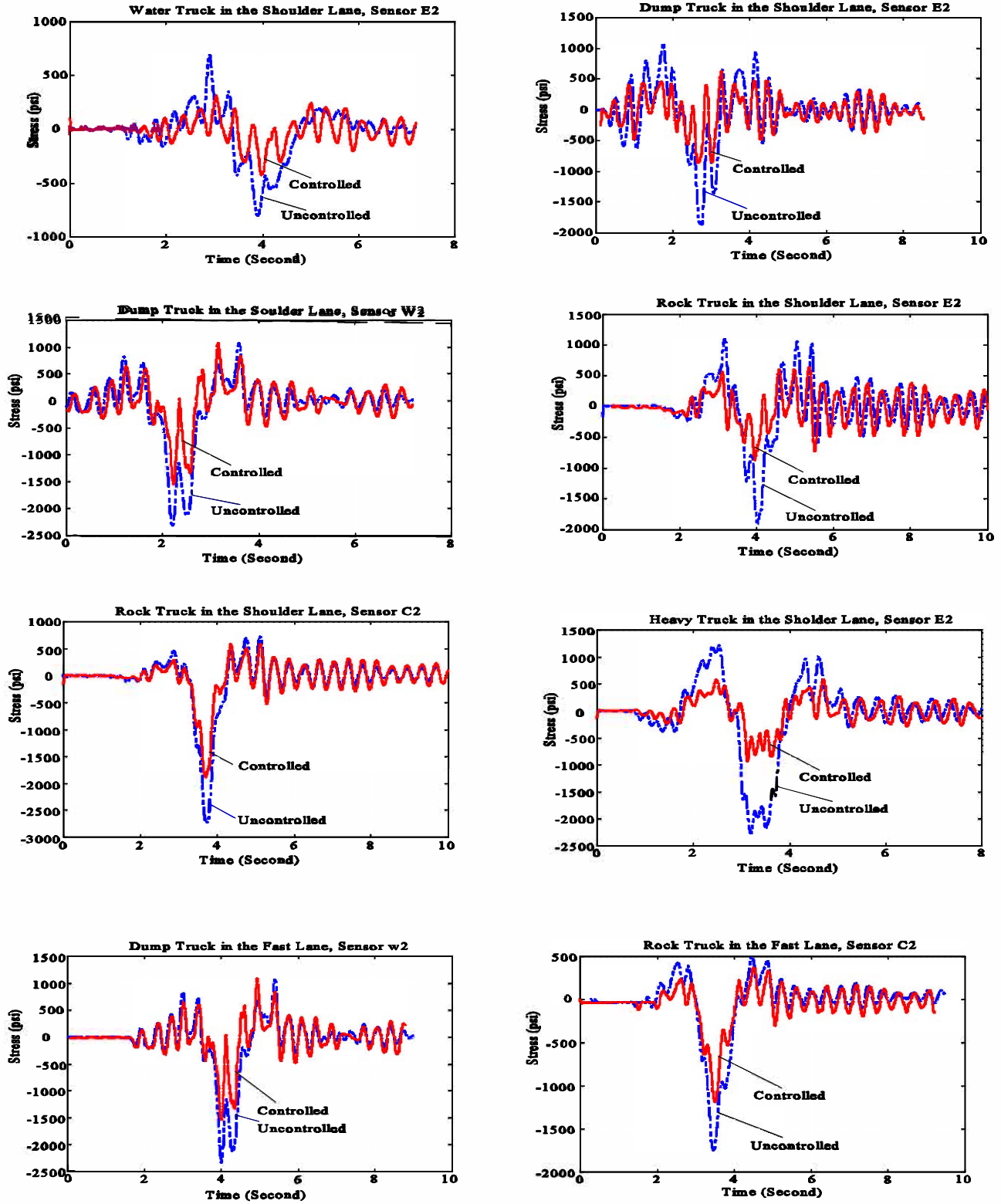
Figure 3.9 Field Test Results, Uncontrolled vs. SAVA Controlled

22

Table 3.4 Dynamic Stress Range under the Different Truck Test

(Trucks Driving in the Shoulder Lane)

(psi)

Test Trucks	Sensors (Strain Gauges) Location											
	E1	E2	E3	E4	C1	C2	C3	C4	W1	W2	W3	W4
A. Water Truck (26k)	1368	_1484_	1750	1308	1341	_1434_	1905	1360	901	_708_	1022	/
B. Controlled	1363	(730)	1658	1331	1329	(1144)	1849	1389	1059	(584)	1016	/
A. Dump Truck (54.7k)	3943	_2934_	4488	3688	3755	_3283_	3918	4109	2373	_1930_	2408	/
B. Controlled	4046	(1497)	4511	3571	3823	(2569)	3880	4043	2410	(1613)	2364	/
A. Rock Truck (79.5k)	3759	_3007_	3876	3391	3710	_3431_	4244	3768	2852	_1962_	2408	/
B. Controlled	3806	(1509)	3963	3418	3765	(2474)	4183	3866	2965	(1505)	2474	/
A. Heavy Truck (120k)	3960	_3506_	4502	3813	4263	_4585_	4713	4682	2453	_1853_	2210	/
B. Controlled	3950	(1504)	4641	3936	4221	(3375)	4804	4527	2493	(1288)	2256	/

E --- East Girder, C --- Center Girder, W --- West Girder; Data inside ( ) are from the span with SAVA

Table 3.5 Dynamic Stress Range under the Different Truck Test

(Trucks Driving in the Fast Lane)

(psi)

Test Trucks	Sensors (Strain Gauges) Location											
	E1	E2	E3	E4	C1	C2	C3	C4	W1	W2	W3	W4
A. Water Truck (26k)	612	_555_	879	580	1003	_789_	1088	1072	1425	_1348_	1790	/
B. Controlled	658	(435)	964	717	1025	(626)	1143	1106	1470	(1010)	1847	/
A. Dump Truck (54.7k)	2232	_2280_	3676	2663	2308	_2350_	2726	3026	5953	_3395_	5271	/
B. Controlled	2374	(1804)	3831	2809	2325	(1858)	2761	3048	5980	(2619)	5465	/
A. Rock Truck (79.5k)	1525	_1378_	1800	1364	2373	_2237_	2805	2251	5258	_3187_	4255	/
B. Controlled	1643	(810)	1810	1594	2508	(1560)	2783	2417	4963	(2028)	4233	/

E --- East Girder, C --- Center Girder, W --- West Girder; Data inside ( ) are from the span with SAVA

Another series of tests conducted in May 1997 is presented here to emphasize the effectiveness of the SAVA system. The truck (weighing 57,000 lb) was traveled over the bridge first with the valves open in that mode. The SAVA behaved like a simple shock absorber. Next, the oil was drained from the SAVA and the test was repeated with the valves open. With no oil, the SAVA offers no resistance. The results of the two tests are compared in Figure 3.10. The data again confirms the observations made earlier. The SAVA, operated as a damper, has very little effect on the maximum stress range (at the center girder) but it does achieve a dramatic reduction of the oscillation that accompanies the passage of the vehicle. The vibratory motion of the east and west girders are reduced considerably. It is noted that a pure stiffener would do little to damp out the residual vibration.

A test with the same rock truck was then conducted with the SAVA operational. The results for the case when SAVA provides control, when the SAVA acts like a damper, and when the hydraulic oil is removed from the SAVA are compared in Figures 3.11 and 3.12. The data indicates a 40% reduction of the peak stress range, irrespective of which lane the truck travels in.
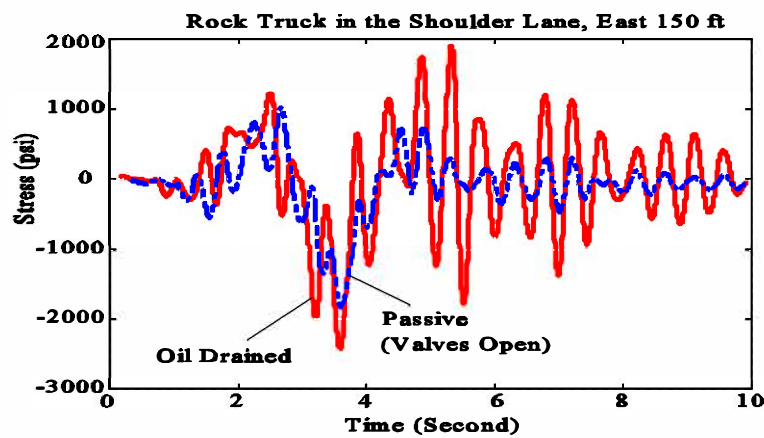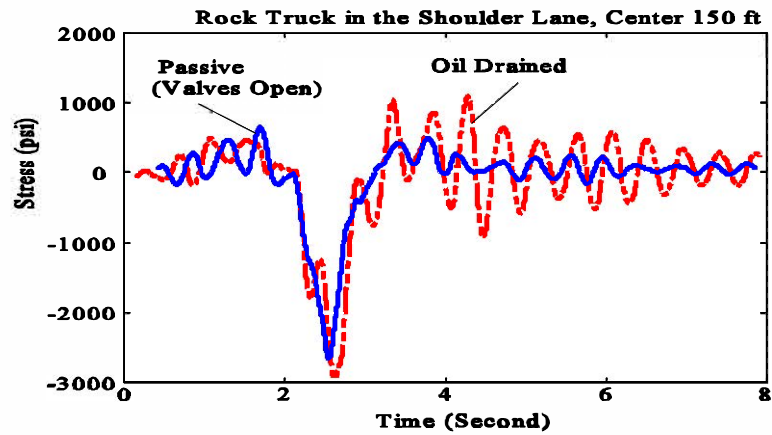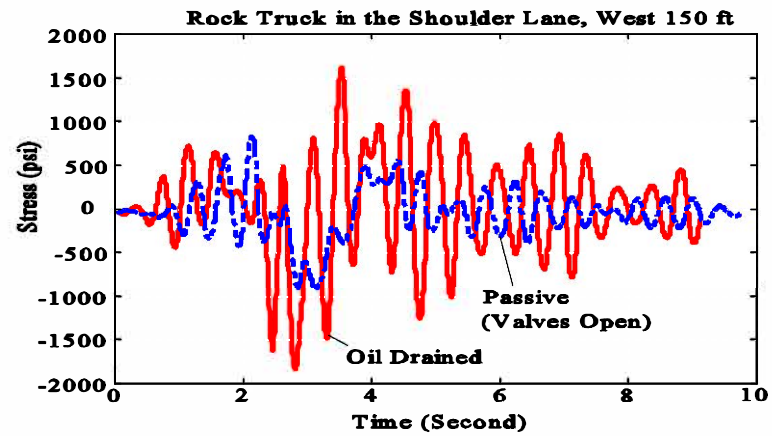
Figure 3.10 Comparison of Dynamic Test, 61 kips Truck Run over the Right Lane

25
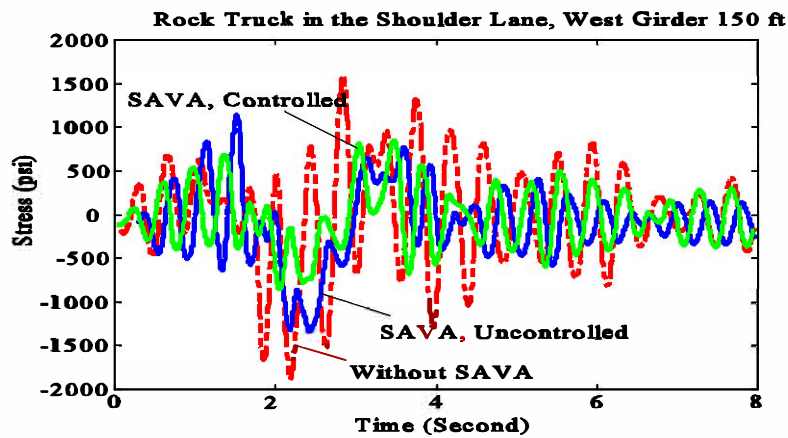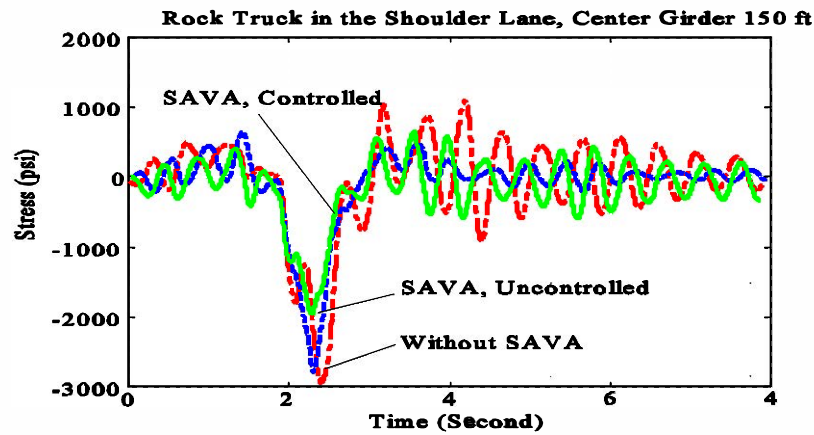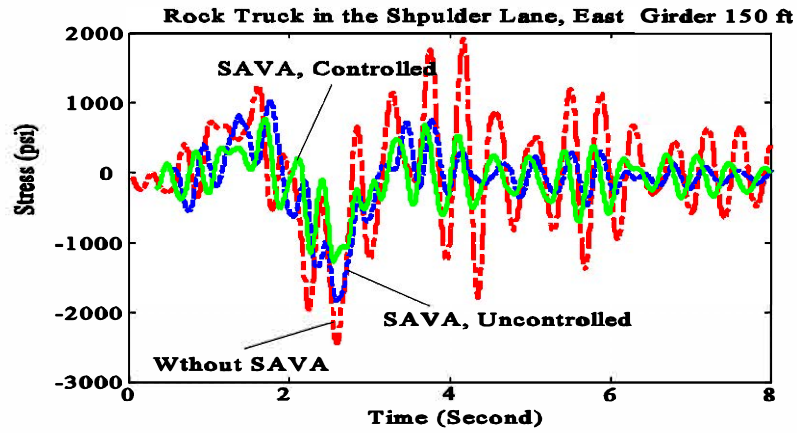
Figure 3.11 Comparison of Dynamic Test, 61 kips Truck Run over the Right Lane
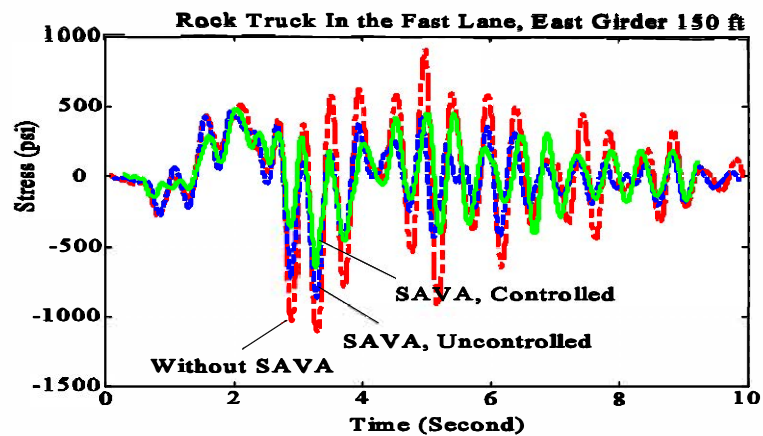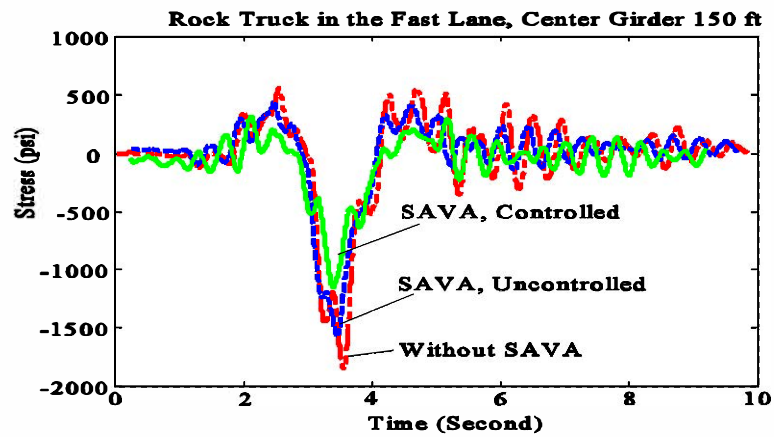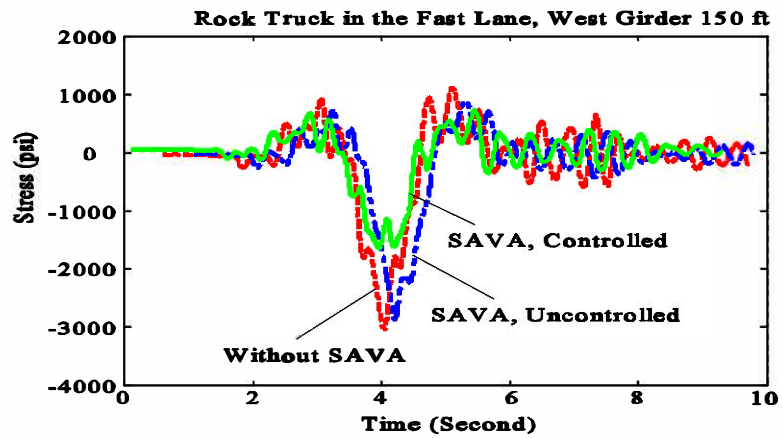
Figure 3.12 Comparison of Dynamic Test, 61 kips Truck Run Over the Left Lane

3.3.3 Impact Factor: Test Results. Figures 3.13 and 3.14 are the field test data in which both the dynamic and static responses, at the same measurement points, are given. The impact is here considered as the ratio of the dynamic maximum stress to the static maximum stress. For example, the rock truck moving in the right lane results in a 25% impact factor, which is within the expected limits assumed by NCHRP 299. The impact factor at the east girder is much higher than the NCHRP 299 guidelines would suggest (30%). A compilation of the impact factors that were recorded for each of the test vehicles at the span center points of the east, central, and west girders, when the truck travels in the right lane, is given in Table 3.6. The impact factors measured when the vehicles traveled in the left lane are recorded in Table 3.7.

Referring to Table 3.6, what is immediately obvious is that the SAVA control dramatically reduces the impact level. A similar observation is made with regard to the data in Table 3.7. Two general observations are also possible. First, the heavy truck appears to produce the smallest impact levels (less vibration). The maximum impact factor on the center girder was produced by the rock truck. In fact, in the two mid-spans (span 2 and 3), the rock truck produces impacts that are almost twice the maximum assumed by NCHRP 299. The results of the impact factor tests were used in the fatigue analysis presented below.
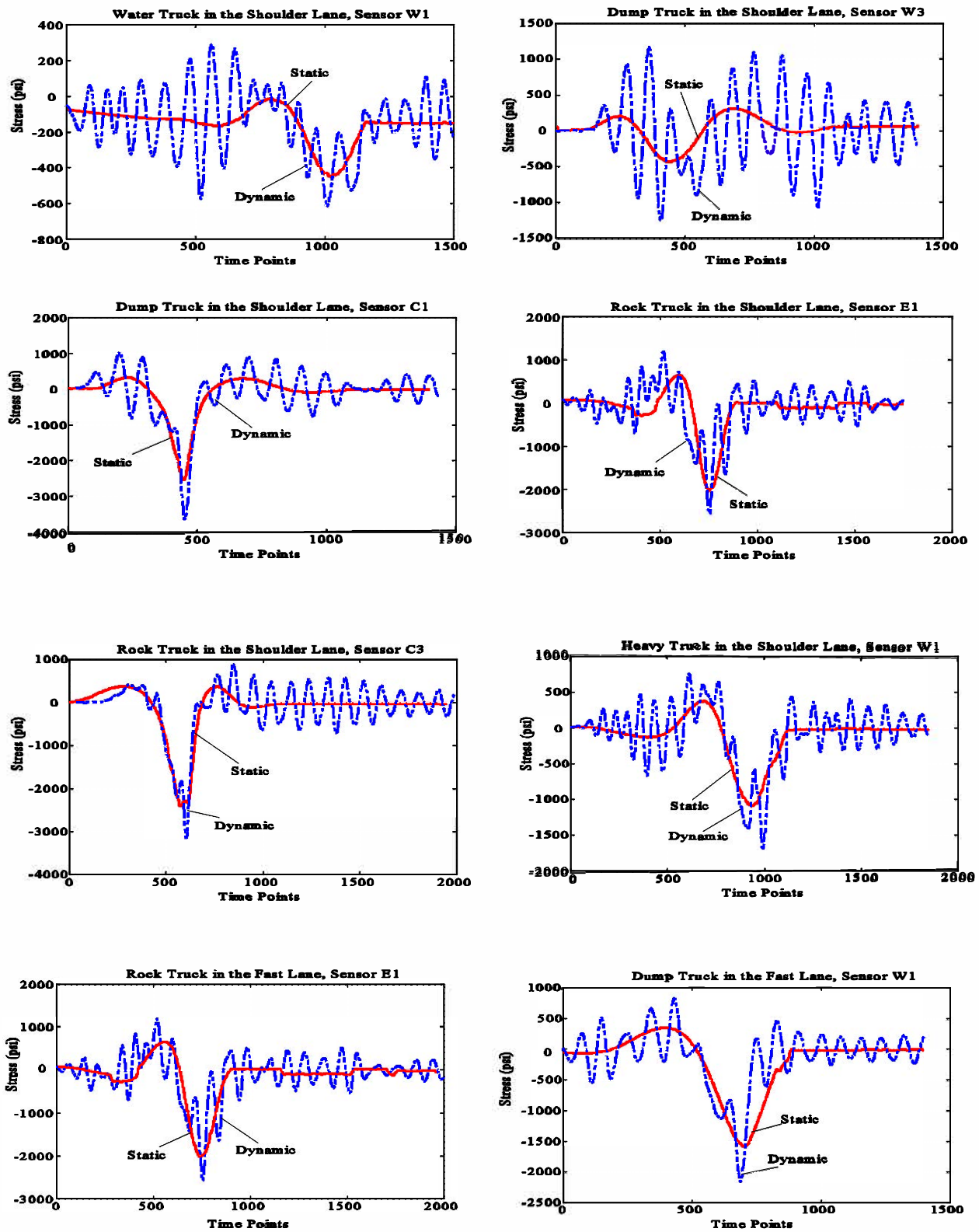
Figure 3.13 Field Test Results, Dynamic vs. Static Responses

29
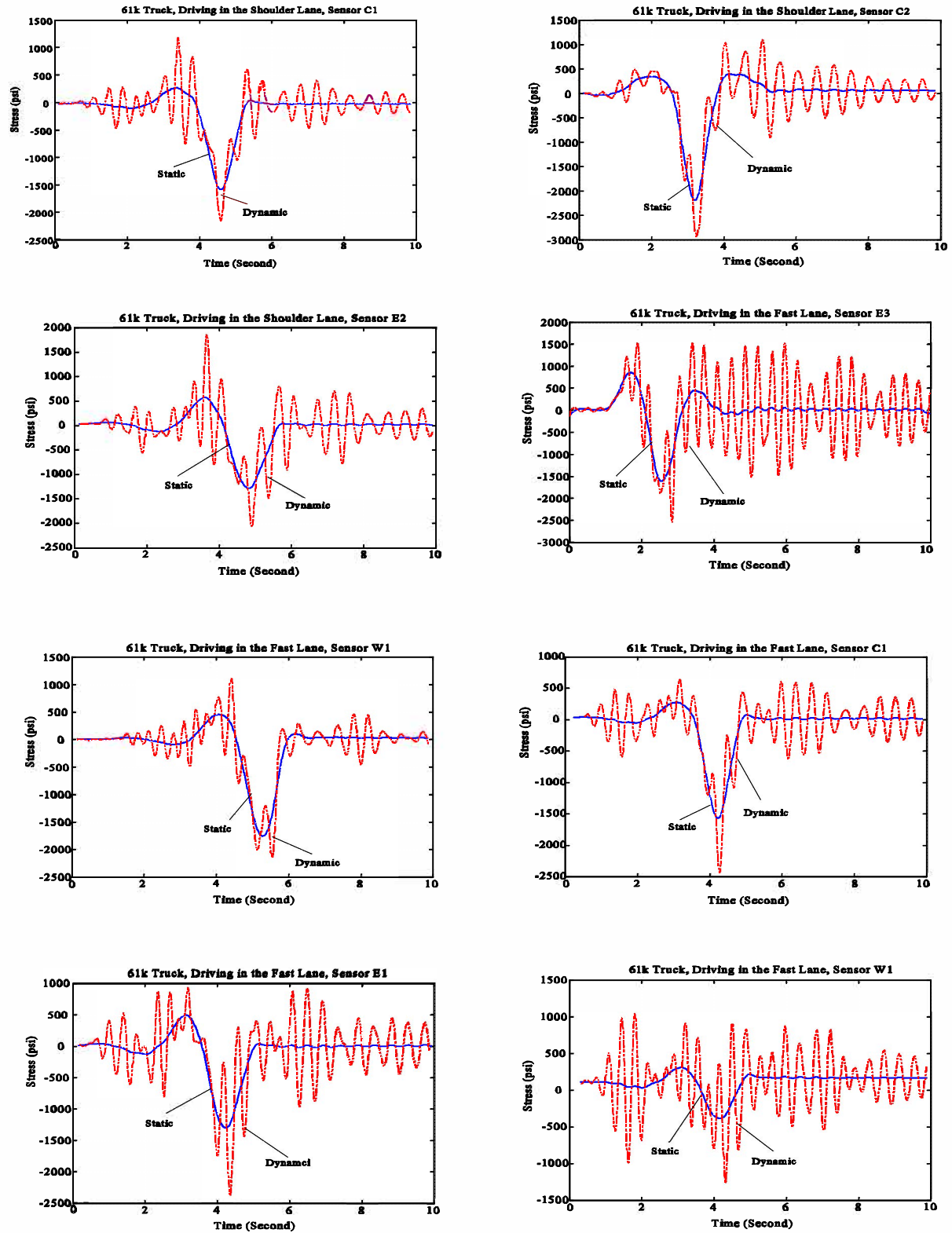
Figure 3.14 61k Truck Field Test Results, Dynamic vs. Static Response

Table 3.6 Impact as a Percentage of Static Load
(Trucks in the Right Lane)

(%)

Test Trucks	Sensor Location											
	E1	E2	E3	E4	C1	C2	C3	C4	W1	W2	W3	W4
Water Truck (26k)	55.6	(36.9)	47.3	28.7	9.7	(5.6)	34.6	5.3	108.8	(48.7)	137.7	/
Dump Truck (54.7k)	110.3	(37.9)	71.7	112	46.7	(5.7)	37.2	33.5	167.8	(137.4)	226.7	/
Rock Truck (79.5k)	40.9	(4.4)	29.9	57.2	55.1	(20.3)	52.4	22.5	222.3	(120.2)	184.6	/
Heavy Truck (120k)	20.1	(2.6)	11.4	5.95	23.9	(13.9)	16.5	8.3	67.1	(33.0)	63.8	/

E --- East Girder, C --- Center Girder, W --- West Girder; Data inside ( ) are from the span with SAVA installed

Table 3.7 Impact As A Percentage of Static Load
(Trucks in the Left Lane)

(%)

Test Trucks	Sensors (Strain Gauges) Location											
	E1	E2	E3	E4	C1	C2	C3	C4	W1	W2	W3	W4
Water Truck (26k)	162.7	(55.0)	140.2	145.7	33.4	(8.4)	40.4	30.1	22.7	(5.0)	34.9	/
Dump Truck (54.7k)	318.8	(227.6)	307.3	323.7	34.7	(42.3)	58.7	81.9	86.0	(31.4)	93.4	/
Rock Truck (79.5k)	148.4	(83.0)	116.9	163.8	20.2	(18.5)	42.0	58.3	40.0	(42.9)	66.6	/
Heavy Truck (120k)	/	/	/	/	/	/	/	/	/	/	/	/

E --- East Girder, C --- Center Girder, W --- West Girder; Data inside ( ) are from the span with SAVA installed

CHAPTER 4

FATIGUE EVALUATION PROCEDURE FOR THE TEST BRIDGE

This chapter provides first a review of the procedures that can be applied to determine the remaining fatigue life of a previously constructed bridge. Those methods are then employed to determine the probable remaining fatigue life of each of the spans of the test bridge. The analysis contrasts the expected fatigue life of the bridge with and without the vibration control system attached. This analysis includes a discussion of the procedures needed to calculate both the remaining safe life and the remaining mean life of the girders of the bridge. The procedure was tailored for application to the test bridge. That approach results in less uncertainty and hence, a more reasonable estimate of remaining life. The fatigue life of the bridge increases remarkably with the application of the structural control system, as the data demonstrates.

4.1 Fatigue Evaluation Procedure (per NCHRP 299): A Review

4.1.1 Scope. This evaluation procedure is applicable to virgin (uncracked and unrepaired) girders subjected to primary stresses that are normally determined by simulation or field test. It does not cover the evaluation of repaired or cracked girders.

4.1.2 Approach. The remaining fatigue life for a critical location is obtained by first determining a nominal stress range at that location for the truck traffic crossing the bridge and, then, calculating the life corresponding to this stress range based on an estimated truck volume. Two different estimates of remaining life can be obtained: the remaining mean life and the remaining safe life. These two different estimates of remaining life provide a useful indication of fatigue safety and facilitate reasonable and cost-effective decisions regarding replacement, maintenance, and the possible retrofit of an aged bridge with a SAVA system.

The remaining mean life reflects a 50% probability that the actual remaining life will exceed the remaining mean life. The remaining mean life is the same for redundant and nonredundant bridge girder systems.

The remaining safe life provides a higher degree of safety. The remaining safe life is different for redundant and nonredundant girders, because different levels of safety are provided for the two cases. **<u>Specifically, the probability that the actual remaining life will exceed the remaining safe life is 97.7% for redundant girders and 99.9% for nonredundant girders</u>**. To achieve these desired levels of safety, appropriate reliability of safety factors are applied to the stress range calculated by the basic procedure. To account for improved analysis accuracy, a safety factor of 1.35 is applied for the procedure calculating the stress range. This safety factor, yields the same probability of failure as the basic procedure.

The ratio of the total mean fatigue life, in cycles to failure, to the total safe fatigue life is constant for various cases (different bridges, detail, etc.). This ratio is about 5 for the redundant girders of this bridge. The ratio of the stress range, corresponding to the mean and safe life, is equal to the cube roots of the ratios (1.71) for a redundant system. The ratio of remaining mean and safe life in years is not the same as the ratio of the total life in cycles to failure, because the life (in years) is not directly proportional to the number of cycles to failure if a compound growth rate is

involved, and the same number (age of the bridge) must be subtracted from the total mean and safe lives to get the remaining mean and safe lives.

4.1.3 Stress Range. The nominal stress range can be obtained either directly from the field testing or from the calculated stress-range histograms obtained from the simulation of the dynamic response of the bridge using the standard fatigue truck. The fatigue damage caused by a given number of cycles of the effective stress range is the same as the damage caused by an equal number of different stress ranges defined by the histograms of stress spectrum. This root-mean-cube formula (Miner's Law), Equation (4.1), is the basis for the AASHTO allowable fatigue stresses.

$$S_{re} = (\Sigma f_i \, S^3_{ri})^{\frac{1}{3}}$$
(4.1)

where f_i is the fraction of stress ranges within an interval i, S_{ri} is the mid width of stress interval i, and S_{re} is the effective stress range.

4.1.4 Standard Fatigue Truck. The fatigue truck represents a composite of different types and weights trucks that might be found in actual traffic. As a high percentage of fatigue damage to a typical U.S. bridge is done by 4- and 5-axle semi-trailers [5], the axle spacing and load distribution of the standard fatigue truck approximates the spacing and load distribution for those multi-axle trucks. Measurements of actual trucks have shown that a spacing of 30' between the main axles is representative of a composite truck. The dual axles on the semi-trailers are represented by single axles on the standard fatigue truck.

The gross weight of the standard fatigue truck used in this evaluation procedure is 54 kips. This is an effective weight that represents the actual truck traffic spectrum from recent (1981) WIM studies [1] that included 30 sites nationwide and more than 27,000 trucks. The WIM measuring systems were undetectable to drivers and included some overweight trucks not found in typical FHWA load meter studies. **A higher gross weight than 54 kips may be used to reflect real growth in truck weights with time.**

4.1.5 Impact Factor. For fatigue evaluations, the impact factor defines the increase in static stress range, rather than the increase of peak stress, and is caused by dynamic effects. The impact factor used for fatigue is intended to be an effective value that averages all trucks in the traffic, rather than a safe extreme value. Theoretically, the effective value for a particular bridge could be obtained by a root-mean-cubed relationship similar to the relationship for effective stress range, but a sufficient quantity of data would rarely be available to permit such a calculation.

The effective impact factor varies considerably from bridge to bridge. It is normally a function of the natural frequency of the bridge or the span length of the bridge, the natural frequencies of the truck suspensions, and the surface roughness and/or the "bump" at the entrance to the bridge. NCHRP 299 suggests then an impact factor of 15% be used to represent an average value of the effective impact factor for bridges with a normal amount of surface roughness, and a good joint at the bridge abutment. (The data obtained during the course of this project indicates that the 15% guideline severely underestimates the actual conditions at the test bridge.)

4.1.6 Section Modules. The section modules of the girders can be obtained by dividing the moment of inertia by the distance from the neutral axis to the expected crack initiation location in the girder. That section modules can

then be used to calculate the stress range, S_r, if a simulation is used. The computed and measured stress values obtained at the Walnut Creek bridge test site agreed closely. This was made possible because the FEM of the bridge and been adjusted to reflect the modal test data, and the field measured position of the neutral axis.

For the composite deck construction, the computed section modules in positive bending regions should be increased by 30%. The factored section modules reflects the section modules of the girders and deck combined. In the test bridge, the 1st and 4th spans of the test bridge have effective composite section modules of 1390 in³ , while the 2nd and 3rd spans have reduced modules of 1140 in³. This difference reflects the common design practice of increasing the flange thickness of continuous girders at the entrance and exit sections of steel bridges.

4.1.7 Reliability Factor. When calculating the remaining mean life, it is unnecessary to apply a reliability or safety factor to the calculated stress range, as this is the best estimate of the actual stress range. In contrast, when calculating the remaining safe life, a reliability or safety factor should be applied to the calculated stress range to achieve a desired level of safety; that is, a desired probability that the actual life will exceed the safe life. The corresponding overall safety factor used for the redundant girder construction employed on the test bridge was 1.35 [1]. This factor incorporates the respective uncertainties of loading, analysis, and fatigue life.

4.1.8 Finite Life. If the maximum stress range for a bridge (based on a fatigue truck analysis), when weighted by the reliability factor, is above the limiting value for infinite life, then the remaining fatigue life must be calculated.

4.1.9 Remaining Safe Life (NCHRP 299). The measured stress range of the Walnut Creek bridge for two test truck is compared to S_c in Table 4.1, where S_c is the compressive dead load stress which can be employed to check the finite life of a highway bridge [5]. The remaining safe life (Y_f , in years) or the remaining mean life (Y_m , in years) corresponding to the factored stress range, $R_s \times S_{re}$, can be calculated from

$$Y_f = \frac{f \times K \times 10^6}{T_a \times C \times (R_s \times S_{re})^3} - a \tag{4.2}$$

in which: T_a = the estimated lifetime average daily truck volume; C = the cycles per truck passage counted using the rainflow technique; a = the present age of the bridge in years ; $R_s \times S_{re}$ = the factored stress range obtained from testing or simulation; R_s = reliability factor; K = the detail constant; f = a factor to account for the difference between the mean and allowable SN curves. Specific values of the parameters used in Equation (4.2) are defined in a later section.

Table 4.1 Infinite Fatigue Lives Checking of the Walnut Creek Bridge

Critical Points	Comparison of Sc vs. Measured Stress Range (ksi)		Finite Life Check Required
	Dump Truck	Rock Truck	
E1	5.06 >A	4.93 >A	Yes
E2	5.74 >B	5.28 >B	Yes
E3	7.06 >B	5.47 >B	Yes
E4	4.70 >A	3.96 >A	Yes
C1	6.91 >A	4.39 >A	Yes
C2	8.39 >B	5.23 >B	Yes
C3	7.71 >B	5.11 >B	Yes
C4	8.31 >A	5.64 >A	Yes
W1	8.64 >A	7.02 >A	Yes
W2	6.97 >B	5.55 >B	Yes
W3	7.36 >B	5.76 >B	Yes
W4	/	/	/

Note: A = 3.60 ksi, the Sc for the 1st and 4th spans; B = 4.40 ksi, the Sc for the 2nd and 3rd spans.

The estimated lifetime average daily truck volume T_a, was calculated using reference [1], which relies on the present truck volume, T, the present age of the bridge, a, and the compound annual growth rate, g. According to the recent traffic investigation by ODOT, the total daily traffic volume in two-direction traffic is designed to be 18,800 or 9,400/day in one-direction (from 1970, 26 years ago). Assuming 30% of the traffic are trucks and 85% of those trucks are in the shoulder or slow lane, then $9,400 \times 30\% \times 85\% = 2,397$. Assuming a growth rate of 4%, then the average daily truck volume in the shoulder lane adjusted for future growth is: $T_a = 2,397 \times 1.3 = 3,116$.

4.1.10 Detail Constant K and SN Curve. The SN diagram has an endurance of fatigue limit, S_e, which is a stress level below which the material has an "infinite" life. When evaluating fatigue life, the "infinite" life of the bridge is assumed to be 2×10^6 and the endurance fatigue limit is equal to 0.367 times the present AASHTO allowable stress range for the design of the bridge [1]. When the factored stress range is below this value, all of the stress cycles in the spectrum are below the constant amplitude fatigue limit.

The test bridge falls in the "C" category [1]. The mean stress range, S, that the girders can sustain for a given number of cycles, N, is given by

$$NS_{95}{}^b = A \tag{4.3}$$

Fisher et al., [18] proposed that the slope b be taken as 3.0 and also proposed values of A for each detailed category, where A is the intercept at 2,000,000 cycles. The value of A, together with the slope 3.0, defines the fatigue strength of each category, and is the basis for the present AASHTO allowable fatigue stresses for that category. For convenience in calculating the remaining life in years, a new detail constant, K, is used in the fatigue evaluation of the bridge. K is related to A by the simple relationship:

$$K = \frac{A}{365 \times 10^6} \tag{4.4}$$

The value of K for the detailed category "C" is 12 [1].

The allowable and mean SN curve for a given detail are assumed to be parallel on a log-log plot. Consequently, the ratio of stress ranges for the two curves is the same at all cyclic lives. For Categories B through E', the ratio of mean to allowable stress range does not vary greatly and averages 1.243. Because of the power of 3 in the fatigue Equation (4.1), the corresponding ratio of mean to safe lives is equal to 1.92. The average ratio of mean to safe lives for Categories A to F is 2.05. Thus, the value of f which is a constant in the SN equation, is taken as 2.0 while calculating mean life in this fatigue evaluation of this bridge. The value of f is 1.0 for calculating the remaining safe life.

4.1.11 Other Modifying Factors.   Usually, the corrosion factor is an important factor in considering the SN curve of the bridge. **For most steel bridges, the fatigue life is not significantly affected by corrosion.** Therefore, corrosion is not considered in the fatigue evaluation of this bridge. However, if there is some unsuitable design details and unusual environmental conditions, then they can increase susceptibility of the bridge to corrosion. A study by NCHRP (Project 10-22) details the relationship between corrosion of bridge members and fatigue life. This study was made specifically for weathering steels, but most of the conditions that contribute to corrosion of such steels also apply to painted steels. NCHRP project 12-18 [7], "Guidelines for Evaluating Corrosion Effects in Existing Steel Bridges," describes guidelines for evaluating corrosion effects in existing steel bridges.

4.1.12 Damage Summing Method-Miner's Rule.   To account for the damage accumulation caused in the past years and to predict the remaining life of the test bridge, both the effective stress ranges concept and the linear damage rule have been used here. The linear damage rule is commonly known as Miner's Law. In Miner's Law, the "cycle ratio" is defined as n/N, where n is the number of cycles at stress level S and N is the fatigue life in cycles at stress level S; the damage fraction, D, is defined as the fraction of life depicted by an event or a series of events, and the damage fraction, D_i, at stress level S_i is equal to the cycle ratio, n_i/N_i. Failure is assumed to occur when the summation of damage fractions equals 1, or

$$\Sigma D_i = \Sigma \frac{n_i}{N_i} \geq 1 \tag{4.5}$$

At any critical location on the test bridge, the damage fraction D, caused in the past years can be obtained from the average daily truck volume (T_a), the past years (a), and the effective stress level (S_r). For the uncontrolled case, the effective stress level at this location was assumed to be the same in the future as in the past, its fatigue life (N) is

a constant. For the controlled case, the stress level is changed in the future, the fatigue life (N) will change also. Once the damage caused in the past at the old stress level is accumulated, both the remaining live for the two cases can be obtained based on using the old and new stress levels, respectively.

4.2 Rainflow Cycle Counting (A Review)

To predict the life of a component, it is necessary to reduce its complex load history into a number of events which can be compared to the available constant amplitude test data. This process of reducing a complex load history into a number of constant amplitude events involves what is termed "cycle counting".

Rainflow counting has become a generic term that describes any cycle counting method which attempts to identify closed hysteresis loops in the stress-strain response of a material subjected to cyclic loading. At present, a number of rainflow counting techniques are in use. If the stress-time history being analyzed begins and ends at the stress value having the largest magnitude, whether it occurs at a peak or valley, all of the methods will yield identical results. However, if an intermediate stress value is used as a starting point, these methods will yield results that are similar but not identical in all cases. While rainflow counting can be completed manually for relatively simple load histories in simulation, more complex loading histories, such as the field test results, the method is better implemented through the use of computers. The following text reviews the rainflow counting method.

The reversals included in a complex cycle cause the same amount of fatigue damage as individual simple cycles of the same size; therefore, the complex cycle is first decomposed into several individual cycles of different sizes that are represented by an equivalent number of cycles of the same size. The method of decomposing the complex cycle is the key to the rainflow method.

The complex cycle begins and ends at the same moment, the base moment, which means the time history has been removed from the effects of the offset and preload of the bridge. The complex cycle consists of three stages. Stage 1 is between the beginning and the minimum moment (or stress, strain and voltage output) of the cycle; Stage 2 is between the minimum moment and the maximum moment of the cycle; Stage 3 is between the end and the maximum moment. If the entire curve is above or below the base stress, Stage 2 does not exist.

The complex cycle can then be decomposed into a primary cycle and one or more higher order cycles. The algebraic difference between the maximum and the minimum moment is the moment range for the primary cycle. Each higher order cycle begins and ends at the same moment referred to as the base moment for that cycle. Each higher order cycle has one peak or valley, and the algebraic difference between this peak and valley and the base moment for that cycle is the moment range for the cycle. A cycle of any order may include higher order cycles.

Within each stage, the primary cycle follows a path without reversal. When the path of the complex cycle reverses within a stage, the primary cycle moves vertically to intersect its path at a later point. This vertical line is the base moment for the next higher order cycle. Fatigue damage is proportional to the moment range, S_r, cubed and the stress range is proportional to the moment range. Thus, each higher order cycle makes $(M_{ri}/M_{rp})^3$ times as much damage as the primary cycle, and the equivalent number of cycles (primary cycles) for a complex cycle is

$$N_e = 1 + \left(\frac{M_{r1}}{M_{rp}}\right)^3 + \left(\frac{M_{r2}}{M_{rp}}\right)^3 + \ldots + \left(\frac{M_{rn}}{M_{rp}}\right)^3 \tag{4.6}$$

in which, M_{rp} is the moment range for the primary cycle, and M_{ri} is the moment range for a higher order cycle. Thus, Equation (4.6) consequently neglects any effects of fatigue limit and the mean value of the moment on the equivalent number of cycles.

The foregoing procedure can be clarified through the use of an example. Figure 4.1 shows a moment history and the resulting count procedure in the rainflow counting methods. The following discussion describes the manner in which each rainflow path was determined. As shown in Figure 4.1, the given moment time history begins and ends at the moment value of greatest magnitude (point A). Rainflow is initiated at each reversal in the moment history.
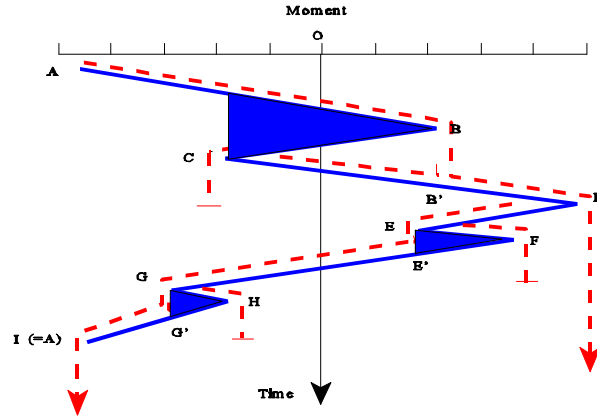
Figure 4.1 Rainflow Counting Demonstration

(1) Rain flows from A over B and D and continues to the end of the history since none of the conditions for stopping rainflow are satisfied.

(2) Rain flows from B over C and stops opposite D, since both B and D are local maximums and the magnitude of D is greater than B.

(3) Rain flows from C must stop upon meeting the rain flow from A.

(4) Rain flows from D over E and G and continues to the end of the history , since none of the conditions for stopping rainflow are satisfied.

(5) Rain flows from E over F and stops opposite G, since both E and G are local minimums and the magnitude of G is greater than E.

(6) Rain flows from F must stop upon meeting the rainflow from D.

(7) Rain flows from G over point H and stops opposite A, since both G and A are local minimums and the magnitude of A is greater than G.

(8) Rain flows from H and must stop upon meeting the rainflow from D.

Having completed the above, we combine events to form complete cycles. In this example, events A-D and D-I are combined to form a full cycle. Event B-C combines with event C-B (of moment range C-D) to form an additional cycle. Similarly, cycles are formed at E-F-E and G-H-G .

As a practical example, the rainflow counting process for one time history obtained from the test bridge, at the point of Center Beam, North 350', is illustrated in Figures 4.2 and 4.3.1 thru 4.3.3.

First, the original time history was filtered, the offset was removed, the smaller moment ranges were neglected, and finally the peaks and valleys were chosen (Figure 4.3.2).
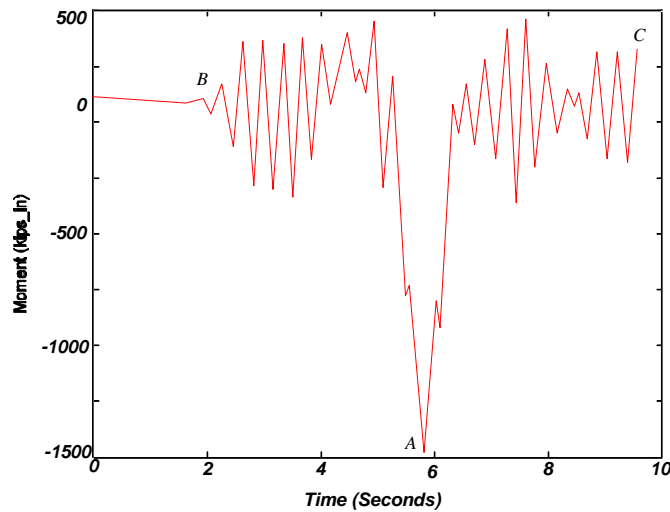
Figure 4.2 Test Sample, Peak-Value Values
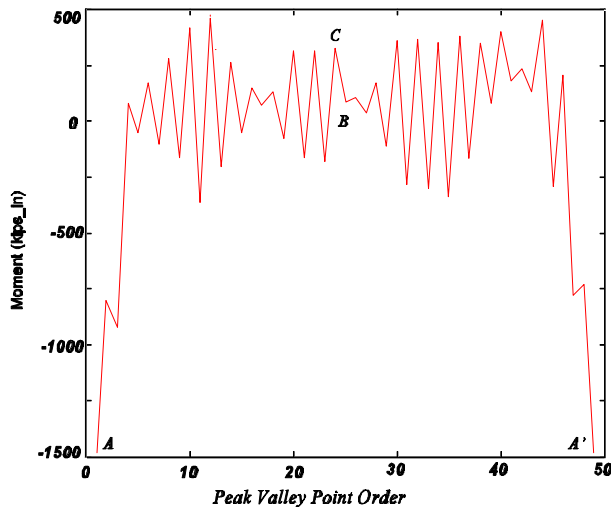
Figure 4.3.1 Rearranged Peak-Value Values
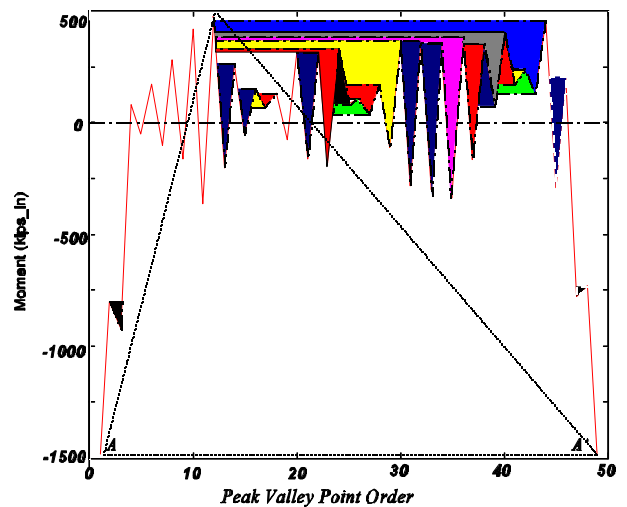
Figure 4.3.2 Counted Closed Cycles
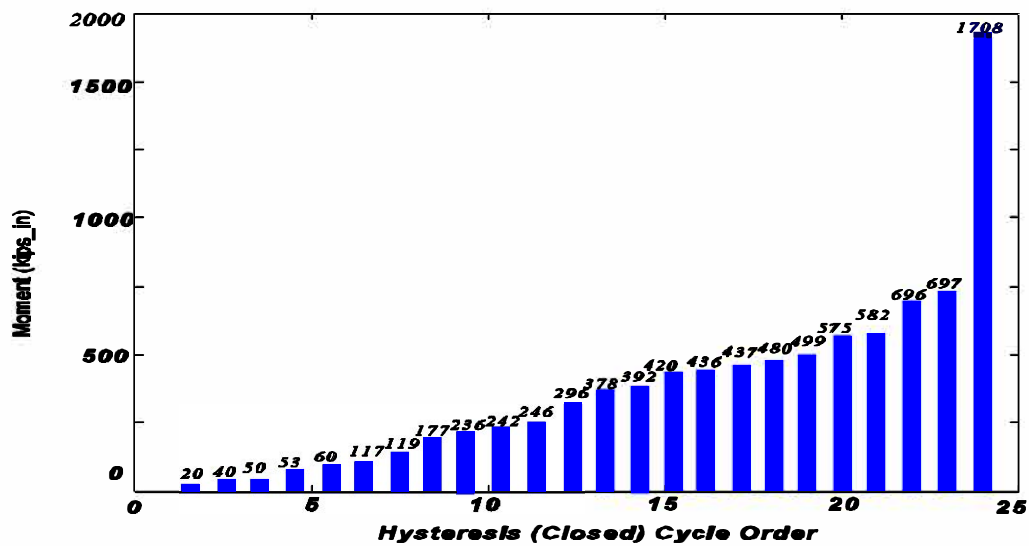
Figure 4.3.3 Rainflow Counting Results

Next, the peak-valley history was rearranged as the beginning and ending at the moment value of greatest magnitude (point A), and the points B and C were connected.

Finally, the effective cycle of this history can be calculated by substituting the values in Figure 4.3.3 into Equation (4.14), and all the effective cycles for different test trucks were obtained using the same procedure. They are listed in Tables 4.2 to 4.5.

Table 4.2 Effective Stress Cycles Via Rainflow Counting;
Uncontrolled Response (Right Lane, 65 mph)

Test Trucks	Sensors (Strain Gauges) Location											
	E1	E2	E3	E4	C1	C2	C3	C4	W1	W2	W3	W4
Water Truck (26k)	1.323	1.286	1.230	1.551	1.085	1.002	1.041	1.184	2.577	1.974	2.127	/
Dump Truck (54.7k)	1.694	1.429	1.605	1.847	1.663	1.063	1.161	1.212	3.519	2.979	3.101	/
Rock Truck (79.5k)	1.264	1.728	1.917	1.857	1.631	1.144	1.271	1.362	3.163	2.479	3.018	/
Heavy Truck (120k)	1.079	1.087	1.169	1.128	1.062	1.046	1.061	1.040	1.416	1.866	1.703	/

E --- East Girder, C --- Center Girder, W --- West Girder, / --- No Data

40

**Table 4.3 Effective Stress Cycles Via Rainflow Counting;
Uncontrolled Response, (Left Lane, 65 mph)**

Test Trucks	Sensors (Strain Gauges) Location											
	E1	E2	E3	E4	C1	C2	C3	C4	W1	W2	W3	W4
Water Truck (26k)	2.050	2.120	2.061	2.753	1.193	1.262	1.116	/	1.045	1.518	1.435	/
Dump Truck (54.7k)	2.967	2.092	2.023	2.169	1.639	1.055	1.354	1.393	1.155	1.741	1.327	/
Rock Truck (79.5k)	1.186	1.126	1.500	2.223	1.004	1.005	1.027	1.012	1.003	1.006	1.020	/
Heavy Truck (120k)	1.776	1.798	2.056	2.571	1.015	1.018	1.091	1.131	1.009	1.007	1.062	/

E --- East Girder, C --- Central Girder, W --- West Girder, / --- No Data

**Table 4.4 Effective Stress Cycles Via Rainflow Counting;
Controlled Response, (Right Lane, 65 mph)**

Test Trucks	Sensors (Strain Gauges) Location											
	E1	E2	E3	E4	C1	C2	C3	C4	W1	W2	W3	W4
Water Truck (26k)	1.495	1.656	2.182	1.834	1.056	1.013	1.180	1.146	2.265	2.413	3.408	/
Dump Truck (54.7k)	1.864	1.547	1.974	1.856	1.130	1.207	1.189	1.172	2.864	3.025	2.197	/
Rock Truck (79.5k)	1.446	1.361	1.252	1.272	1.260	1.214	1.387	1.242	2.763	2.778	2.871	/
Heavy Truck (120k)	1.079	1.087	1.169	1.128	1.063	1.028	1.080	1.065	1.536	1.910	1.763	/

E --- East Girder, C --- Center Girder, W --- West Girder, / --- No Data

Table 4.5 Effective Stress Cycles Via Rainflow Counting;
Controlled Response, (Left Lane, 65 mph)

Test Trucks	Sensors (Strain Gauges) Location											
	E1	E2	E3	E4	C1	C2	C3	C4	W1	W2	W3	W4
Water Truck (26k)	2.211	2.523	2.314	2.258	1.143	1.021	1.133	1.301	1.064	1.082	1.065	/
Dump Truck (54.7k)	2.617	3.084	2.674	2.902	1.491	1.675	1.778	1.715	1.307	1.407	1.251	/
Rock Truck (79.5k)	1.308	1.159	1.195	1.518	1.007	1.010	1.017	0	1.003	1.013	1.013	/
Heavy Truck (120k)	/	/	/	/	/	/	/	/	/	/	/	/

E --- East Girder, C --- Center Girder, W --- West Girder

4.3 Remaining Fatigue Life of Walnut Creek Bridge

The purpose of this section is to demonstrate the effectiveness that the SAVA has on the fatigue life remaining of the test bridge. **The projections are based entirely on the measurements obtained from field tests conducted at the test bridge**.

Three different tests were employed:

(1) pre SAVA (prior to installation of SAVA),

(2) post SAVA-Passive-SAVA system operated as a system of simple non-adjusting dampers, and

(3) post SAVA-Semiactive-SAVA system operated as a system of automatically adjustable stiffness/dampers.

In each case, a calibrated truck was traveled over the bridge at or near the posted speed limit. As described above, the test was conducted with escort vehicles, which were used to slow down vehicles behind the test truck. The traffic control made it possible to have the truck on the bridge without other vehicles. In fact, there were no other vehicles on the bridge for 10 seconds before the truck reached the bridge and for an additional 10 seconds after the truck had completely traversed the bridge.

What is important to note is that the trucks used represent a spectrum of the vehicles that typically cross the bridge. The dynamic response of the bridge to each truck passing was recorded and used directly in the remaining life formula, Equation (4.1). What is produced is a comparison of the projected life remaining between the SAVA uncontrolled and controlled operation of the bridge. In each case, the basic parameters are $f = 1$ (for the remaining safe life) or $f = 2$ (for the remaining mean life); $K = 12$; $T_a = 3116$; and $R_s = 1.0$ (for the remaining mean life) or $R_s = 1.35$ (for the remaining safe life). The cycle count C is listed in Tables 4.2 through 4.5. The results of the remaining life analysis are listed in Tables 4.6 through 4.9.

<p align="center">Table 4.6 Remaining Safe Life (Ys) Evaluation,
Based on Water Truck, Dump Truck, Rock Truck, and Heavy Truck Dynamic Test (Years)</p>

Critical Points	E1	E2	E3	E4	C1	C2	C3	C4	W1	W2	W3	W4
Water Truck (26.7 klbs)												
No Control	369.6	244.7	176.5	353.1	480.5	214.5	161.1	419.2	676.5	440.8	561.5	/
Controlled	368.8	(2614)	210.5	335.7	493.7	(855.2)	175.6	391.1	406.8	(3334)	566.5	/
Dump Truck (54.7 klbs)												
No Control	-13.9	-8.05	-17.0	-12.5	-12.1	-11.0	-8.52	-11.4	-0.42	1.49	1.62	/
Controlled	-14.8	(213.8)	-17.3	-11.4	-12.7	(38.5)	-8.12	-10.7	-1.46	(66.4)	2.94	/
Rock Truck (79.5 klbs)												
No Control	-8.0	-12.4	-14.8	-9.1	-11.2	-13.7	-13.1	-9.1	-7.1	0.4	1.2	/
Controlled	-8.5	(167.7)	-15.4	-9.6	-11.9	(35.8)	-12.7	-10.5	-8.0	(110.5)	0.0	/
No SAVA	-15.2	-17.8	-17.9	-14.7	-17.0	-17.4	-17.2	-13.7	-13.6	-10.6	-9.6	/
Heavy Truck (120 klbs)												
No Control	-16.1	-3.37	-18.2	-10.6	-18.7	-18.3	- 19.5	-17.6	-14.3	15.0	-11.8	/
Controlled	-16.1	(260.6)	-18.9	-12.0	-18.5	(-6.73)	-19.8	-16.7	-14.8	(96.1)	-12.6	/

Note: The data shown in parentheses is the fatigue life at the points of span with SAVA installed.

Table 4.7 Remaining Mean Life (Ym) Evaluation,
Based on Water Truck, Dump Truck, Rock Truck, and Heavy Truck Dynamic Test (Years)

Critical Points	E1	E2	E3	E4	C1	C2	C3	C4	W1	W2	W3	W4
Water Truck (26.7 klbs)												
No Control	1917	1307	966.9	1836	2461	1154	890.8	2159	3424	2266	2862	/
Controlled	1914	(12963)	1134	1753	2526	(4306)	962.8	2022	2098	(16495)	2887	/
Dump Truck (54.7 klbs)												
No Control	29.5	58.4	14.3	36.5	38.6	43.7	56.1	42.0	95.9	105.3	107.0	/
Controlled	26.2	(1150)	13.2	42.0	35.6	(288.0)	58.1	45.3	90.8	(424.8)	112.5	/
Rock Truck (79.5 klbs)												
No Control	58.7	37.1	25.3	53.1	42.8	30.7	33.4	53.2	62.9	99.1	104.1	/
Controlled	55.9	(923.0)	22.2	51.0	39.7	274.1	35.5	46.6	58.9	(640.9)	98.3	/
No SAVA	21.4	9.2	8.2	23.9	12.6	10.7	11.7	28.6	28.9	43.3	48.0	/
Heavy Truck (120 klbs)												
No Control	22.5	85.4	12.2	49.7	10.0	11.8	6.08	15.6	31.8	175.7	43.7	/
Controlled	22.9	(1385)	9.9	42.9	11.1	(68.8)	4.30	20.0	29.0	(574.6)	39.6	/

Note: The data shown in parentheses is the fatigue life at the points of span with SAVA installed

Table 4.8 Remaining Safe Life (Ys) of Walnut Creek Bridge,
SAVA No Control vs. SAVA Controlled (years)

Critical Points		E2,	Difference	C2,	Difference	W2,	Difference
Water Truck							
No Control	Ys	244.7		214.5		440.8	
Controlled	Ys	2614	**2369.3**	855.2	**640.7**	3334	**2893.2**
Dump Truck							
No Control	Ys	-8.10		-11.0		1.49	
Controlled	Ys	213.8	**221.9**	38.5	**49.5**	66.4	**64.9**
Rock Truck							
No Control	Ys	-12.4		-13.7		0.40	
Controlled	Ys	167.7	**180.1**	35.8	**49.5**	110.5	**110.1**
Heavy Truck							
No Control	Ys	-3.37		-18.3		15.0	
Controlled	Ys	260.6	**264.0**	-6.73	**11.57***	96.1	**81.1**

*The SAVA control system is not very effective to the heavy truck which has small dynamic impact

Table 4.9 Remaining Mean Life (Ym) of Walnut Creek Bridge,
SAVA No Control vs. SAVA Controlled (years)

Critical Points		E2,	**Difference**	C2,	**Difference**	W2,	**Difference**
Water Truck							
No Control	Ym	1307		1154		2266	
Controlled	Ym	12963	**11656**	4306	**3152**	16495	**14229**
Dump Truck							
No Control	Ym	58.4		43.7		105.3	
Controlled	Ym	1150	**1091.6**	288.0	**244.3**	424.8	**319.5**
Rock Truck							
No Control	Ym	37.1		30.7		99.1	
Controlled	Ym	923.0	**885.9**	274.1	**243.4**	640.9	**541.8**
Heavy Truck							
No Control	Ym	85.4		11.8		175.7	
Controlled	Ym	1385	**1299.6**	68.8	**57.0**	574.6	**398.9**

4.4   Observations

What is most obvious is that the SAVA control system effects a tremendous change in the projection of remaining life for every vehicle tested. **That is the entire point of the exercise**. It matters not what truck is used, the increase in the safe life is no less than 50 years. One might wonder what the outcome might have been had a standard fatigue truck been used in the test. Of course, the standard fatigue truck (used for design) does not include a compliant chassis. The test results at the bridge make it very clear that no matter what kind of suspension used, the dynamic interaction of the bridge and an actual truck produces actual impact factors that are 2 to 5 times larger than that suggested by NCHRP 299. On the other hand, the data presented here produces far more conservative results than the hypothetical fatigue truck. In fact, the 57 klbs dump truck, with a 14' long wheel base produces a dynamic response that will always produce loading conditions that exceed any fatigue truck analysis.

The essential observation is that the controlled SAVA system can extend service life by a minimum of five decades.

REFERENCES

[1] F. Moses, C.G.Schilling, and K.S.Raju, National Cooperative Highway Research Program Report 299, "Fatigue Evaluation Procedures for Steel Bridges", Case Western Reserve University, Cleveland, Ohio, November, 1987.

[2] Mark F. Green, David Cebon, and David J. Cole, "Effects of Vehicle Suspension Design on Dynamics of Highway Bridges", Journal of Structural Engineering, Vol. 121, No. 2, February, 1995.

[3] Julie A. Bannantine, Jess J. Comer, James L. Handrock, "Fundamentals of Metal Fatigue Analysis", Prentice Hall, Englewood Cliffs, New Jersey 07632.

[4] Thomas D. Gillespie, "Fundamentals of Vehicle Dynamics", Society of Automotive Engineers, Inc. 400 Commenwealth Drive, Warrendale, PA 15096-0001.

[5] "Recommendations for the Fatigue Design of Structures", European Convention for Constructional Steelwork, Sept. 24, 1982.

[6] "Recommended Design Loads for Bridges," by the ASCE Committee on Loads and Forces on Bridges, P. G. Buckland, Chmn., Journal of the Structural Division, ASCE, Vol. 107, No. ST7, July, 1981.

[7] "Steel, Concrete, and Composite Bridges, Part 10: Code of Practice for Fatigue", BSI BS 5400, British Standards Institute (England), 1980.

[8] Schilling, C. G., et al., "Fatigue of Welded Steel Bridge Members Under Variable-Amplitude Loadings", NCHRP Report 188,1978.

[9] Schilling, C. G., and Klippstein, K. H., "New Method for Fatigue Design of Bridges", Journal of the Structural Division, ASCE, Vol. 104, No ST#, March, 1978.

[10] Miner, M. A., "Cumulative Damage in Fatigue", Transactions of the American Society of Mechanical Engineers, Vol. 67, 1945.

[11] "Standard Specifications for Highway Bridges:, 13th ed., AASHTO, 1983 and Interim Specifications through 1986.

[12]. Albrecht, P., "Analysis of Fatigue Reliability:, Department of Civil Engineering, University of Maryland, College Park, MD, Jan., 1981.

[13] Albrecht, P., and Duerling, K., "Probabilistic Fatigue Design of Bridges for Truck Loading", Department of Civil Engineering, University of Maryland, College Park, MD, Jan., 1979.

[14] Albrecht, P., "Fatigue Reliability Analysis of Highway Bridges", Department of Civil Engineering, University of Maryland, College Park, MD, Jan., 1982.

[15] Albrecht, P., and Naeemi, A. H., "Performance of Weathering Steel in Bridges", NCHRP Report 272, July, 1984.

[16] Albrecht, P., and Friedland, I. M., "Fatigue Limit Effect on Variable Amplitude Fatigue of Stiffeners", Journal of the Structural Division, ASCE, Vol. 105, No. ST212, Dec., 1979.

[17] Fisher, J. W., et al., "Detection and Repair of Fatigue Damage in Welded Highway Bridges", NCHRP Report 206, June, 1979.

[18] Fisher, J. W., et al., "Fatigue Strength of Steel Beams with Welded Stiffeners and Attachments", NCHRP Report 147, 1974.

[19] Fisher, J. W., et al., "Effect of Weldments on the Fatigue Strength of Steel Beams", NCHRP Report 102, June, 1970.

SEMIACTIVE VIBRATION ABSORBERS (SAVA) AT THE I-35 WALNUT CREEK BRIDGE

A PROJECT FUNDED BY OKLAHOMA DEPARTMENT OF TRANSPORTATION

ODOT PROJECT ENGINEER: DAVID OOTEN, PE

SUB-REPORT # 3:

VEHICLE DYNAMICS MODELING, AND TESTING

CENTER FOR STRUCTURAL CONTROL
UNIVERSITY OF OKLAHOMA
http://www.coe.ou.edu/research/cstructc/

PROJECT MANAGER:

WILLIAM N. PATTEN, Ph. D, P.E., (PI)

RESEARCH ENGINEERS:

JINGHUI SUN, Ph. D.
GANG SONG, Ph. D.
GUANGJUN LI
JAESOO LEE

AUGUST, 1997

TABLE OF CONTENTS

Nomenclature

$m_{1..6}$	mass	kg
$Z_{1..7}$	displacement	m
θ_1, θ_2	rotation	radius
Z_{d1}, Z_{d9}, Z_{d3}, Z_{d4}	road profiles at the points of tire contact	m
$K_{1..8}$	stiffness coefficient	N/m
$C_{1..8}$	damping coefficient	N/(m/s)
J_{G5}, J_{G6}	intertia	kgm/s
K_s	stiffness of suspension	N/m
K_t	stiffness of tire	N/m
M	sprung mass	kg
m	unsprung mass	kg
C_s	damping coefficient	N/(m/s)
Z	displacement of sprung mass	m
Z_r	road profile	m
Z_u	dispalcement of unsprung mass	m

Introduction

The development of a retrofit control technology for bridge could only be accomplished with a clear understanding of how heavy trucks interact with the structure when they travel over the bridge. Described in this section are various findings and observations about truck and truck/bridge dynamics that were used ultimately to craft an effective control design for the SAVA system. We first review the results of quasi-static crawl tests for various trucks. Next, observations are made on the dynamic response of the bridge when those trucks cross the bridge at/or near the posted speed limit. Next we describe the process used to model the very important chassis compliance of a test vehicle. We then present comparisons of the simulated response of the bridge/truck with actual field data. Next we describe the results of certain field tests that indicate the very strong coupling that naturally occurs between the truck chassis and the bridge. The section closes with experimental evidence that proves that when the SAVA system is used to control the bridge, the degree of dynamic coupling between the truck and the bridge is substantially reduced.

1.   Crawl Tests

Four trucks were used to test the bridge quasi-statically. Figure 1.1 presents the wheel loading and axle spacing of these four trucks. The water truck and the dump truck are owned by ODOT. The rock truck is owned by Cleveland County, OK, District 2, and the heavy truck is owned by Dolese Brothers Inc. of OKC. The guasi-static tests were conducted with traffic control provided by ODOT and the Oklahoma Highway Patrol. Traffic was stopped just prior to each test. The trucks were traveled in the right lane at approximately 1 mile/hour. The test results are shown in Figures 1.1 thru 1.4. The time traces are the scaled output of the strain gauges mounted at the bottom flange in the center in each span of the east girder.
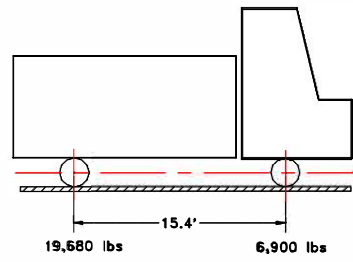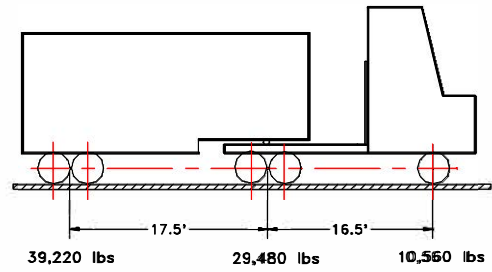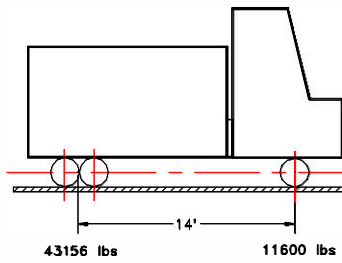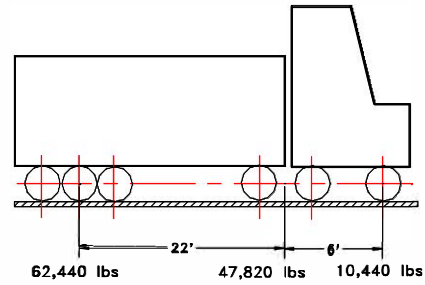
Figure 1.1 Test Trucks' Wheel Loads and Axle Spacing
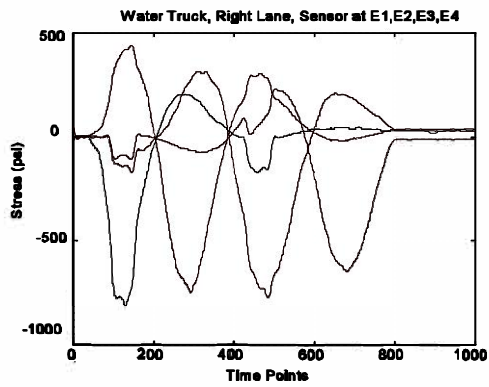
Figure 1.2 Crawl Test Data of Water Truck
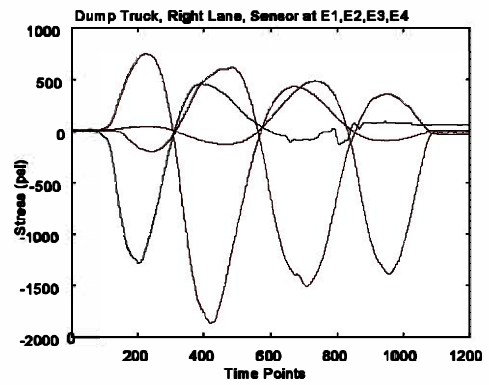
Figure 1.3 Crawl Test Data of Dump Truck

2
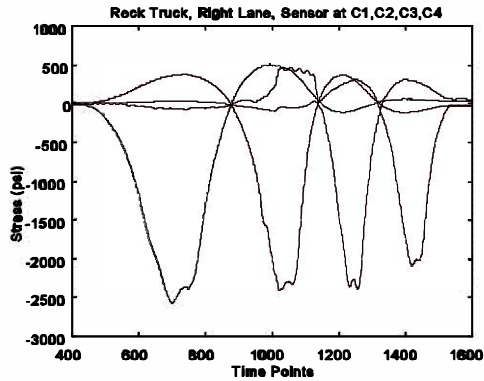
Figure 1.4 Crawl Test Data of Rock Truck   **Figure 1.5 Crawl Test Data of Heavy Truck**
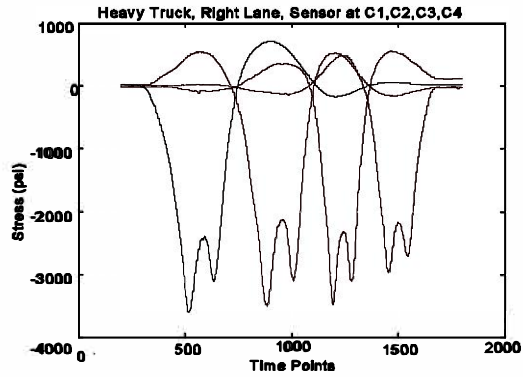
This test data, along with the modal test data (see Subrepot # 2) was used to tune and validate FEM of the bridge.

2.   Dynamic Truck Testing

Almost all of the truck tests were conducted at or near the posted speed limit (70 mph). Those tests were conducted with vehicles that slowed down trailing traffic to 50 mph. This made it possible to drive the test truck across the bridge with no other vehicles on the bridge. Tests were conducted in both the right and left lanes of the two lane bridge. The tests were conducted prior to installation of the SAVA system. Tests were also conducted after the SAVA system was installed. Four modes of SAVA operation were tested:

(1) With control,

(2) With the valves open (the SAVA actuator acts like a simple viscous damper in this mode),

(3) The valve closed (the SAVA system becomes a fixed stiffener), and

(4) With the fluid drained from the actuator (the SAVA system provides no resistance to the vibration; this mode is equivalent to not having the SAVA system installed).

The results of those various tests were used in the modal analysis, the control design, and the fatigue analysis. Limited space makes it impossible to reproduce anything but a few examples of the test results. The data presented here provides a typical example of time histories obtained when the vehicles were traveled over the bridge prior to the installation of SAVA. The results are posed so as to indicate the actual impact levels that occur.

Presented here are the scaled output of various strain gauges. Figure ?.6 from Subreport #2 is reproduced here to show the strain gauge locations.

3
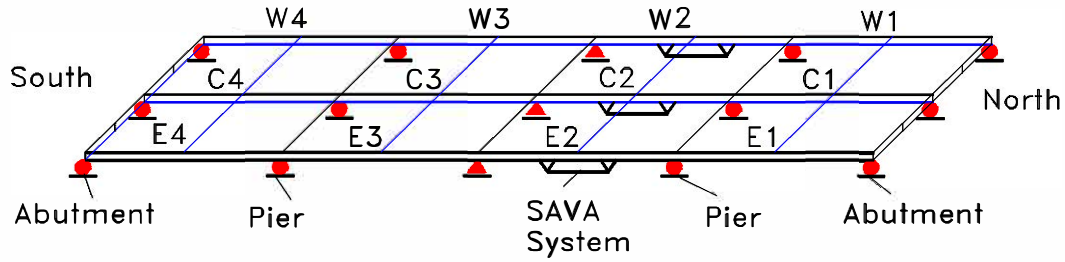
Figure 2.1 Strain Gauge Locations

The rock truck was tested in the right lane. The recorded stress at the bottom flange of the center girder in the middle of the first span of the bridge is shown in Figure 2.2. Next, we decompose the response in Figure 2.2 into the mean valve (Figure 2.3) and the vibratory component (Figure 2.4). Figure 2.5 is a comparison of the mean value with the time history of the crawl test for this truck measured at the same location. The comparison suggests that the mean comparison is close in magnitude to the static load. Using this decomposition, then we can establish a reasonable idea of the impact factor for a truck at the various locations on the bridge. For example, the impact level at C_1 for the rock truck is based on the ratio of the maximum vibratory stress range (1,500 psi) and the quasi-static stress range (2,500 psi). The ratio is 0.6. Recall that NCHRP 299 suggests a maximum of 0.3. We note that when the truck travels in either lane, the central girder experiences the smallest impact relative to the other girders. As an example the stress history at the east girder in the 1st span at the center of the girder (E1) is shown in Figure 2.6 for the rock truck test. The decomposition of the signal into a quasi-static and vibratory component is shown in Figures 2.7 and 2.8. The impact level is then $I = (1050-(-1100)) / (650-(-1500)) = 1$.
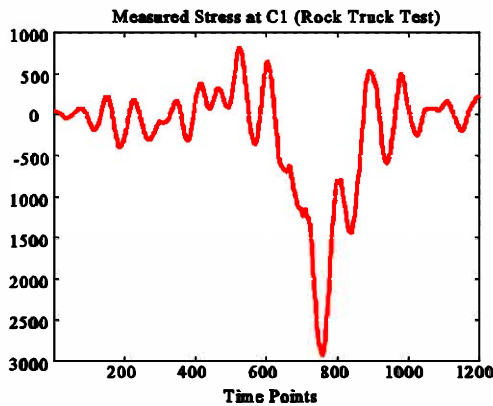
Figure 2.2 Stress Response of Rock Truck
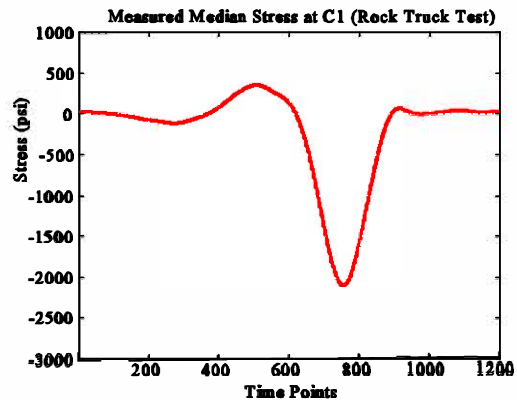
Figure 2.3 Measured Median of Dynamic Stress

4
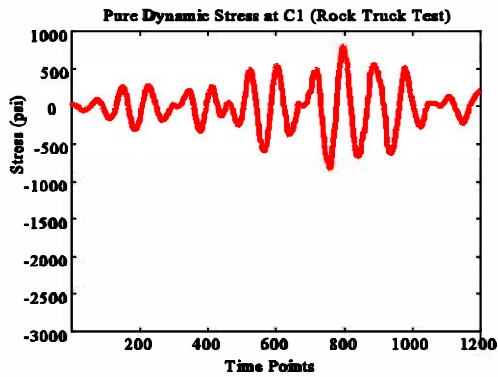
Figure 2.4 Pure Dynamic Stress Response
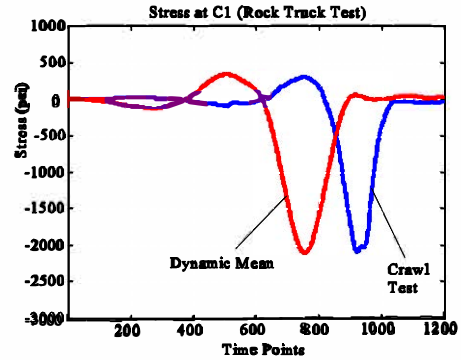
Figure 2.5 Comparison of Crawl Test with Measured Median
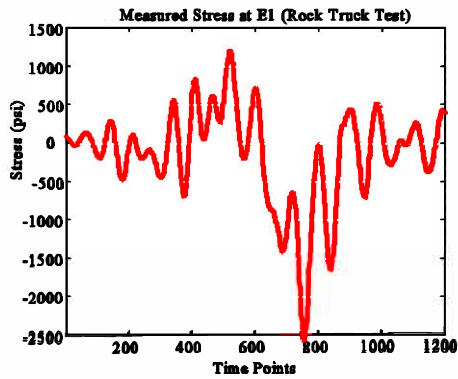
Figure 2.6 Stress Response of Rock Truck
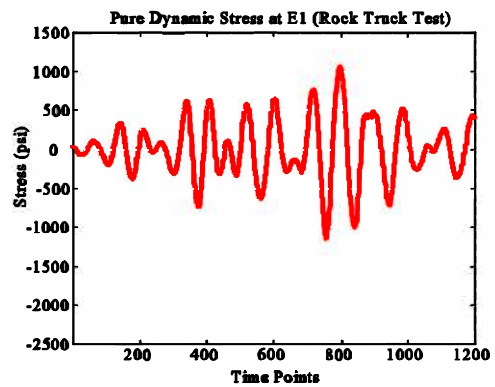
Figure 2.7 Pure Dynamic Stress Response
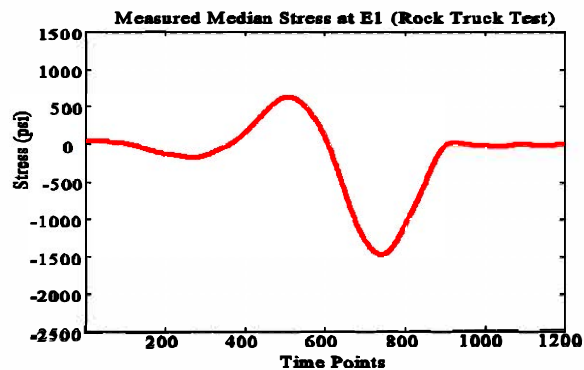
Figure 2.8 Measured Median of Dynamic Stress

The dump truck used in the tests also exhibited significant vibratory dynamics. The stress measurement at location E1 for a right lane test is shown in Figure 2.9. The decomposition of the time trace into mean and vibratory components is shown in Figures 2.10 and 2.11. Figure 2.12 provides a comparison of the mean and quasi-static tests results at that location. The apparent impact factor was I=2.0.
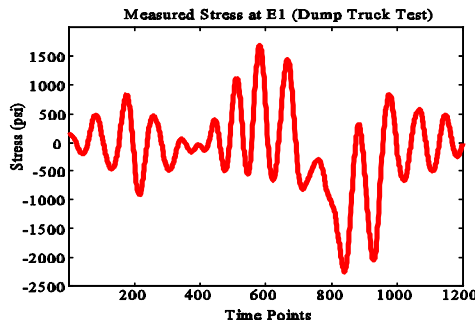
Figure 2.9 Stress Response of Dump Truck
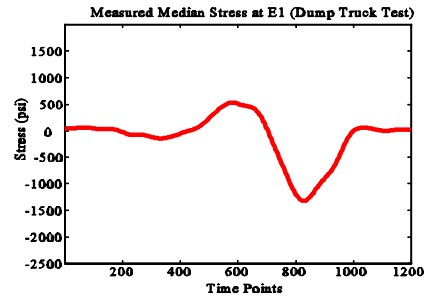
Figure 2.10 Measured Median of Dynamic Stress
of Dump Truck Test
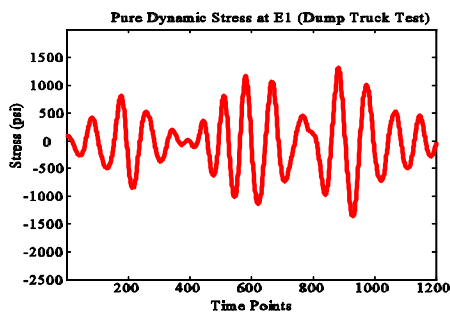
Figure 2.11 Pure Dynamic Stress Response
of Dump Truck Test
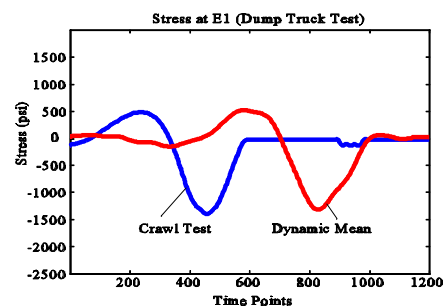
Figure 2.12 Comparison of Crawl Test
with Measured Median

The heavy truck response exhibited less oscillation than the lighter trucks. Figure 2.13 is the stress time history at E3, and Figures 2.14 and 2.15 are the mean and vibratory components of the stress. Figure 2.16 depicts a comparison of the quasi-static stress versus the mean stress at that point. The apparent impact ratio is approximately 0.25. Aside from the weight and wheel base differences of the three trucks, the only other significant difference between the vehicles is that the heavy truck had no compliance in the suspension. **<u>The results indicate that a truck suspension design is a significant component of a truck vibration response.</u>** The next section recounts the methods used to identify plausible dynamic models of the suspensions of the trucks used in the testing.
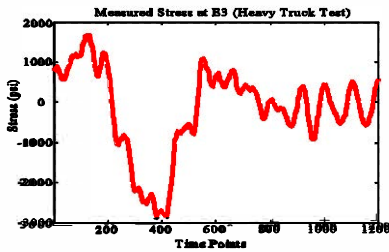
Figure 2.13 Stress Response of Heavy Truck
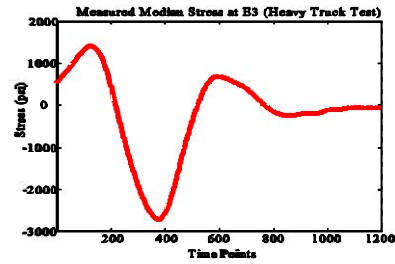
Figure 2.14 Measured Median of Dynamic Stress
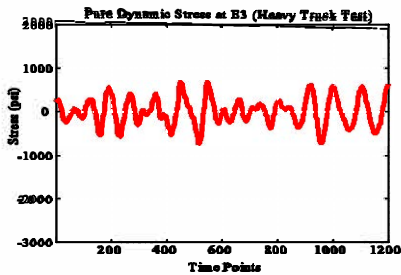
Figure 2.15 Pure Dynamic Stress Response
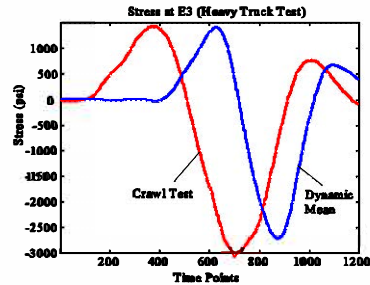
Figure 2.16 Comparison of Crawl Test

with Measured Median

3.   Truck Modeling

A dynamic model of the suspension of each of the test vehicles was developed to conduct the design analysis. The modeling of a truck suspension typically begins with an in-plane analysis of a full vehicle. In most cases, that model is then able to be simplified to a system of so called quarter vehicles, each representing the significant compliance and mass components at each axle group. We begin by describing the full vehicle analysis and use the rock truck as an example. A seven degree of freedom kinematic structure was assumed.   The pitch angles remain small, which justifies a linear model. It is assumed that relative motion occurs between tractor and trailer at the fifth wheel.

A test system was setup on the rock truck to validate the mathematical model.   Figures 3.1 and 3.2 show the sensor layout and truck geometry in the truck test.

Figures 3.4 and 3.5 indicate the compliance model of the truck chassis. The rear tandem is treated as a single axle.
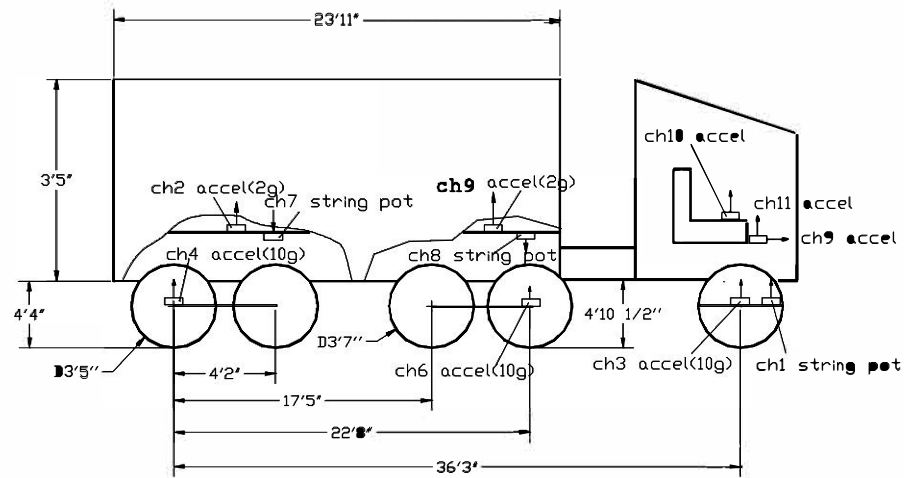
Figure 3.1 Sensor Layout on the Rock Truck
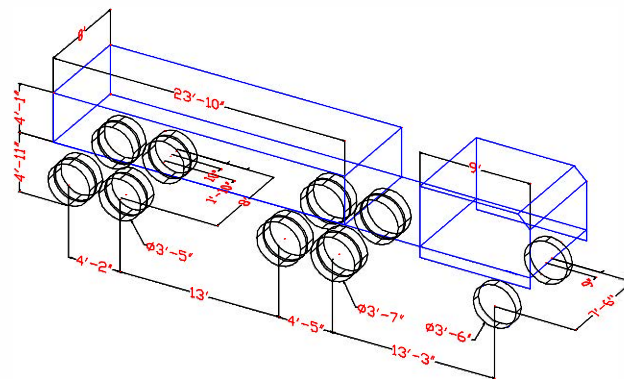
Figure 3.2 Geometry of the Rock Truck
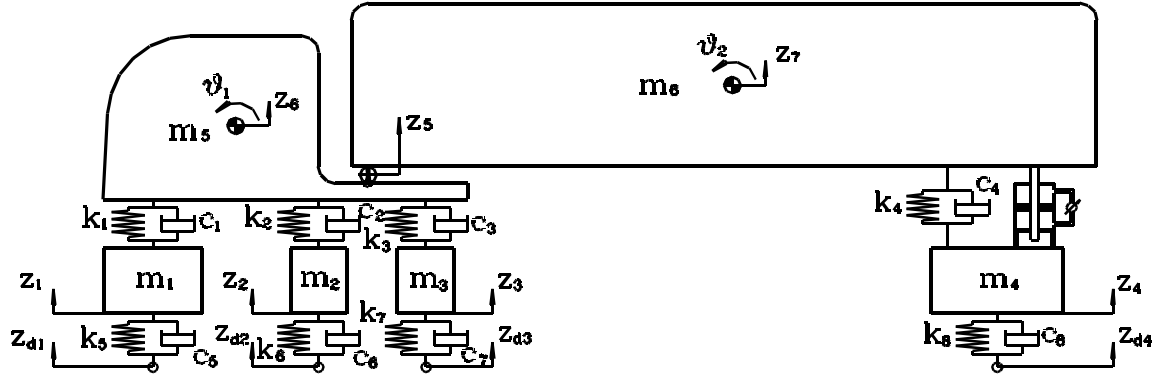
Figure 3.3 Dynamic Model of Four Axle Tractor-Trailer
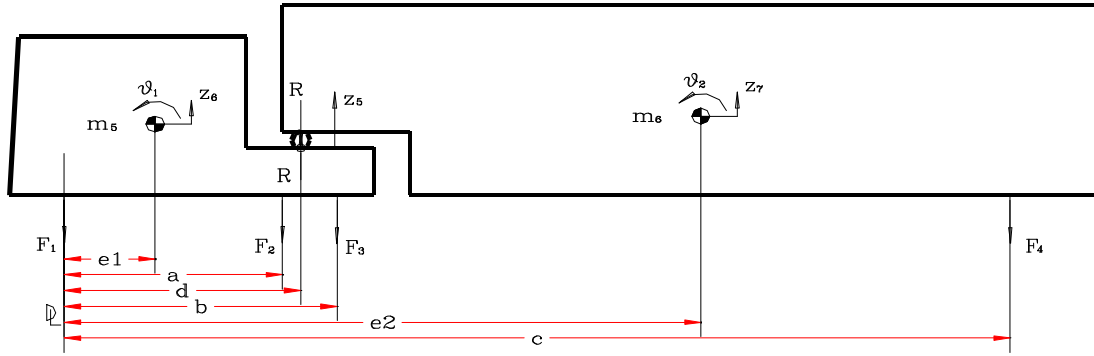
Figure 3.4 Kinematic Layout of Rock Truck

Each axle group is represented as an unsprung mass. The vehicle is characterized by seven generlized coordinates, five vertical displacements z_1 to z_4 and z_8 and two rotations (θ_1 **to** θ_2). The coordinates Z_{d1}, Z_{d9}, Z_{d3} and Z_{d4} are the absolute positions of the bridge deck at the point of tire contact; these are referred to as the road profile.
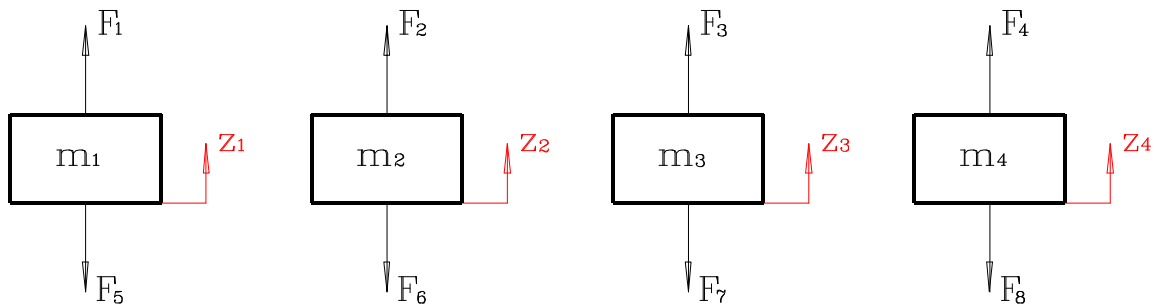
Figure 3.5 Free Body Diagram of Axles

The spring and the damping forces of the truck suspension systems can be obtained from the geometric

9

relationships and expressed as follows

$$F_1 = k_1\{ -z_1 + z_5 - d\theta_1 \} + c_1\{ -\dot{z}_1 + \dot{z}_5 - d\dot{\theta}_1 \}$$
$$F_2 = k_2\{ -z_2 + z_5 - (d-a)\theta_1 \} + c_2\{ -\dot{z}_2 + \dot{z}_5 - (d-a)\dot{\theta}_1 \}$$
$$F_3 = k_3\{ -z_3 + z_5 + (b-d)\theta_1 \} + c_3\{ -\dot{z}_2 + \dot{z}_5 + (b-d)\dot{\theta}_1 \}$$
$$F_4 = k_4\{ -z_4 + z_5 + (c-d)\theta_2 \} + c_4\{ -\dot{z}_4 + \dot{z}_5 + (c-d)\dot{\theta}_2 \}$$
$$F_5 = k_5(z_1 - z_{d1}) + c_5(\dot{z}_1 - \dot{z}_{d1})$$
$$F_6 = k_6(z_2 - z_{d2}) + c_6(\dot{z}_2 - \dot{z}_{d2})$$
$$F_7 = k_7(z_3 - z_{d3}) + c_7(\dot{z}_3 - \dot{z}_{d3})$$
$$F_8 = k_8(z_4 - z_{d4}) + c_8(\dot{z}_4 - \dot{z}_{d4})$$

(3.1)

Using the above relationships, the following system of governing differential equations is obtained

$$m_1\ddot{z}_1 = F_1 - F_5$$
$$m_2\ddot{z}_2 = F_2 - F_6$$
$$m_3\ddot{z}_3 = F_3 - F_7$$
$$m_4\ddot{z}_4 = F_4 - F_8$$
$$(m_5 + m_6)\ddot{z}_5 - m_5(d-e_1)\ddot{\theta}_1 + m_6(e_2-d)\ddot{\theta}_2 = -(F_1+F_2+F_3+F_4)$$
$$\{ J_{G5} + m_5(d-e_1)^2 \}\ddot{\theta}_1 - m_5(d-e_1)\ddot{z}_5 = dF_1 + (d-a)F_2 + (d-b)F_3$$
$$\{ J_{G6} + m_6(e_2-d)^2 \}\ddot{\theta}_2 + m_6(e_2-d)\ddot{z}_5 = (d-c)F_4$$

(3.2)

We next cast the equations in space format with x_1 thru x_7 representing the five translations and two rotations. The component x_8 thru x_{14} are the velocities defining.

$$\dot{X} = EX + FX_d$$

(3.3)

$$X = \{ x_1\ x_2\ x_3\ x_4\ x_5\ x_6\ x_7\ x_8\ x_9\ x_{10}\ x_{11}\ x_{12}\ x_{13}\ x_{14} \}^T$$

$$E = \begin{bmatrix} [\,0\,] & [\,I\,] \\ 7\times 7 & 7\times 7 \\ \hline M_1^{-1}A_1 & M_1^{-1}B_1 \\ M_2^{-1}A_2 & M_2^{-1}B_2 \end{bmatrix}, \quad F = \begin{bmatrix} [\,0\,] \\ 7\times 4 \\ \hline M_1^{-1}C \\ \hline [\,0\,] \\ 3\times 4 \end{bmatrix}$$

(3.4)

$$X_d = \{ Z_{d_1}\ Z_{d_2}\ Z_{d_3}\ Z_{d_4} \}^T$$

10

The entries in E and F are given in Table 1 at the close of this Subreport.

The selection of parameter values was guided by published data on the truck's chassis components and by testing. The process required a trial and error procedure. The parameters that were found to provide a best fit to the test data are listed in Table 2. The eigenvalues of the model are

$$\frac{eig(A)}{2\pi} = \begin{Bmatrix} -2.2974 \pm 13.2530i \\ -2.4488 \pm 10.0070i \\ -1.7078 \pm 9.7754i \\ -1.5721 \pm 9.3764i \\ -0.1529 \pm 1.5670i \\ -0.1215 \pm 2.6782i \\ -0.2764 \pm 2.2427i \end{Bmatrix} \tag{3.5}$$

4. Test Simulation of Road/Truck Dynamics

The damped natural frequencies of the various inertial components are:

- Steering axle 13.45 Hz
- Tractor tandem axle #1 10.29 Hz
- Tractor tandem axle#2 9.92 Hz
- Rear tandem axle 9.51 Hz
- Pitch mode, tractor 2.26 Hz
- Pitch mode, trailer 1.52 Hz
- Heave mode entire truck 2.68 Hz

Recalling that the first three modes of the bridge are 2.55 Hz, 2.95 Hz and 3.3 Hz, then the result here raises a serious issue. The heave and pitch modes of the truck are extremely close to the fundamental frequencies of the bridge. When the truck chassis is vibrating, it will resonate with the bridge producing dynamic deflections that are not accounted for in the codes that describe bridge design or analysis. The result is typical for all of the vehicles tested. (We note, however, that the trailer pitch mode decreases with wheel base). It is also worth noting, that we have analyzed four plate girder bridges along I-35 with spans ranging from 80 feet to 125 feet and find that all of those bridges have first modes between 2.6 Hz and 3 Hz. This is a serious problem.

In order to simulate the response of the system, a road profile characterized by white noise with a constant RMS velocity was employed. A time history of the road profile is shown in Figure 4.1. Figures 4.2 thru 4.3 depict comparison of various transfer function of the system for the simulation versus actual experimental tests (conducted on I-35 near the Walnut Creek Bridge).
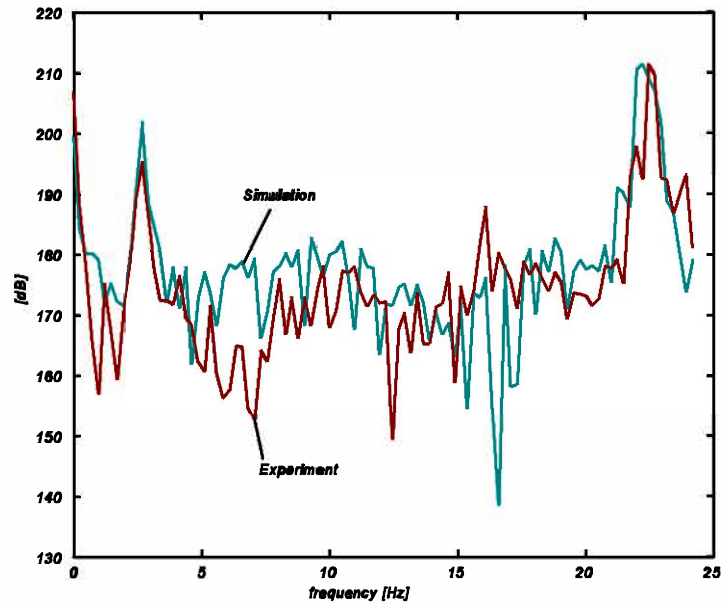
Figure 4.1 Time History of the Road Profile
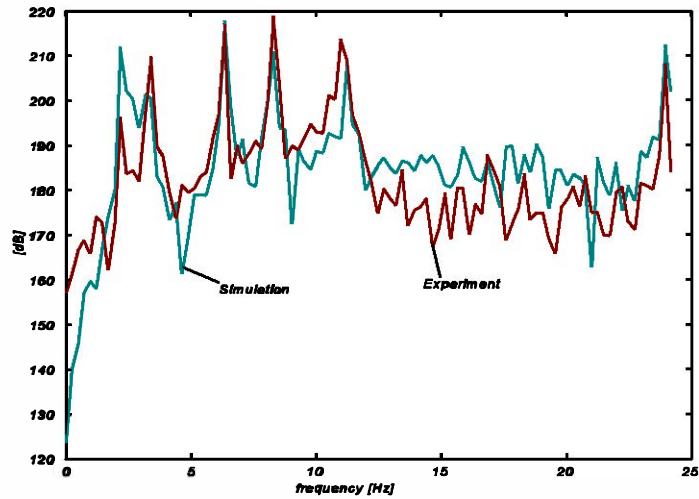
**Figure 4.2 Comparison of simulation and experiment
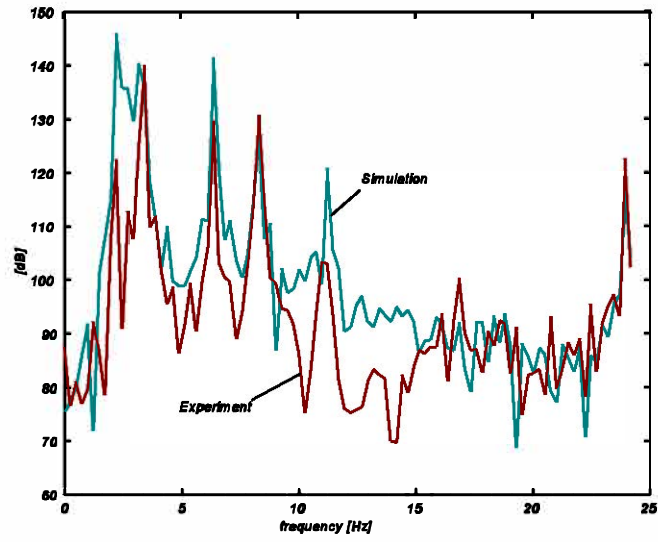of acceleration of trailer unsprung mass**

**Figure 4.3   Comparison of simulation and experiment
of acceleration of trailer sprung mass**

Table 4.1 Parameter in Matrices E and F

$$X_1 = [\ddot{z}_1, \ddot{z}_2, \ddot{z}_3, \ddot{z}_4]^T$$
$$X_2 = [\ddot{z}_5, \ddot{x}_6, \ddot{x}_7]^T$$
$$\dot{Z} = [\dot{z}_1, \dot{z}_2, \dot{z}_3, \dot{z}_4, \dot{z}_5, \dot{x}_6, \dot{x}_7]^T$$
$$Z = [z_1, z_2, z_3, z_4, z_5, x_6, x_7]^T$$
$$Z_d = [z_{d1}, z_{d2}, z_{d3}, z_{d4}]^T$$

$$M_1 = \begin{bmatrix} m_1 & 0 & 0 & 0 \\ 0 & m_2 & 0 & 0 \\ 0 & 0 & m_3 & 0 \\ 0 & 0 & 0 & m_4 \end{bmatrix}, \quad M_2 = \begin{bmatrix} m_5 + m_6 & -m_5(d-e_1) & m_6(e_2-d) \\ -m_5(d-e_1) & J_{G5} + m_5(d-e_1)^2 & 0 \\ m_6(e_2-d) & 0 & J_{G6} + m_6(e_2-d)^2 \end{bmatrix}$$

$$A_1 = \begin{bmatrix} -(c_1+c_5) & 0 & 0 & 0 & c_1 & c_1 d & 0 \\ 0 & -(c_2+c_6) & 0 & 0 & c_2 & -c_2(d-a) & 0 \\ 0 & 0 & -(c_3+c_7) & 0 & c_3 & c_3(b-d) & 0 \\ 0 & 0 & 0 & -(c_4+c_8) & c_4 & 0 & c_4(c-d) \end{bmatrix}$$

$$B_1 = \begin{bmatrix} -(k_1+k_5) & 0 & 0 & 0 & k_1 & k_1 d & 0 \\ 0 & -(k_2+k_6) & 0 & 0 & k_2 & -k_2(d-a) & 0 \\ 0 & 0 & -(k_3+k_7) & 0 & k_3 & k_3(b-d) & 0 \\ 0 & 0 & 0 & -(k_4+k_8) & k_4 & 0 & k_4(c-d) \end{bmatrix}$$

(4.5)

$$A_2 = \begin{bmatrix} a_{51} & a_{52} & a_{53} & a_{54} & a_{55} & a_{56} & a_{57} \\ a_{61} & a_{62} & a_{63} & a_{64} & a_{65} & a_{66} & a_{67} \\ a_{71} & a_{72} & a_{73} & a_{74} & a_{75} & a_{76} & a_{77} \end{bmatrix}, \quad B_2 = \begin{bmatrix} b_{51} & b_{52} & b_{53} & b_{54} & b_{55} & b_{56} & b_{57} \\ b_{61} & b_{62} & b_{63} & b_{64} & b_{65} & b_{66} & b_{67} \\ b_{71} & b_{72} & b_{73} & b_{74} & b_{75} & b_{76} & b_{77} \end{bmatrix}$$

$$C = \begin{bmatrix} k_5 & 0 & 0 & 0 \\ 0 & k_6 & 0 & 0 \\ 0 & 0 & k_7 & 0 \\ 0 & 0 & 0 & k_8 \end{bmatrix}$$

where the elements of a matrix A_2 are

$$a_{51} = c_1 , \quad a_{52} = c_2 , \quad a_{53} = c_3$$
$$a_{54} = c_4 , \quad a_{55} = -(c_1 + c_2 + c_3 + c_4)$$
$$a_{56} = c_1 d + c_2 (d-a) - c_3 (b-d) , \quad a_{57} = -c_4 (c-d)$$

$$a_{61} = -c_1 d , \quad a_{62} = -c_2 (d-a) , \quad a_{63} = -c_3 (b-d)$$
$$a_{64} = 0 , \quad a_{65} = c_1 d + c_2 (d-a) + c_3 (b-d)$$
$$a_{66} = -c_1 d^2 - c_2 (d-a)^2 - c_3 (b-d)^2 , \quad a_{67} = 0$$

$$a_{71} = 0 , \quad a_{72} = 0 , \quad a_{73} = 0 , \quad a_{74} = -c_4 (d-c)$$
$$a_{75} = c_4 (d-c) , \quad a_{76} = 0 , \quad a_{77} = -c_4 (c-d)^2$$

(4.6)

and the elements of a matrix $\boldsymbol{B_2}$ are

$$b_{51} = k_1 , \quad b_{52} = k_2 , \quad b_{53} = k_3$$
$$b_{54} = k_4 , \quad b_{55} = -(k_1 + k_2 + k_3 + k_4)$$
$$b_{56} = k_1 d + k_2 (d-a) - k_3 (b-d) , \quad b_{57} = -k_4 (c-d)$$

$$b_{61} = -k_1 d , \quad b_{62} = -k_2 (d-a) , \quad b_{63} = -k_3 (b-d)$$
$$b_{64} = 0 , \quad b_{65} = k_1 d + k_2 (d-a) + k_3 (b-d)$$
$$b_{66} = -k_1 d^2 - k_2 (d-a)^2 - k_3 (b-d)^2 , \quad b_{67} = 0$$

(4.7)

$$b_{71} = 0 , \quad b_{72} = 0 , \quad b_{73} = 0 , \quad b_{74} = -k_4 (d-c)$$
$$b_{75} = k_4 (d-c) , \quad b_{76} = 0 , \quad b_{77} = -k_4 (c-d)^2$$

Table 4.2 Dynamic Parameters of the Truck Model

Symbols	Unit	Value	Symbols	Unit	Value
m_1	Kg	250	c_1	N/sec/m	6.13e+3
m_2	Kg	544	c_2	N/sec/m	8.75e+3
m_3	Kg	500	c_3	N/sec/m	8.75e+3
m_4	Kg	794	c_4	N/sec/m	1.75e+4
J_{G5}	$Kg \cdot m^2$	5.26e+3	c_5	N/sec/m	8.75e+2
J_{G6}	$Kg \cdot m^2$	6.3e+4	c_6	N/sec/m	1.75e+3
k_1	N/m	2.63e+5	c_7	N/sec/m	1.75e+3
k_2	N/m	3.68e+5	c_8	N/sec/m	3.5e+3
k_3	N/m	3.68e+5	a	m	4.064
k_4	N/m	2.36e+5	b	m	5.359
k_5	N/m	7.88e+5	c	m	10.414
k_6	N/m	1.58e+6	d	m	4.572
k_7	N/m	1.58e+6	e_1	m	1.83
k_8	N/m	3.15e+6	e_2	m	7.49

5.   Test vs. Simulation of Bridge/Truck Dynamics

Tests of most of the vehicles on the bridge suggest that a simple quarter car model at each significant axle group can sufice for a dynamic model of the truck. The quarter car model is shown in Fig. 5.1. The compliance parameters as well as the sprung and unsprung mass values can be established from the truck manufacturers literature. The quarter car model neglects the pitch modes of the vehicle. The longer the truck, the lower are the pitch mode frequencies.

Once the FEM of the bridge was completed then it was used to simulate the response of the different test trucks used. In each case quarter car models were used to represent the truck. A comparison of the simulated and experimentally measured response for each of the four trucks is shown in Fig. 5.2. The differences in the traces reflect the fact that the initial conditions of the trucks actual dynamics are not known. The results verify the appropriateness of a simplified chassis model for the trucks.
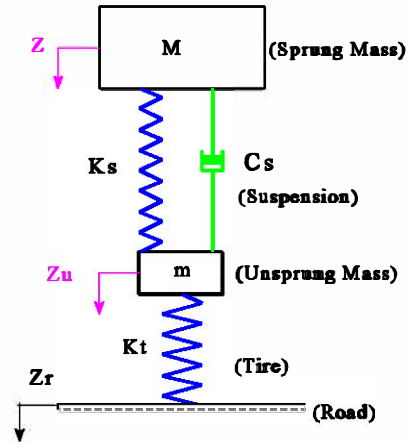
Figure 5.1 A Quarter Car Model
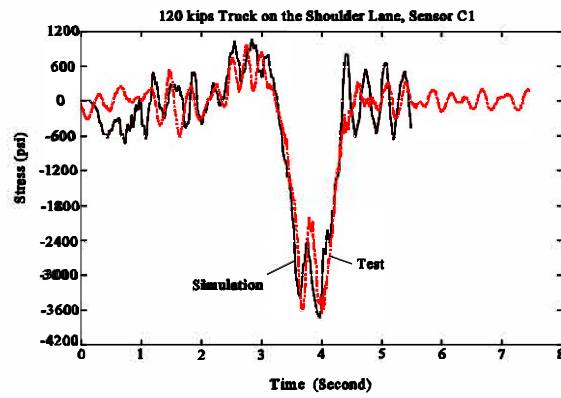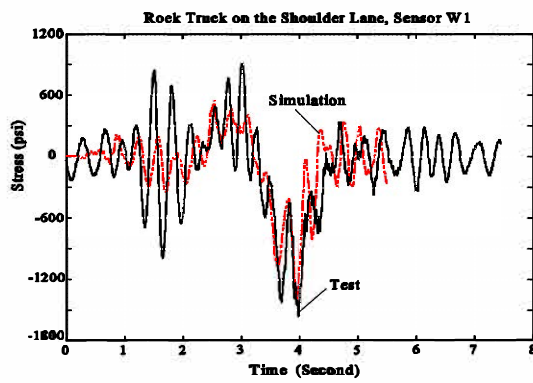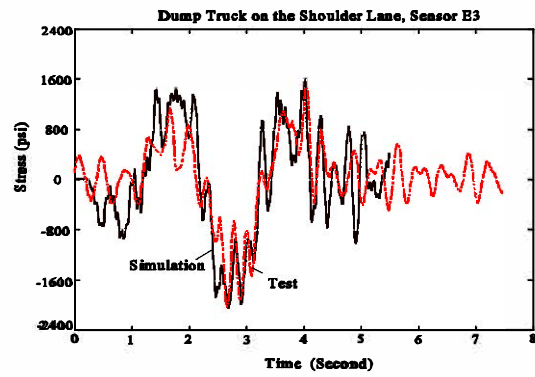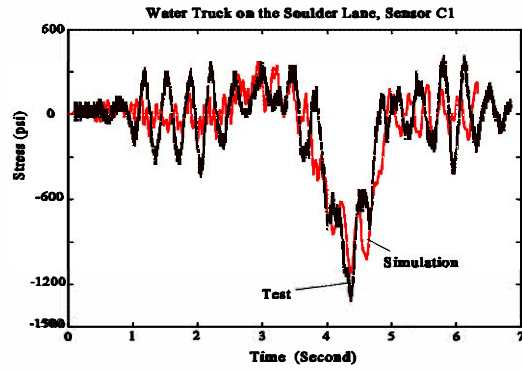
Figure 5.2 Comparison of the Simulated and Measured Dynamic Response

18

6.   Bridge Truck Coupling

This last section of Subreport #4 provides an indication of the effect that the SAVA control system has on a trucks principal models of motion. We have reported in an earlier section that the rock truck has at least two modal frequencies that are very close to one or more of the bridges modal frequencies.

The testing of the instrumented rock truck produced data that provides some insight. Figures 6.1 and 6.2 are fast Fourier Transformers (FFTs) of the accelerometer mounted on the rear axle, and the accelerometer mounted on the trailer body above the rear axle. Each figure contrasts the response spectra first when the truck is traveling on an arbitrary section of the road. Next the FFTs of the response with the truck on the bridge with the SAVA system operating in the control mode and the passive mode are shown. Figure 6.1 indicates that the axle dominate mode is attenuated when the truck is on the bridge. Similar comparisons are made in Figures 33. Figures 32 and 33 also confirm that the control effects a substantial reduction of the absolute acceleration of the axle and the trailer body. This of course reflects the fact that the bridge vibrates less when the control is used.
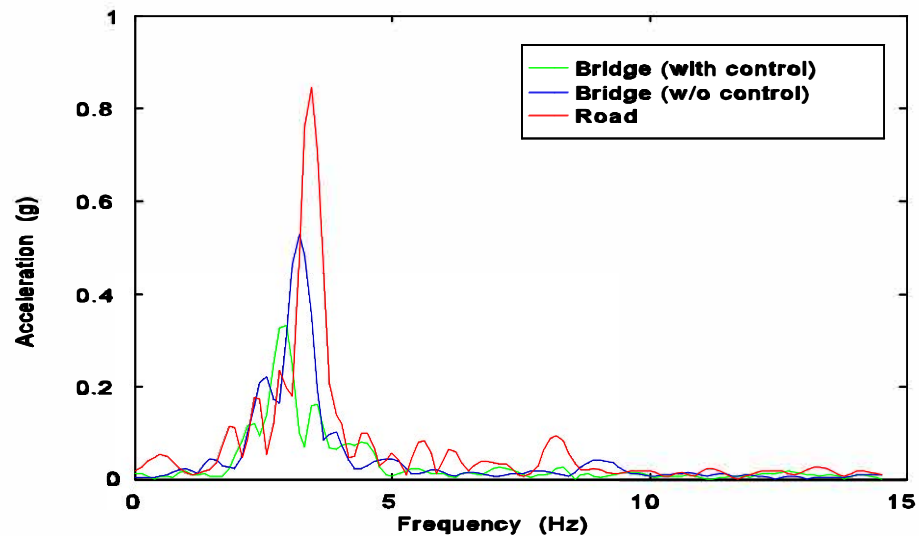
**Figure 6.1 Comparison of FFT of Rock Truck Test, Controlled vs. No Control
& Truck on Road, Acceleration Measured at Rear Frame**

19
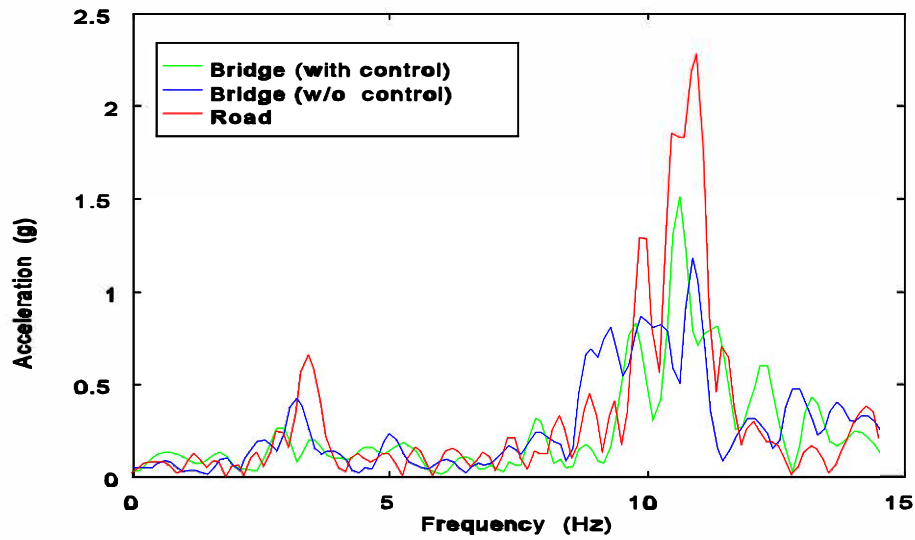
**Figure 6.2 Comparison of FFT of Rock Truck Test, Controlled vs. No Control
& Truck on Road, Acceleration Measured at Rear Axle**

Closure

This Subreport described the dynamics of the vehicles used in the testing. The quasi-static response of the bridge was first presented for each of the four trucks. Next, the dynamic response of the bridge to the passage of a truck at the posted speed limit was discussed. A description of the process used to determine a dynamic model of a tractor trailer was also provided. The truck models were then used with the FEM of the bridge to verify test data. Finally, the spectral response of a truck was examined to determine the effect that the control mode of the SAVA system has on the trucks motion.

SEMIACTIVE VIBRATION ABSORBERS (SAVA) AT THE I-35 WALNUT CREEK BRIDGE

A PROJECT FUNDED BY OKLAHOMA DEPARTMENT OF TRANSPORTATION

ODOT PROJECT ENGINEER: DAVID OOTEN, PE

SUB-REPORT # 4:

Design and Implementation of A Semiactive Structure Control System

---

CENTER FOR STRUCTURAL CONTROL
UNIVERSITY OF OKLAHOMA
http://www.coe.ou.edu/research/cstructc/

PROJECT MANAGER:

WILLIAM N. PATTEN, Ph. D, P.E., (PI)

RESEARCH ENGINEERS:

GUANGJUN LI
JINGHUI SUN, Ph. D.
GANG SONG, Ph. D.

AUGUST, 1997

TABLE OF CONTENTS

NOMENCLATURE

A	The plant matrix	
A^*	The bridge/actuator coupled system plant matrix	
A_v	Hydraulic Valves Orifice Area	m^2
A_p	Effective Piston Area of Actuator	m^2
A_{vmax}	Maximum hydraulic orifice area	m^2
A_{vmin}	Minimum hydraulic orifice area	m^2
B	The control input matrix	
B^*	The bridge/actuator coupled system control input matrix	
c1	Damping coefficient of truck suspension	N*s/m
C	General damping matrix	
C_b	Bridge damping matrix	
C_t	Truck damping matrix	
d	Truck disturbance	N
D	Truck disturbance input matrix	N
E	Young's module	N/m^2
$g(\Delta P)$	Nonlinear damping function	
F	Boundary of truck disturbance amplitude	N
f(x)	Truck disturbance input	N
H	Height of moment arms	m
I	Inertia of the bridge girder	m^4
K	General stiffness matrix	
K_b	Bridge stiffness matrix	
K_t	Truck stiffness matrix	
k1	Stiffness of tire	N/m
k2	Stiffness of suspension	N/m
L	Span length of the bridge	m
l_0	Beam element length	m
M	General mass matrix	
M_b	Bridge mass matrix	
M_t	Truck mass matrix	
m1	Mass of tire	kg
m2	Mass of truck body	kg

Q	Weighing matrix of control	
u	Semiactive control force matrix (for bridge control)	
v	Truck traveling speed	m/s
V	Lyapunov function	
w	static weight of truck	kg
W	Width of moment arms	m
$\bar{x}$	State vector of bridge	m
$\bar{y}$	Generalized coordinate of bridge	
$\bar{z}$	Generalized coordinate of bridge/truck coupled system	
$\dot{z}_0$	initial velocity of truck suspension	m/s
α	Coefficient of hydraulic damper	N/m^2
ΔP	Differential pressure of hydraulic damper	N/m^2
ϵ	Hydraulic damper leakage coefficient	N/m^2
γ	Coefficient of hydraulic damper	N/m^2
ρ	Density of hydraulic damper	N/m^2

ABSTRACT

The service life of highway bridges has been decreased because of dynamic loads induced by heavy truck traffic. A program of research is being conducted by Center for Structural Control, the University of Oklahoma to extend the fatigue life of highway bridges by retrofitting them with Semiactive Vibration Absorbers (SAVA).

The report describes the design and performance of the SAVA control system which has been installed on Walnut-Creek highway bridge of I-35 near Purcell, Oklahoma. The report first describes the control logic design developed for this project. Next the results of field tests are reviewed to demonstrate the effectiveness of the design.

CHAPTER 1

INTRODUCTION AND BACKGROUND

1.1   Introduction

A semiactive vibration absorber is an energy storage and dissipation device. The energy is produced by the vibration (deflection and velocity) of the bridge. The vibration is a direct byproduct of the passage of vehicles over the bridge. This report describes the development, installation and field testing of a Semiactive Vibration Absorber (SAVA) for bridges. The system consists of a load transfer assembly and a controllable hydraulic cylinder. The report describes the SAVA system, the control logic and hardware that were employed. The performance of the SAVA system is discussed in detail.

1.2   Reviews of the Literature

1.2.1. Bridge Dynamics. Research on the dynamic response of bridges subjected to moving vehicle loads date back to the work of Jeffcott [17] in 1929. In that early study, the vehicle was modeled as a traveling load, and the effects of the suspension dynamics were neglected. Recently, more sophisticated vehicle models that include suspension dynamic have been employed. Veletsos [30], for example, presented the results of simulations of the coupled bridge-vehicle system. His system model included the significant structural compliance. Patten et al., [1] has also examined the coupled bridge/vehicle dynamics and extended that analysis to the treatment of the bridge vibration control problem.

1.2.2. Bridge Control Theory. One of the earliest attempts to address the possibility of active control applications to structures was made by Chubbier [30] in 1960. Soong [19] recently reviewed research in the structural controls area. The practical issue of how to configure an active bridge control system was posed by Abdel-Rohman [28] in 1980. The kinematic arrangement proposed there is similar to that utilized on the test bridge. Their work differs in that they proposed an active (powered) control system. A more recent examination of the active control problem for highway bridges was recently authored by Lin and Trethewey [29]. The semiactive control of a bridge was first discussed by Patten et al., [1]. That work demonstrated that if a semiactive system was designed properly, it can achieve mitigation levels similar to those achieved with active control.

1.2.3. Semiactive Vibration Dampers. Since Karnopp [3] first introduced the concept of semiactive automotive suspensions in 1973, there have since been hundreds of papers authored that address semiactive automotive control, including the control of suspension shock absorbers, semiactive motor mounts, and semiactive seats. A recent review of semiactive automotive technology was offered by Ivers and Miller [32] 1991. There are three types of semiactive (SA) actuators underdevelopment. Patten [15] has described the physics that governs the use of a hydraulic SA actuator. He presented laboratory results that confirm the important effects caused by compressibility, air entrainment, nonlinear flow and the coupling between the hydrodynamics and the structural dynamics. Lemaire [33] has recently reported progress on the development of a casual model of the actuator dynamics of a semiactive damper that employs elector-rheological (ER) fluid. Spencer [20] has described similar progress in the development of an adjustable damper that employs magneto-rheological (MR) fluids. ER fluids and MR fluids offer an alternative means of quickly

restricting flow, without requiring the mechanical manipulation of a valve. Imposing a magnetic field in the area of a constriction can increase the shear modules of these fluids many orders of magnitude. The fluid can in effect be turned into a solid in milliseconds. This prevents flow through the orifice. ER and MR fluid dampers may provide a cost effective alternative to hydraulic SA dampers, if various parasitic problems can be overcome. Both fluids for example tend to loose their desirable characteristics if they remain dormant for any length of time. In addition, MR fluids are abrasive, and high cycle loading tends to wear the cylinder components out prematurely.

CHAPTER 2

CONTROL DESIGN

    This section first describes the dynamics of the bridge/vehicle/actuator system. Next, the techniques used to establish a control law for the SAVA system are presented.

2.1. Motion Equations of the Bridge

    The finite element (FE) method was employed to produce a dynamic reduced order model of the bridge structure. The model assumes that the motion consists of planer displacements and rotation only. This is in contrast to the full finite element model (FEM) of the bridge developed for modal analysis purposes. In spite of the pronounced skew of the bridge, the modal analysis of the field test data indicates that the maximum out-of-plane motions are less than 5% of the maximum in-plane motions, thus justifying the use of a simplified model. The bridge motion equations, can be written as

$$M_b \{\ddot{y}\} \; + \; C_b \{\dot{y}\} \; + \; K_b \{y\} \;\; = \;\; \Gamma u \; + \; d(t) \quad ; \; y \in R^{\,m} \tag{2.1}$$

where M_b, C_b, K_b are mass, damping and stiffness matrices of the bridge. y is a vector of the global nodal displacements and rotations. u is the vector of control force. Γ is a mapping (matrix) between the generalized coordinates y and the control inputs u. $d(t)$ represents the exogenous external inputs to the bridge (the truck wheel loads). We next write Equation 2.1 in state space form

$$\dot{x} \;\; = \;\; A\,x \; + \; B\,u \; + \; D(t) \tag{2.2}$$

where $\quad x_1 \; = \; y; \;\; x_2 \; = \; \dot{y}; \;\; x \; = \; [x_1, \, x_2]^T$

and

$$A \; = \; \begin{bmatrix} 0 & I \\ -M_b^{-1}K_b & -M_b^{-1}C_b \end{bmatrix} \quad B \; = \; \begin{bmatrix} 0 \\ M_b^{-1}\Gamma \end{bmatrix} \quad D \; = \; \begin{bmatrix} 0 \\ d(t) \end{bmatrix} \tag{2.3}$$

The matrix A is referred to as the plant$,$ B is the control input and D the disturbance.

    Equation (2.2) represents a linear nontime varying system. It provides the setting for the determination of a best control u that drives the state of the system x to its equilibrium (static) position in the face of the unknown disturbances $D(t)$. The design of that control will be discussed in a later section.

    In order to employ Equation (2.2) in a design study it is important to restrict the size of the matrices A and B (or equivently $,M_b$, C_b, $,K_b$). Recall that the full FEM of the bridge had over 4,000 DOF. In order to establish a workable model, a reduced order model of the bridge is required. Modal reduction methods are available, but the presence of the damping in the system makes that approach problematic. The approach taken in this study was to

introduce a course grid of finite elements (a master-slave approach) and generate a smaller model, taking care to match the modal characteristics of the full model (see Subreport #2 for a complete discussion of this topic).

2.2 Truck/ Bridge Dynamics

The system model reflects the reality that it is virtually impossible to characterize the vehicle disturbances. One can measure the response of the bridge in a straight forward fashion. Measurements that define the time varying load imposed by the tires on the bridge were not available for this study. On the other hand, one can analyze the effectiveness of a control design by constructing an analytical model of a vehicle and reformulate the disturbance in terms of the compliance of the bridge/tire interface. Recall that the vehicle model (see Subreport #4) can be described generally as

$$M_t \ddot{\bar{z}} + C_t \dot{\bar{z}} + K_t \bar{z} = k (f.\bar{y} - z) \qquad (2.4)$$

where $\bar{y}$ is the absolute motion of the bridge deck at the point(s) of interface between the tire and the superstructure. The expression represents the forces applied by the bridge to the tire. Those same forces must then act on the superstructure, with equal magnitude and opposite sign. The coupled bridge/truck system equations of motion can then be written as

$$M_b \{\ddot{y}\} + C_b \{\dot{y}\} + K_b \{y\} = -K\{y - F(t)z\} + \Gamma u \qquad (2.5)$$

$$M_t \ddot{z} + C_t \dot{z} + K_t z = K \{y - F(t) z \} \qquad (2.6)$$

where K is the compliance of the tires, and F is a time varying transformation between the isolated points on the bridge structure where the tires are located at any moment and the entire global vector of the bridges generalized coordinates.

The system can then be written as

$$M \ddot{\bar{y}} + C \dot{\bar{y}} + K^* \bar{y} = B^* u \qquad (2.7)$$

where

$$M = \begin{bmatrix} M_b & 0 \\ 0 & M_t \end{bmatrix} \qquad C = \begin{bmatrix} C_b & 0 \\ 0 & C_t \end{bmatrix} \qquad K = \begin{bmatrix} K_b + g(t) & 0 \\ 0 & K_t - g(t) \end{bmatrix} \qquad (2.8)$$

Defining the state vector $r = [y, \dot{y}]^T$, then the sate space form of the bridge/truck model is

4

$$\dot{r} = \overline{A}(t)r + \overline{B}u \qquad (2.9)$$

The time varying nature of the plant matrix makes the use of Equation 2.7 impractical as a design tool, but it can be used to simulate the performance of the bridge truck system for a given control law. The physics that govern the semiactive actuators (SAVA) are discussed next.

2.3 SAVA Dynamics

The governing differential equation for a semiactive damper is

$$\Delta\dot{P} = -\alpha A_p V_{rel} - \gamma \, sign(\Delta P) A_v \sqrt{\frac{2}{\rho}|\Delta P|} \qquad (2.10)$$

where $\alpha,$ γ are parameters and V_{rel} is relative velocity of actuator piston, sign is a sign function, A_v is the orifice area of the control valve which is bounded by the inequalities

$$A_{vmin} \quad A_v \quad A_{vmax} \qquad (2.11)$$

Here, $A_{Vvmin} = 0$ and A_{vmax} is the maximum orifice area possible.

Noting that the relative velocity across an actuator can be related in a routine way to the generalized coordinates of the bridge FEM. Then we can write Equation (2.10) as

$$\Delta\dot{P}_i = -\alpha_i A_p G_i z - \gamma_i sign(\Delta P_i) A_{vi} \sqrt{\frac{2}{\rho}|\Delta P_i|} \quad i=1,2,..... \qquad (2.12)$$

where the subscript i is indicitation of the ith actuator. If we define the vector of differential pressures as $\Delta\overline{P} = \{\Delta P_1, \Delta P_2,......\}$, then

$$\begin{aligned}
\Delta\overline{P} &= -\alpha A_p \overline{G}z - \gamma \, sign(\Delta\overline{P})\overline{A}_v \sqrt{\frac{2}{\rho}|\Delta\overline{P}|} \\
&= -\alpha A_p \overline{G}z + g(\Delta\overline{P})\overline{A}_v
\end{aligned} \qquad (2.13)$$

We now combine the actuator equations with the system equation. Defining $Z = \{z, \Delta\overline{P}\}$ and noting that

$$\overline{u} = L A_p \Delta\overline{P} \qquad (2.14)$$

where L is the moment arm length and A_p is the area of the actuator, then it can be shown that the combined bridge and actuator dynamics takes the form

$$\dot{X} = A^*X + B\overline{g}(X)\overline{A_v} + d \qquad (2.15)$$

where X is the vector of global nodal displacements of the bridge along with the differential pressure.

2.4 Controller Design

For the purpose of the discussion here, A is assumed to have unique eigenvalues with negative real parts, indicating that the bridge/actuator system is inherently stable. A Lyapunov control design is used. The following instantanious form is selected

$$V = X^T Q X \qquad (2.16)$$

where $Q > 0$. The quadratic function represents a form of the kinetic and potential energy of the system. A good control design will manage to dissipate the system energy that is caused by the passage of a vehicle (the disturbance d). The dissipation rate is obtained by differentiating V

$$\dot{V} = \dot{X}^T Q X + X^T Q \dot{X} \qquad (2.17)$$

Substitute Equation 2.13 into Equation 2.15, then

$$\dot{V} = X^T(A^TQ + QA)X + X^TQBg(X)A_v + X^TQd \qquad (2.18)$$

The object of the control design is then to maximize the negativity of $\dot{V}$ or

$$\max\{-\dot{V}\} \qquad (2.19)$$

Because A has negative eigenvalues, then it can be shown that Q can be selected to force the expression

$$A^TQ + QA = P \qquad (2.20)$$

to be negative. That guarantees that the first term on the right hand side of Equation (2.18) is always dissipative. The last term on the right hand side of Equation (2.18) reflects the disturbances effect on the total dissipation. We cannot control the disturbance; instead, the control is designed to dissipate any energy imparted by the disturbance. The last expression is there for irrelevant and is neglected.

In order to assure the dissipation of energy, then the second term on the right side must be prevented from becoming positive. That goal is achieved by selecting a valve area setting (A_V) in accordance with the following rule

$$A_{vi} = \left\{ \begin{array}{ll} A_{vmax} & \text{if } X^T Q B g_i(X) < 0, \qquad i = 1,...N \\ A_{vmin} & \text{if } X^T Q B g_i(X) \geq 0 \end{array} \right\} \qquad (2.21)$$

This simple rule guarantees that the SAVA actuators are always operating to reduce the amount of energy being stored in the bridge. Block diagram of the control is shown in Figure 2.1.
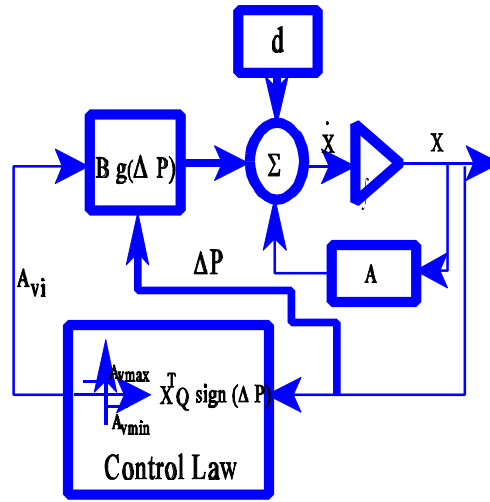
Figure 2.1 Block Diagram of Lyapunov Control Law

The selection of an appropriate Q for the design is not straight forward. That selection process was accomplished by a trial and error method, using simulation to adjust the entries in the matrix. The resulting control law is referred to as a bistate control.

CHAPTER 3

TUTORIAL

Examples of the SAVA design is provided here. First, a simple Pin-Pin girder is adopted with section properties identical to those that define the test bridge girders. We assume that the SAVA has been attached, and that a truck with a suspension travels over the bridge. In the interest of simplicity we assume a quarter vehicle model (single axle) of the truck. Because the girder is Pin-Pin, then a 50' long SAVA assembly (Figure 3.1).
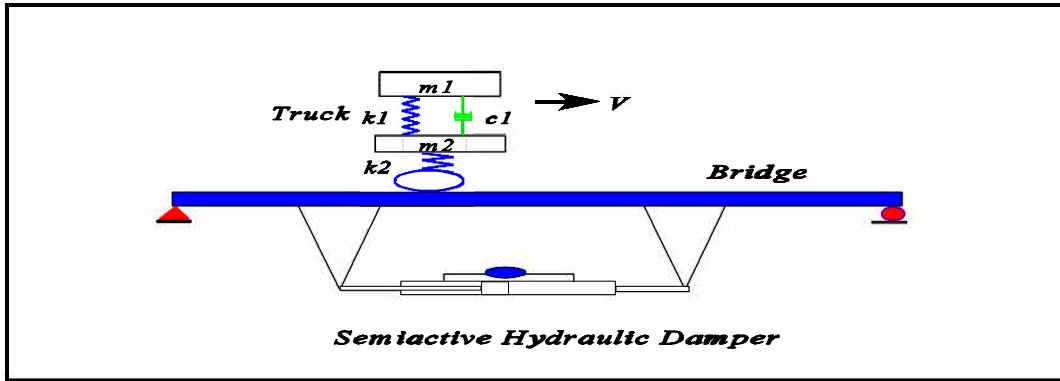
Figure 3.1 Simple Beam Bridge Coupled with Truck Layout

The static weight of the quarter vehicle was 79.5 klb. The truck is assumed to travel at 65 mph. The deflection time history (via simulation) is shown in Figure 3.2.
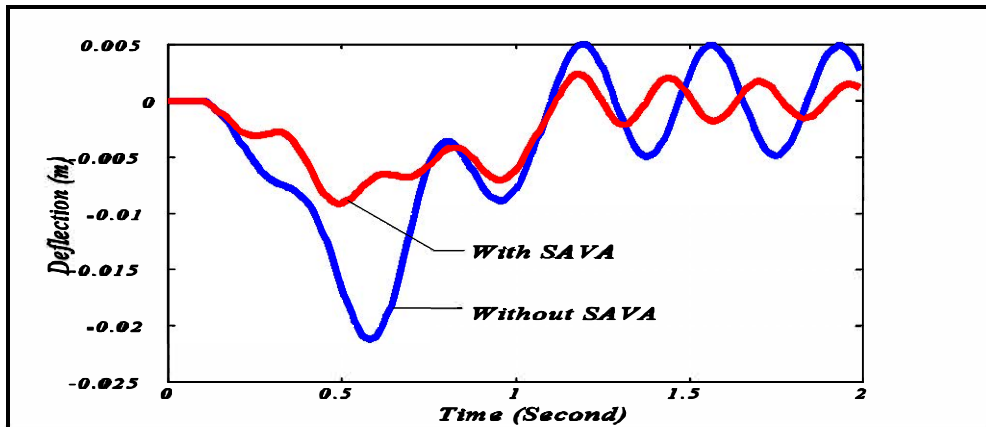
Figure 3.2 Deflection of Simulation Controlled vs. Uncontrolled

While the reduction of maximum deflection is obviously beneficial, the objective of the control design is the reduction of stress range and stress cycles. If that is accomplished, then the remaining fatigue life of the structure can be prolonged. The stress at any point is indicated by the second derivative of the deflection. In order to get reasonably good estimates of the moments at a point, the Finite Element Mesh must be small. Figure 3.3 shows the moment time history at the center of the girder.
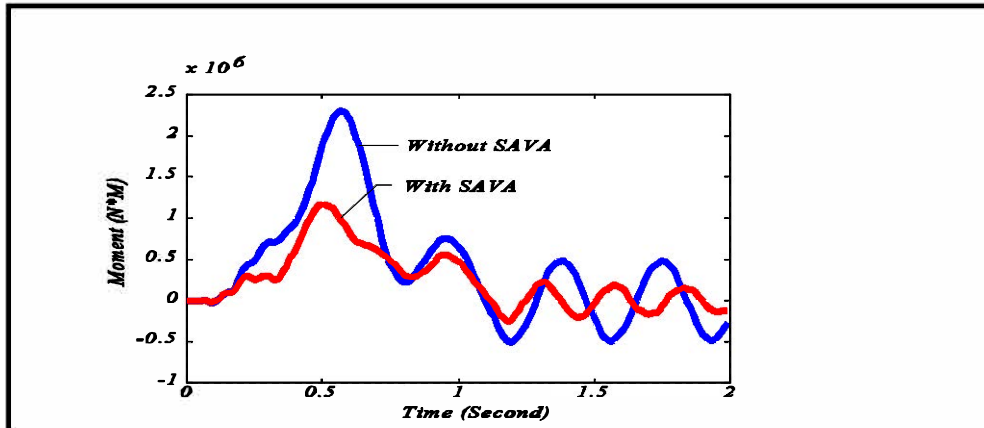
Figure 3.3 Moment Time History at the Center of the Girder (Bottom Flange)

Figure 3.4 depicts the maximum moment for each point along the bridge for the entire time history. The result indicates that simple control law reduces the dynamic stress range considerably.
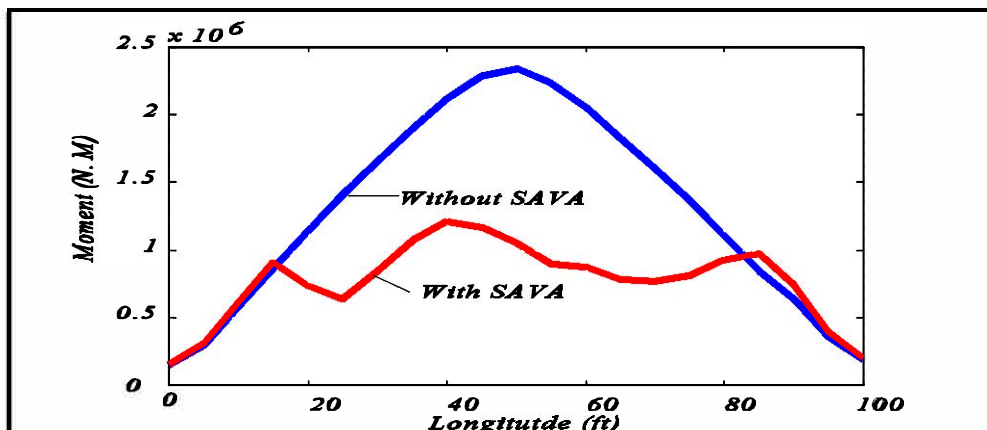
Figure 3.4 Maximum Moment Distribution

Next, the response of a continuous 400' girder. with intermediate supports at 100' intervals, is simulated. A 30' SAVA assembly is assumed to be mounted in the third span (Figure3.5).

9
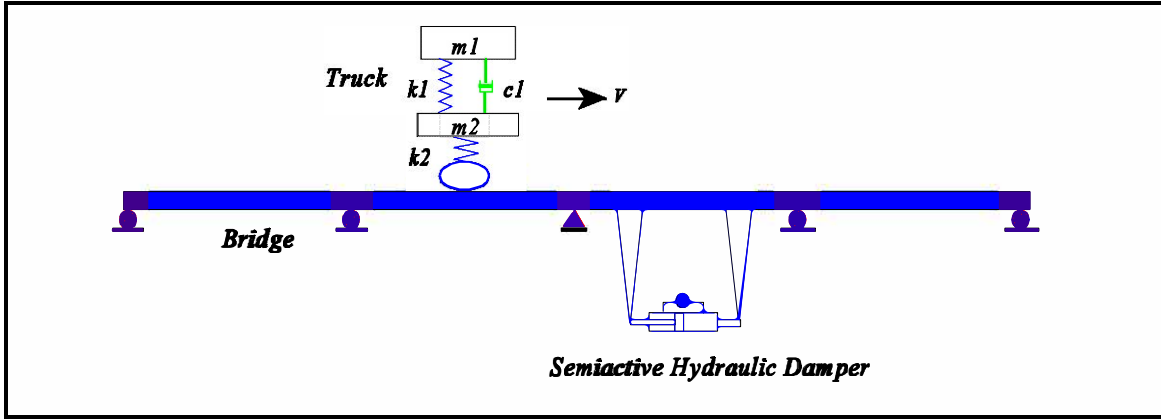
Figure 3.5 Four Span Bridge Coupled with Truck Layout

Again, the parameters used to define the components in this example match the actual construction.

The moment time history at the center of the third span is shown in Figure 3.6
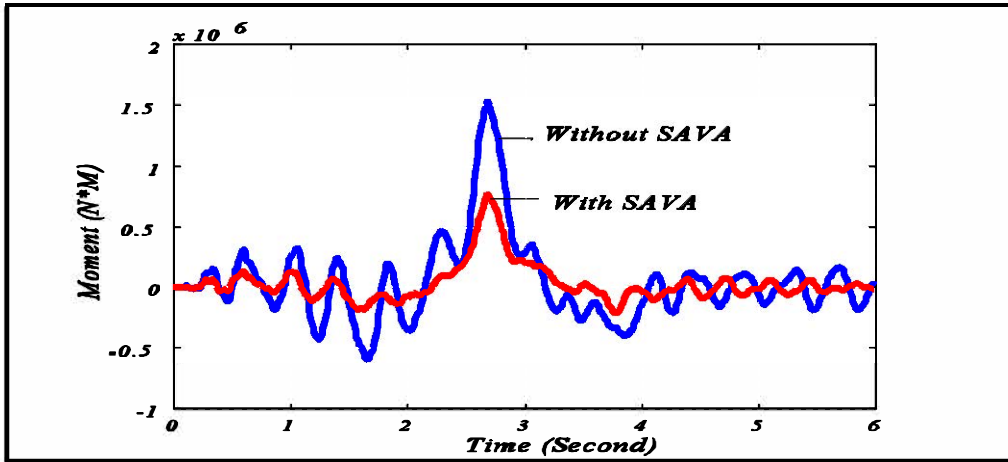
Figure 3.6 Moment Time History at the Center of the Third Span Girder

Figure 3.7 depicts the time history of the control command, and the maximum moments at each point in the controlled (3rd) span are shown in Figure 3.8. Figure 3.9 depicts the moment at every point along the girder when the truck is at the center of the controlled span. The data indicates that the SAVA mounted in a single span, can effect a reduction of moment in the other spans as well. The application of the SAVA system to the test bridge is discussed next.
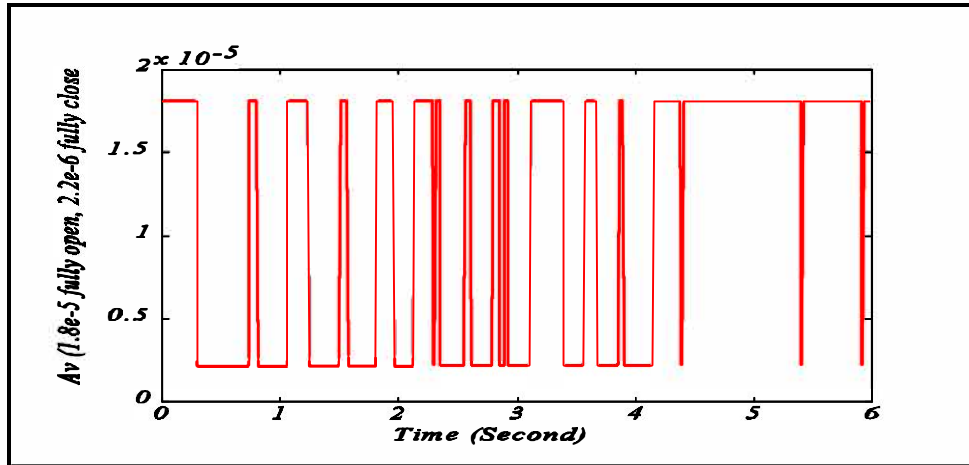
Figure 3.7 The Valve Orifice Time History of the Actuator
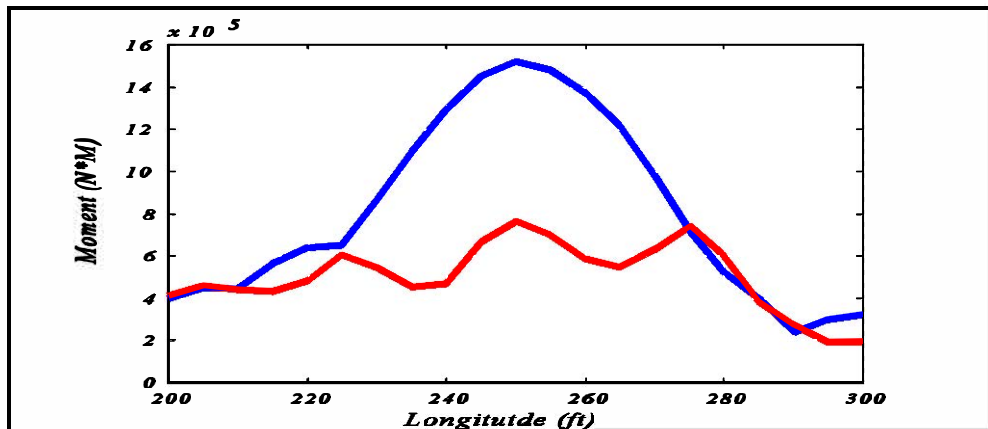
Figure 3.8 Maximum Moment Distribution in Third Span
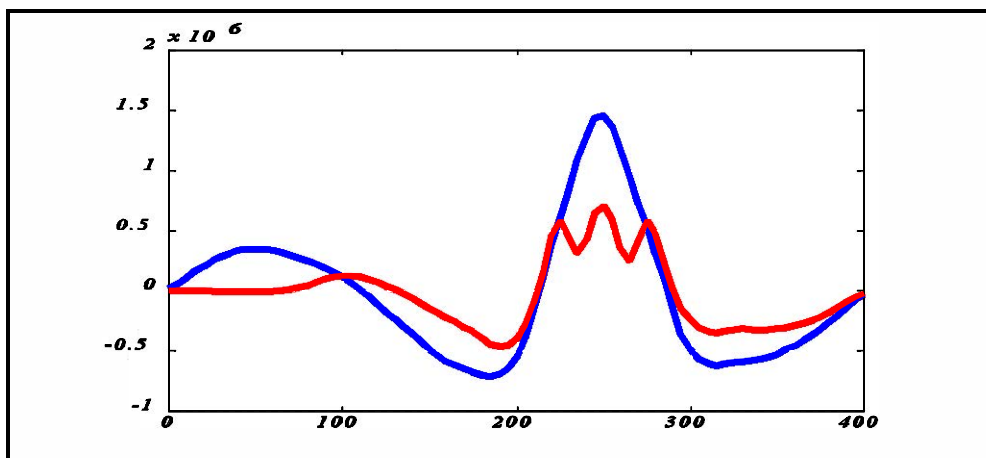
Figure 3.9 Moment Disturbution

11

CHAPTER 4

CONTROLLER IMPLEMENTATION

Figure 4.1 depicts the reduced order model of the bridge that was used to accomplish the real time control of the system. It consists of 11 nodes (22 degrees of freedom).
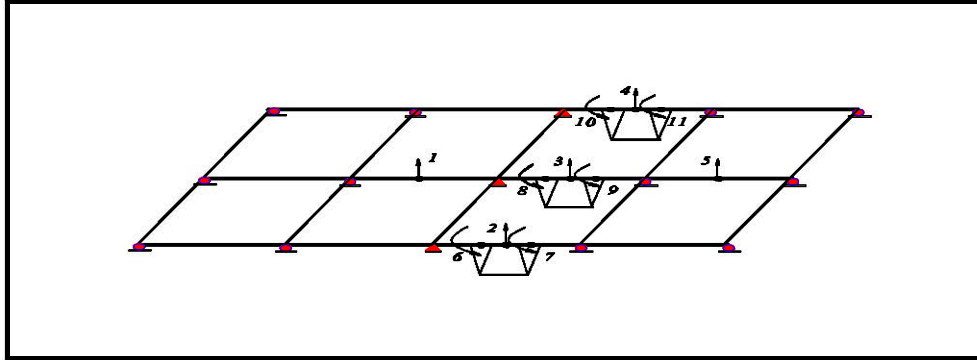
Figure 4.1 Reduced Order Control Bridge Model

Two groups of sensors are used; those associated with each of the actuators, and those associated with the bridge superstructure. Each actuator was outfitted with pressure sensors (2), an LVDT to measure the stroke of the actuator piston and an encoder to monitor the position of the valve. Five strain gauges mounted at points 1, 2, 3, 4 and 5 on the bridge girders were also used. There are less sensors than degrees of freedom (DOFs). This required the development in software of an observer to estimate the unmeasured nodal deflections and rotations. The control system is shown in Figure 4.2
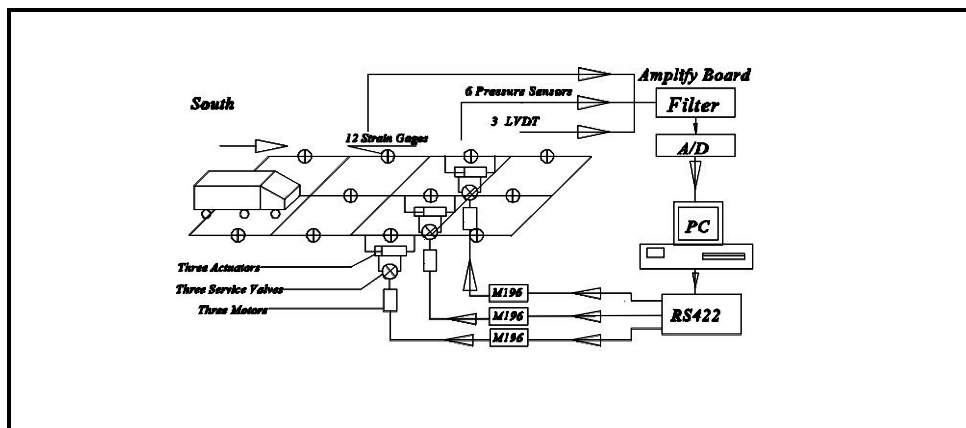
Figure 4.2 Control System Layout

A PC was used to collect all the control sensor outputs, except the encoder outputs. The new values of the valve orifice area (A_v) were computed at each update of the control step. The desired was then transmitted to an Intel® 196 microcontroller mounted near each of the actuators. The microcontroller then provided a closed loop control command to the valve motor. The position of the value was feedback to the microcontroller and the microcontroller then automatically adjusted the value position to the desired final position. The time required to move the valve from open to closed position or vice versa was less than 15 milliseconds. The sensor layout at the SAVA is depicted in Figure 43.
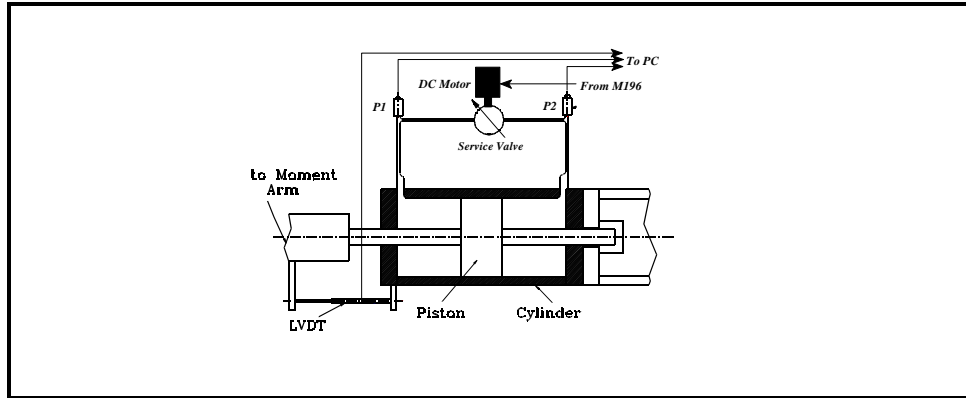
Figure 4.3 Assembly of an Actuator

A flow chart of the algorithm is shown in Figure 4.4.

Start

Initial 196 and AD3100

Offset Calculation

Start Control

Paralell Sampling Data From Three AD3100

Calculate X, ΔP

$X^T Q \, B \, \Delta P > 0$

No

Yes

Sent Open Command to 196

Sent Close Command to 196

Continue

Print Result to File

Stop
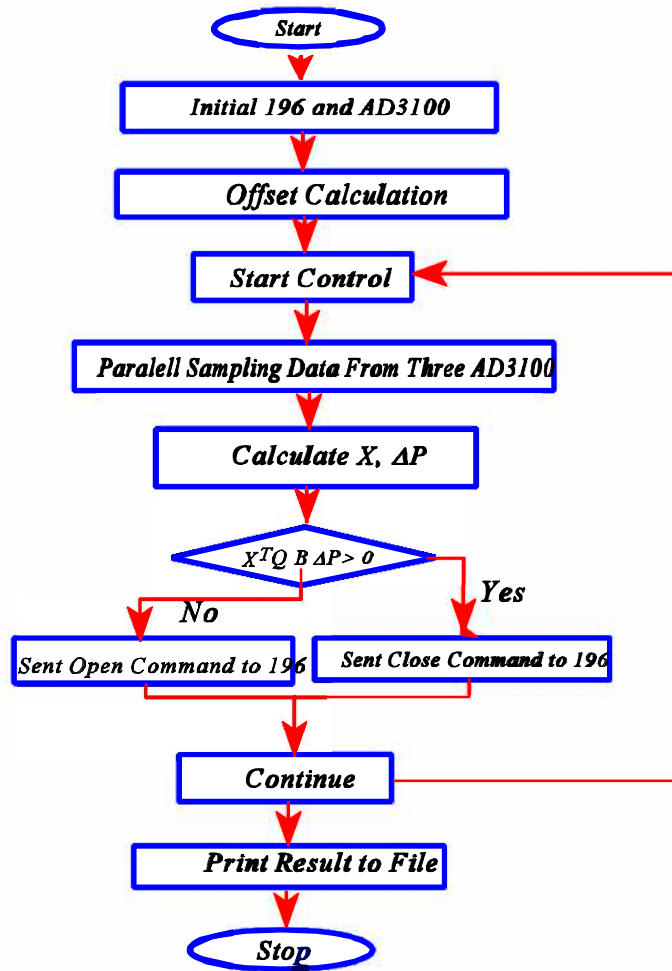
**Figure 4.4 Flow Chart of Experimental Control Program**

4.2 Field Test Results

The first test discussed here was conducted in November, 1996. A rock truck was used in the test (See Subreport #1 for description). The test was conducted to determine the passive (uncontrolled) performance of the SAVA system versus the performance of the bridge prior to the installation of SAVA system. When the valve on a SAVA is fixed open, the SAVA acts like a simple fluid damper, providing some resistance to flexure as a truck passes over the bridge. Figures 4.5 and 4.6 depict the strain time histories at the bottom flange for three girders at the center of the span in which the SAVA was mounted.

The truck was traveling at 65 mph in each test, vehicles traveling behind the test truck slowed the following traffic down, making it possible to have the test truck cross the bridge without any other vehicles on the bridge. An inspection of the data indicates that the SAVA when operated as a passive damper, does provide some reduction of the maximum

14

stress for those girders that are not located near the wheel loads. The passive damper has very little effect on the stress induced in the girders that are proving primary support. The conclusion is that passive dampers are ineffective as a means of extending service life.

Rock Truck in the Right Lane, Sensor C2
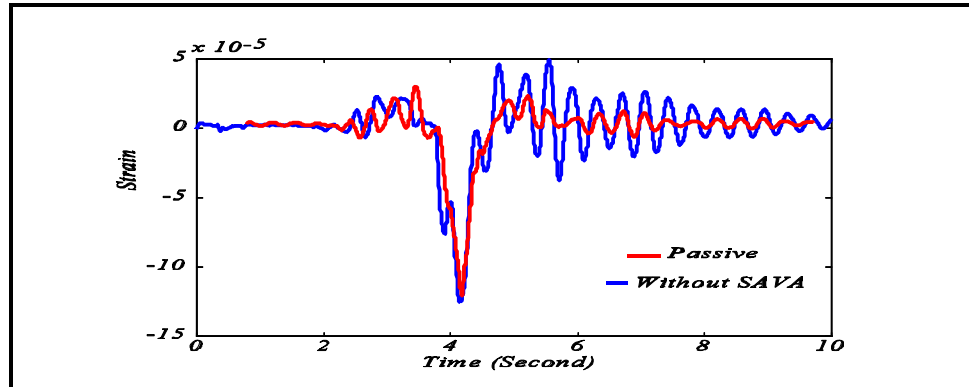
Rock Truck in the Right Lane, Sensor E2
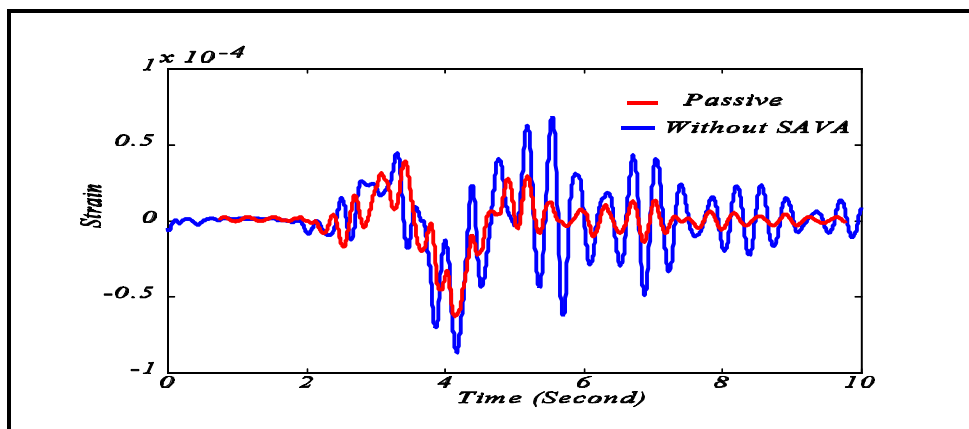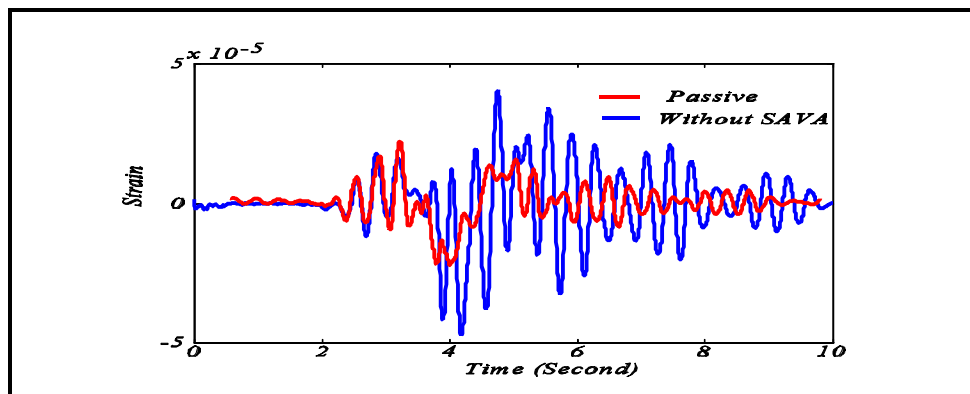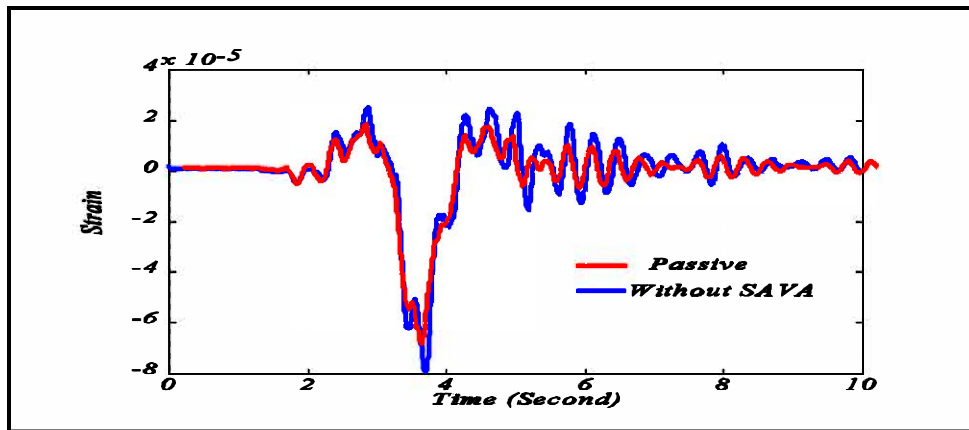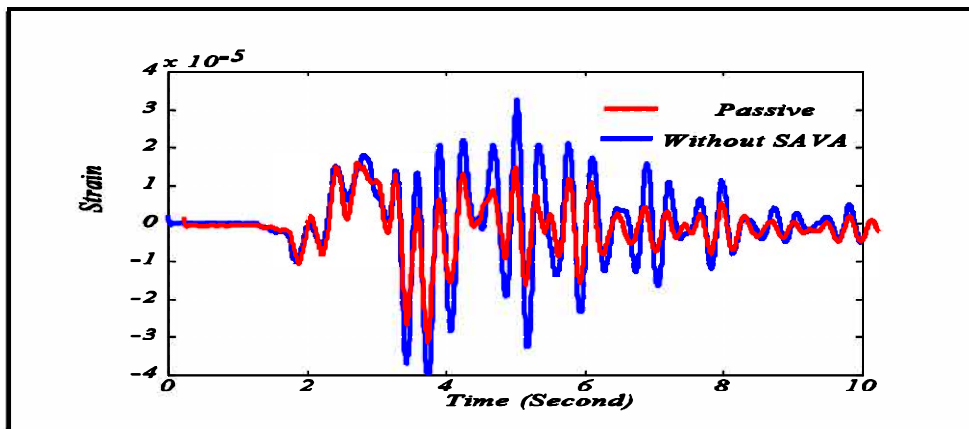

Rock Truck in the Right Lane, Sensor W2

Figure 4.5 Strain Comparison Without SAVA vs. Passive, Rock Truck in the Right Lane

15

Rock Truck in the Left Lane, Sensor C2

Rock Truck in the Left Lane, Sensor E2

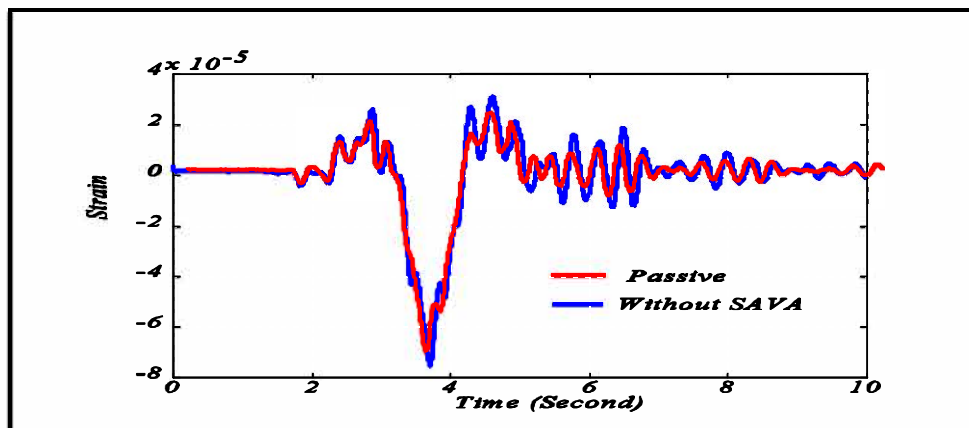**Rock Truck in the Left Lane, Sensor W2**

Figure 4.6 Strain Comparison Without SAVA vs. Passive, Rock Truck on Left Lane

4.3   Controlled Response

Several field tests have been conducted at the bridge to examine the performance of the control system. The tests were needed to debug the design of the controller. The results of a test conducted in April, 1997 are reproduced here to demonstrate the closed loop performance of the SAVA system. The test included four trucks. Figures 4.7 thru 4.11 indicate the controlled and uncontrolled response for each of the test truck. Figures 4.12 depicts the differential pressure in one actuator, the stroke of the piston and the time history of the control command when the heavy truck passed over the bridge.

4.4   Closure

The real time histories of the controlled and uncontrolled response of the bridge provided the basis for the fatigue life study (see Subreport #1).
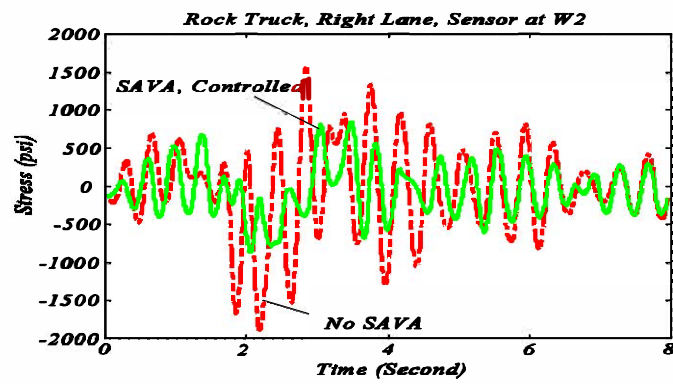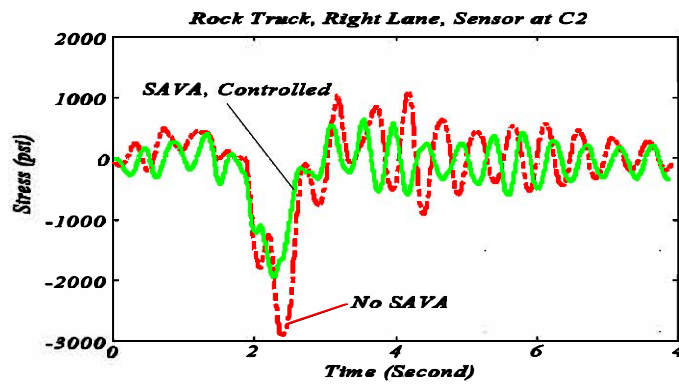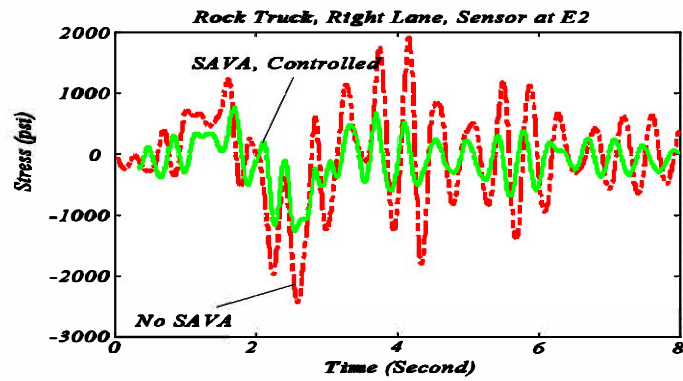
Figure 4.7 SAVA Control vs. No SAVA from the Test Data

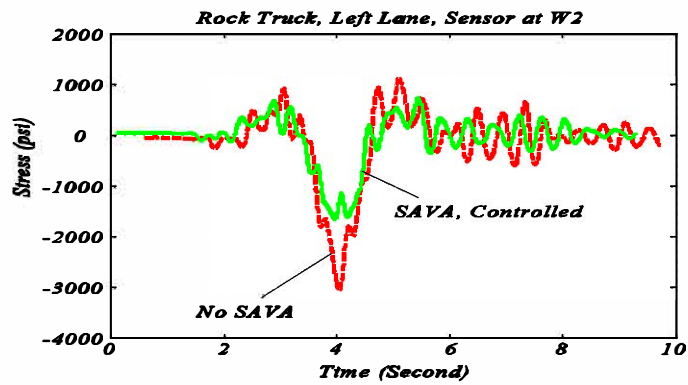**of a 61 kips Truck Traveled in the Right Lane**
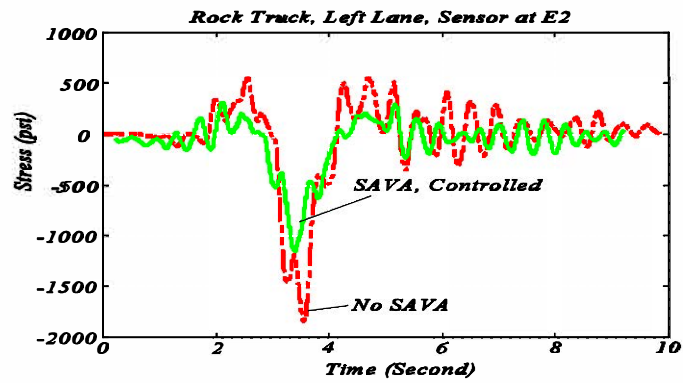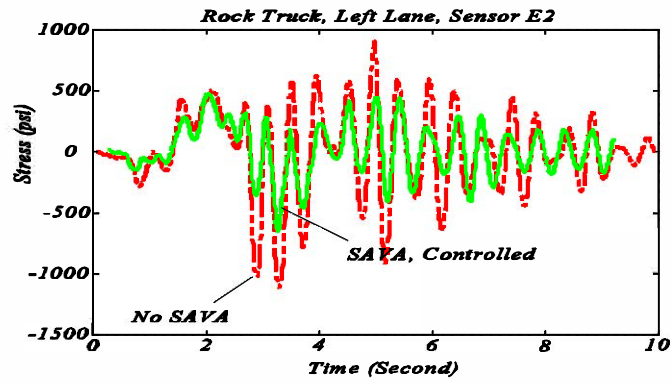
Figure 4.8 SAVA Control vs. No SAVA from the Test Data

of a 61 kips Truck Traveled in the Left Lane

19

Water Truck, Right Lane, Sensor at E2

Water Truck, Right Lane, Sensor at C2

Figure 4.9 SAVA Control Field Test, Water Truck Traveled in the Right Lane

20

Figure 4.10 SAVA Control Field Test, Heavy Truck Traveled in the Right Lane

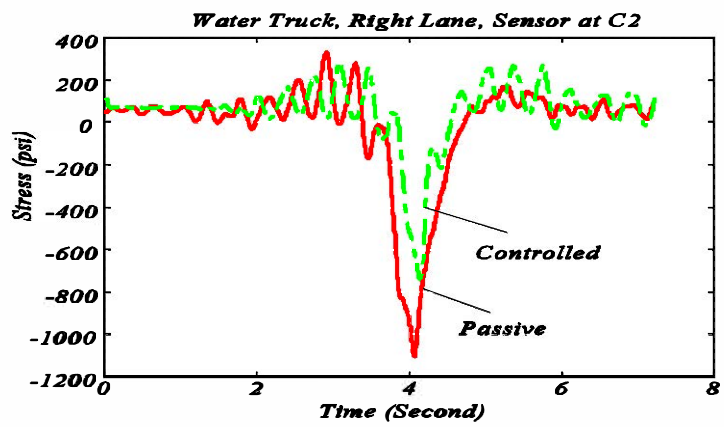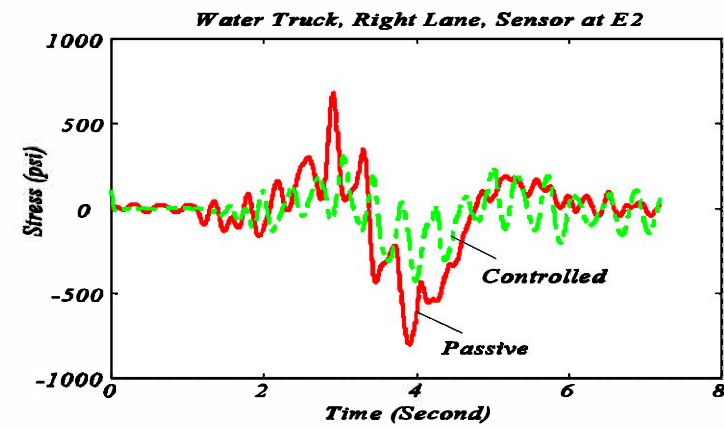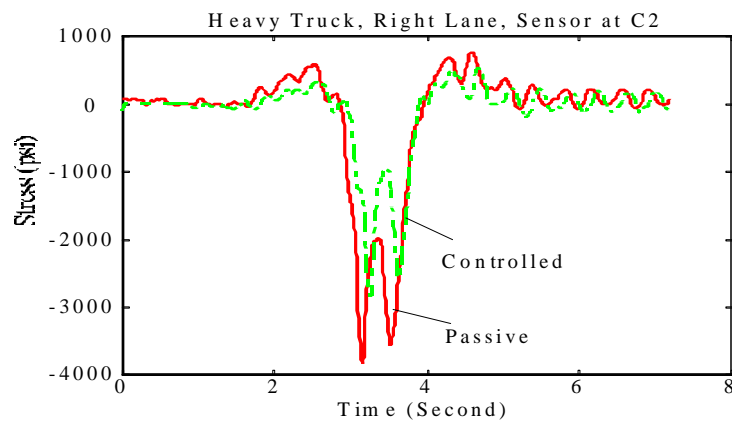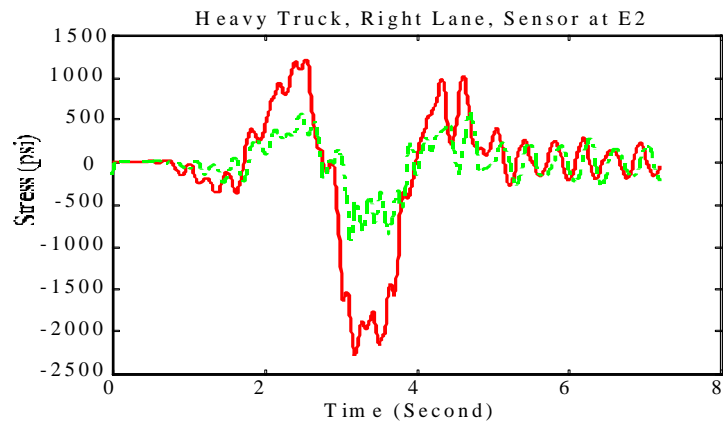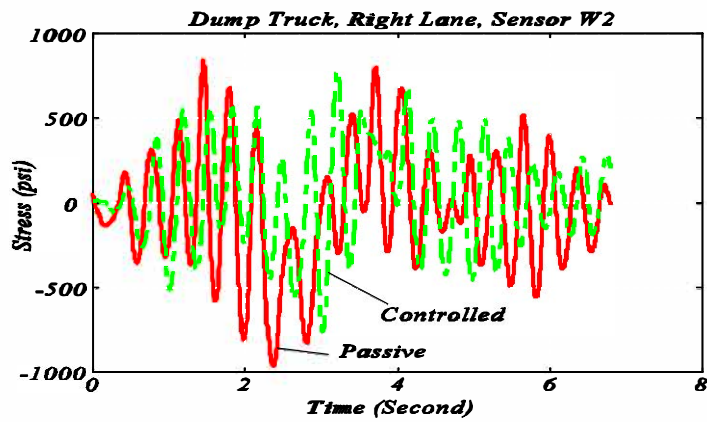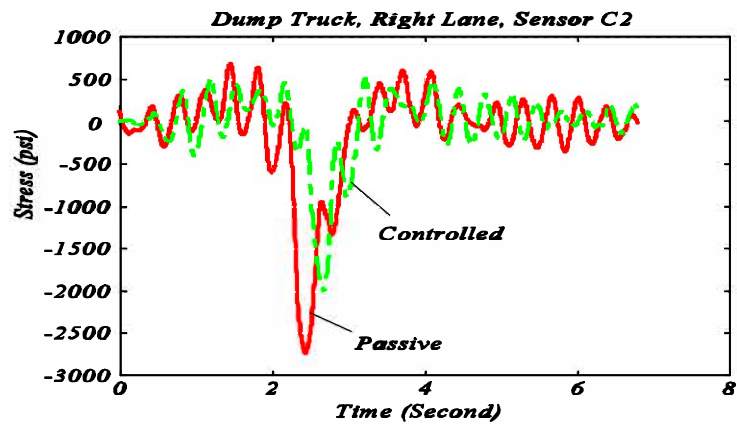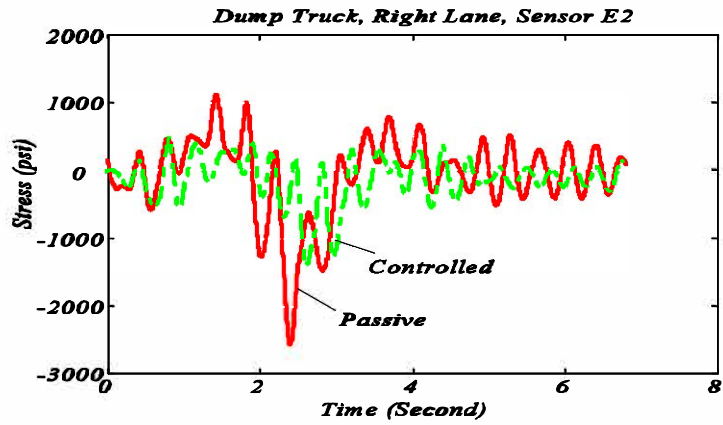**Figure 4.11 SAVA Control Field Test, Dump Truck Traveled in the Right Lane**

References

[1] Patten, W. N., Sack, R. L., He, Q., (1996), " A Controlled Semiactive Hydraulic Vibration Absorber for Bridges", ASCE, Journal of Structural Engineering, 122(2), 187-193.

[2]Crosby, M. J., and Karnopp, D.C., (1973),"The Active Damper-A New Concept for Shock and Vibration Control," 43rd Shock and Vibration Bulletin, Part H, June.

[3] Karnopp, D., (1990),"Design Principles for Vibration Control System Using Semiactive Damper,"Journal of Dynamic System, Measurement, and Control, 1127(4), 449-455.

[4]Feng, Q. and Shinozuka, M., (1990), "Use of a Variable Damper for Hybrid Control of Bridge Response under Earthquake,"U.S. National Workshop on Structural Control Research Proceedings, ed. Housner, George and Masri, Sami, October, Los Angeles, California.

[5] Hrovat, D., Barak, P., and Rabins, M., (1983)," Semiactive Versus Passive or Active Tunes Mass Dampers for Structure Control."Journal of Engineering Mechanics, 109(3), June, 691-701.

[6]Butsuen, T., (1989)," The Design of Semiactive Suspensions for Automotive Vehicle, "Ph.D. Dissertation, Department of Mechanical Engineering, MIT, June.

[7]AASHTO, (1989a) Standard Specifications for Highway Bridges, American Association for State Highway and Transportation Officials, Washington, D.C.

[8] AASHTO, (1989b) Guide Specifications for Fatigue Design of Steel Bridges, American Association for State Highway and transportation Officials, Washington, D.C.

[9]Patten, W., He, Q., Kou, C. C., Liu, L., Sack, R. L., (1994), "Suppression of Vechicle Induced Bridge Vibration Damper (SAVA)," First World Conference on Structure Control Los Angles, CA, Aug. 3-5, FA2 83-89.

[10] Tseng, H. E. and Hedrick, J.K., (1994), "Semiactive Control Laws - Optimal and Sub-Optimal," Vehicle System Dynamics, 23, 545-569.

[11] Patten, W. N., He, Q., He, J., and Hu, J., (1994)," A New Algorithm of Semiactive Control for Suspension with Nonlinear Leaf Spring," ASME Winter Annual Meetting, Chicago, IL, 147-156.

[12] Structural Dynamics Research Corporation (1994), I-DEAS System, Dynamics, Analysis, User's Guide, Vol 2, P-10096B.

[13] Hu, J., (1995), " Research on Semiactive Vibration Damper and Control Algrithms for Highway Bridges," Masters Thsis, Univ. of Oklahoma, School of Aerospace and Mechanical Engineering, Norman, Ok.

[14] Balas, M. J., (1978), "Feedback Control of Flexible System," IEEE Transaction on Automatic Control," AC-23(4), 673-679.

[15] Patten, W. N., He, Q., and Sack, R. L., (1995), "New Life for Highway Bridge via Semiactive Vibration Absorbers (SAVA)," Submitted to ASCE Journal of Bridge Engineering, November.

[16] Petersen, I.R., (1985), "A Riccati Equation Approach to the Design of Stablizing Controllers and Observers for a Class of Uncertain Linear Systems," IEEE Trans. Auto. Control, Vol. AC-30(9), 904-907.

[17] Jeffcott, H. H., (1929), " On the Vibration of Beam under The Action of Moving Loads," Philosophy Magzine, 7(8), 66.

[18] Yao, J. T. P., (1972), "Concept of Structure Control," Journal of Structure Division, ASCE, 98(7), 1567-1574.

[19] Soong, T. T., Hanson, R., (1993), "Recnet Developments in Active and Hybrid Control Research in the U.S.," in Housner, G.W. and Masri, S.F. (eds.), Proceedings of the International Workshop on Structure Control: Honolulu, Hawaii, August 4-7, 1993, University of Southern California, 483-490.

[20] Suhardjo, J., Spenceer, Jr., B.F., and Sain, M. K., (1990), " Feedback-Feedforward Control of Structures under Seismic Excitation," in Casciati, F., Elishakoff, I. and Roberts, J. B. (eds.), Nonlinear Structure Systems under Random Conditions, Elsevier, 69-89.

[21] Brogan, W. L., (1991), Modern Control Theory, Prentice-Hall, New York.

[22] Chu, K.H., Grag, V. K., and Wang, T. L., (1996), "Impact in Railway Prestressed Concrate Bridge," Journal of Structural Engineering, ASCE, 112(5), 1036-1051.

[23] Hwang, E. S., and Nowak, A.S., (1991), "Simulation of Dynamic Load for Bridges," Journal of Structural. Engineering, ASCE, 175(5), 1413-1434.

[24] Wang, T. L., Gray, V. K., and Chu, K. H., (1991), "Railway Bridge/Vehicle Interaction Studies with New Vehicle Model," Journal Structure Engineering, ASCE, 117(7), 2099-2116.

[25] Kobori, T., and Minai, R., (1960). "Analytical Study on Activve Seismic Response Control," Transaction of Architecture Institute of Japan, 66, 257-260.

[26] Yang, J. N., and Giannopoulos, F., (1978), "Dynamic Analysis and Active Control of Two Stayed-cable Bridge," Technical Report No.2, NSF Grant No. ENG-76-2387, School of Engineering and Applied Science, George Washington University, Washington, D.C., Feb.

[27] Yang, J. N., and Giannopoulos, F., (1978), "Active Tendon Control of Slender Structure," Journal of Engineering Mechanics Division, ASCE, 104(EM3), Preceeding Paper 13836, June, 1978,551-568.

[28] Abdel-Roham, M., Quintana, V. H., and Leipholtz, H. H., (1980), " Optimal Control of Civil Engineering Structures," Journal of Engineering Mechanics Division, Proceedings of ASCE, 106(EM1), 57-73.

[29] Lin, Y. H., and Trethewey, M. W., (1993), "Active Vibration Supression of Beam Structures Subjected to moving Loads: A Feasibility Study Using Finite Elements," Journal of Sound and Vibration, 166(3), 383-395.

[30]Feng, Q., and Shinozuka, M., (1990), "Use of a Vibration Damper for Hybrid Control of Bridge Response under Earthquake," U.S. National Workshop of Structural Control Research Proceedings, ed. Housner, George and Masri, Sami, October, Los, Angeles, California.

[30] Veletsos, A. S., and Huang, T., (1970), "Analysis of Dynamic Response of Highway Bridge," Journal of Engineering Mechanics, ASCE, 107(1), 229-246.

[31] Fuller, C. R., and Rogers, C. A., (1992), "Control of Sound Radiation with Active/Adaptive Structures, "Journal of Sound and Vibration, 157(1), 19-39.

[32] Semiactive Suspension Technology: An Evolutionary View. Douglas E. Ivers and Lane R. Miller, "Advanced Automotive Technologies", ASCE, 1991.

[33] Lemaire, E., Grasselli, Y., and Bossis, G. (1994) "Ffield Induced Structure in magneto and electro-rheological fluids." J. de Physique, 2(3), 359.

CONCLUSIONS AND RECOMMENDATIONS

Part 1: Modal Analysis. The success of the research project hinged in large part on the fidelity of the finite element model (FEM) of the test bridge. The model was necessary to verify the current condition and capacity of the superstructure, and to provide a basis for the analysis and design of the adaptive muscle structure (the SAVA System) that has been installed at the site. The model also provides a comprehensive picture of the effect various design features have on the service life and load capacity of the bridge. For example, the CSC has been able to determine the effect that skew has on the stress loading and vibration response of the bridge. The FEM has also made it possible to study the out of plane coupling that arises between a skewed bridge deck and the piers, when the piers are cast perpendicular to the center line of the road. Field tests verify the FEM prediction that significant motion occurs about the weak axis of piers of skew bridges. That action is likely to reduce the load-carrying capacity of pier pile caps and/or to promote scower. The CSC…

    1. recommends that study of the skew effect on bridge service be undertaken.

Once the results are verified for one or two additional skew bridges, then work should be conducted to study potential ways of mitigating the problem. A new bearing detail that allows <u>some</u> elastic lateral deformation is one possible mode of remediation.

The FEM of the test bridge can also be employed to gauge the significance that lateral stiffeners have on service life and vibration. There is some concern that those elements pose a weak link in the design of plate girder systems. A formal study, using the Walnut Creek Bridge model, should be conducted to explore the trade off that occurs when those stiffeners are either reoriented (parallel with the skew) or removed. A very preliminary examination of the question has been conducted by CSC. One concept that emerged from that investigation was the possibility of replacing the rigid stiffeners with a damper/stiffener assembly. That design would reduce local stress, while affording forces that resist the "out of plane" vibration of the girders when a heavy truck passes over.

The validated FEM was essential to the design of the bolt connections between the girder flange and the SAVA moment arm. The "zoom" feature of the code allowed the team to examine the stress distribution at each bolt in the assembly, rather than relying on rule of thumb guidelines for their design. Essential to that bolt design was the need to assure a no-slip condition between the SAVA assembly and the girder. The FEM indicated that the best way to achieve that goal was to rely on the friction developed between the SAVA/girder joint and to utilize tapered bolts. Twenty-five percent of the bolts in the coupling assembly were tapered.

During the course of the project, it was discovered that there is not a commercial FEM code available that is capable of simulating the dynamic response of the bridge when trucks travel across. Trucks have suspensions, and the extremely important resonance condition that has been found to exist between a truck and the bridge, can only be predicted if the coupled dynamics of the bridge/truck system is able to be simulated. The CSC spent a good deal of time developing a software package that can achieve that simulation, but it is not a user-friendly code. As the need to develop bridge-friendly truck suspensions grows, there is going to be a corresponding need by bridge engineers for software package that can be used routinely to conduct those studies.

The current crop of commercially-available FEM software is also unable to provide a means of testing structural control designs for a structure. The CSC team has developed a copyrighted "c" code that utilizes a reduced order model of the bridge, based on the full FEM that makes it possible to simulate the bridge/truck dynamics, in combination with the simulated operation of the hydraulic structural control system. That software code was a key component in the design and analysis of the SAVA system.

The development of a high fidelity FEM of the test bridge was only possible because of the modal testing that was done. The CSC has installed over 60 sensors on the Walnut Creek Bridge. Thirty-two of those sensors were accelerometers that were used in the model testing effort. (Funding for the modal testing sensor system was provided by the U.S. National Science Foundation.) A survey of the literature suggests that the sensor system installed on the Walnut Creek Bridge is perhaps the most accurate and sensor dense application to a bridge in the world. The high accuracy was a result of the development of a unique frequency modulated (FM) signal conditioning design that makes it possible to transmit sensor outputs over long distances, while assuring 99% accuracy (see text). All the electronics integral to the design were designed and fabricated by CSC engineers. It may be possible to patent and commercialize that system. We will await ODOT's recommendation on that.

The robustness of the sensor system design is also significant to possible future investigations. The entire system has been weather-proofed and requires very low maintenance. It is our…

(2) recommendation that the sensor system installed on the Walnut Creek Bridge be used to provide the basis of a long term health monitoring trail test at the bridge.

Other efforts that are underway around the nation to demonstrate the benefits of a bridge health monitoring system are now finding that the integrity and resolution of the sensor system is absolutely essential if small changes in the performance of a bridge are to be detected over long periods of time. The system at the Walnut Creek Bridge meets and exceeds that criteria.

Recent work by the CSC team indicates that it is possible to accomplish an accurate modal test with as few as four to eight accelerometers. (The number varies with the span length and number of spans.) The modal testing was also a success, because of the very unique and portable modal drop hammer that was designed and built by the CSC. A thorough review of the bridge modal literature indicates that the characteristics of the modal hammer used on the Walnut Creek project are far superior to, and much less expensive, than the alternative systems being used by others doing modal test research.

The fact that only a few accelerometers need to be used, that they need only be mounted <u>during</u> a modal test, and the portability of the impact hammer, indicate that the modal testing of a bridge could be conducted in a very short amount of time (perhaps a day). The only time traffic control would be needed is when the drop hammer testing is done (approximately 3-4 hrs.), Critical decisions about load-carrying capacity and condition of an existing bridge should be made with a field-verified FEM of a bridge. The project results indicate that the technology needed to conduct that verification is relatively inexpensive. The PI has formed a company that will offer bridge/structure modal testing and FEM verification services to the DOT's in the Midwest.

Part 2: Fatigue Analysis. <u>The estimate of remaining safe life for the span of the Walnut Creek Bridge, that has the</u> <u>control system mounted on it, indicates that the *SAVA system adds a minimum of 50 years* to the bridge.</u> Those estimates are based on the use of field test data. <u>That estimate is very conservative</u>. An estimate based on the standard fatigue truck with assumed worst case impact values, suggests an increase of over 150 years of safe life.

The research at the test bridge suggests that the assumptions made in NCHRP 299 are not well founded. For example, that guideline suggests that for design/analysis purposes, the static load of a fatigue truck need only be multiplied by 1.15 to reflect the most probable impact due to truck traffic. The guideline suggests that in extreme circumstances, a multiplier of 1.3 be used. The field data obtained, using four different trucks, indicates that the true impact levels are almost always greater than 1.6. For two of the trucks, the impact level at every point on the bridge was greater than 2. The Ontario Highway Bridge design code suggests that the impact factor be increased to 1.5, when the bridge fundamental frequencies correspond to truck chassis fundamental nodes (2 Hz. to 5 Hz.). The Swiss bridge code recommends an increase to 1.8 under the same conditions.

The real problem with NCHRO 299 is that it relies on a static analysis, with correction factors suggested to reflect the dynamics. The CSC strongly…

    (3) recommends that the analysis of service life for bridges be accomplished via dynamic testing and dynamic simulations in order to gauge the important effect of elastic coupling and resonance that occurs between trucks and bridges that have fundamental modes between 2 and 5 Hz.

Part 3: Truck Dynamics. The significance of truck suspension dynamics to the assessment of fatigue life has been pointed out above. The CSC spent considerable effort to understand the mechanisms that describe a truck's suspension. A truck was instrumented, and the data obtained was used to construct a dynamic model of a truck's suspension. Simulations, using the model, agree with the test data obtained during the project. The truck and suspension model were used in conjunction with the verified FEM of the bridge, to enable a design analysis of the SAVA control system. The design would not have been possible otherwise.

What is not clear, is what type (or combination of suspension types) is most bridge-friendly. The CSC…

    (4) recommends that a study be undertaken to determine which passive suspension designs produce the least bridge impact.

It is noted that a suspension that provides isolation of the truck load (the freight) is likely to shed undesirable dynamics to the bridge. It is also important to note that the same study could and should also examine what suspension configuration is the most pavement-friendly. The two criteria may not be congruous.

The technology that the CSC has developed to reduce bridge vibrations is an outgrowth of work that was conducted (successfully) to develop a smart semiactive (low power) suspension control system for vehicles. The CSC…

    (5) recommends that a project be conducted to demonstrate the concept of an intelligent highway bridge.

The bridges would be outfitted with a few vibration sensors and a microcomputer, which would have RF communication capability. When a truck equipped with a smart suspension crosses the bridge, then the bridge microprocessor would broadcast to the truck's chassis computer the fundamental frequencies of the bridge. The smart

truck suspension would then react by adjusting the compliance of the suspension in order to prevent the truck from vibrating at a similar frequency.

A preliminary study shows that the Intelligent Highway Bridge (IHB) concept will reduce future vibration impact damage to an existing bridge. The cost of the system is very small, relative to a SAVA system, and the design would add approximately 15 to 20 years of additional life to a healthy bridge. On the other hand, the SAVA system will always provide much more deflection and stress reduction, because it adds both stiffness and damping to the structure. A controlled truck suspension would effect only the degree of impact.

It is also important to note that the project did not examine the impact problem associated with multiple truck loading. Field testing indicates that it is absolutely wrong to assume that a simple superposition of single truck effects suffice to describe the multi-truck loading. The most aggressive dynamic response occurs, when the truck load pattern is such that the torsion and bending modes of the bridge are fully excited. When that occurs, the displacement is much larger than expected, and the residual vibration continues for many more cycles then is typical of the pure bending response. (This is because there is essentially zero damping in the torsion modes of the bridge.) The CSC…

(6) recommends that a thorough study of the mixed truck pattern effect on bridge dynamic loads be conducted. Simple distribution factors do not account for this serious load condition.

Part 4: SAVA Control System. The SAVA system installed on the Walnut Creek Bridge operates within 15% of the expected (analytical) performance prediction. The project demonstrates that the technology is well founded. The concept relies on the very simple truth that a smart muscle, attached at appropriate points on a girder, can dramatically reduce the peak deflections and stress. The design flattens out the moment diagram, distributing the stress to other parts of the girder that have experienced very little fatigue causing stress over the preceding service life of the bridge.

The hardware design proved to be somewhat conservative. The maximum control forces realized were approximately 25% less than was designed for. This suggests that a somewhat lighter assembly may be possible. The electronics proved to be problematic, but the final installation resolved many of the problems. The CSC has determined that a much simpler electronics package could deliver as much as 95% of the utility of the present design, while requiring much less engineering development. The next SAVA system attached to the bridge will utilize that improved design.

The field testing made it clear that the SAVA system can operate with as few as three sensors per actuator. That dramatic reduction of sensor count does much to raise the reliability of the electrical system. The CSC has demonstrated that it is possible to monitor the control system from a remote location using cellular technology. The circuitry used for that purpose was developed by CSC. Remote monitoring makes it possible to determine the need for field maintenance without realizing the cost of an on-site inspection. The CSC is now developing a simple detector technology that will automatically turn the SAVA control on when a truck is detected. The system is otherwise turned off, saving the batteries that will be relied upon to power the system when in full use. (The system is now operated only when field tests are being conducted.)

The installation of the SAVA system required no traffic stoppage. It did require the cooperation of ODOT in making the work site approachable. ODOT also provided transportation to the bridge of the heavier components of the system. The installation was unusual, in that it relied upon a system of temporary monitors attached to the bridge girders that were used to travel the SAVA system to the appropriate location under the bridge. Chain falls were used to raise the assembly into place.

With suggested improvements, a SAVA system should require only occasional maintenance (perhaps once every year or two) to recharge batteries and re-pressurize the actuators with hydraulic oil.

The only criticism to date of the system, is that the current design protrudes too far below the bottom flange of the rest bridge. The concern is that the reduced freeboard may result in debris making contact with the assembly that could produce a side load that, if unresisted, might damage the SAVA assembly and possibly the girder itself. The present SAVA system has been outfitted with a lateral stiffener system that essentially eliminates the possibility of tree limbs or other debris from causing any significant damage.

The next generation of SAVA will be tested on the Walnut Creek Bridge in 1998-1999. That design will seek to increase the freeboard clearance. Work is now underway to develop a design that can be tucked up between the girders.

With the presence of sensors on a bridge to detect motion and strain, there is the strong possibility that the sensed signals could be used to determine tire loads, axle weights and payload weight of a truck within 1% of the actual value. While that information is not needed to make good control decisions, it could be used to assemble a very accurate time history of the loads that a bridge undergoes. The CSC…

(7) recommends that ODOT commission a study at Walnut Creek to develop the software necessary to measure the number, frequency and amplitude time history of truck loads on the bridge.

That data would be used to develop a very precise estimate of the remaining safe life for the bridge. The data would be unique, in that it would be the first time that dynamic loads on a bridge would have been recorded accurately over a long period of time. Weigh in motion studies are generally inaccurate (more than 5%), and the real issue is not just weight, but the very substantial dynamic loads and their time history. The study may reveal a new approach to the estimation of the effect that truck traffic has on service life.

Closure

The project makes it clear; SAVA control is a viable method of remediating bridges that are near the end of their service life. Using the most conservative estimate possible, the system can add at least 50 years of service to a bridge that will otherwise have to be replaced. This new technology promises to provide at least an interim solution to the decaying bridge infrastructure problem facing America.

One question often asked is, "what effect would SAVA have on a new bridge." The question deserves an examination. It may, for example, be possible to reduce the amount of structure needed to afford the safety and load capacity required from a design. The question deserves to be studied.

The project results indicate that the retrofit of a bridge with SAVA will make it possible to routinely traffic trucks with much heavier axle loads, and possibly shorter distances between axles. That is especially so, if the truck is

equipped with an automatically, adjustable suspension. (The investment in that feature represents a fraction of a penny per ton mile of freight hauled.) The CSC…

(8) recommends a study, supported in part by the Trucking Industry, to explore the possibility of increasing the maximum permissible truck weights if the vehicle is outfitted with an appropriate suspension.

The reduction of deflection and vibration that results from the use of the SAVA bridge control system must necessarily reduce the amount of concrete deck that is needed for bridges. The CSC…

(9) recommends that a study be performed that relates the level of deflection reduction of SAVA to the amount of maintenance monies saved by reducing the frequency of bridge deck repairs.

Finally, the CSC…

(10) recommends that the Walnut Creek Bridge control system be linked to the I-35 Ethernet. That connection would make communication with the bridge very convenient. It would also provide an excellent means of monitoring the real time loading and truck traffic at any remote site also connected to the Ethernet.